IDENTIFICATION OF OPTIMAL PMU LOCATIONS AND SYNCHROPHASOR MEASUREMENTS BASED ESTIMATION OF ELECTROMECHANICAL MODES IN POWER SYSTEM

Ph.D. Thesis

by

JOICE G PHILIP

DISCIPLINE OF ELECTRICAL ENGINEERING

INDIAN INSTITUTE OF TECHNOLOGY INDORE

JULY 2019

IDENTIFICATION OF OPTIMAL PMU LOCATIONS AND SYNCHROPHASOR MEASUREMENTS BASED ESTIMATION OF ELECTROMECHANICAL MODES IN POWER SYSTEM

A THESIS

Submitted in partial fulfillment of the

requirements for the award of the degree

of

DOCTOR OF PHILOSOPHY

by

JOICE G PHILIP

DISCIPLINE OF ELECTRICAL ENGINEERING

INDIAN INSTITUTE OF TECHNOLOGY INDORE

JULY 2019

INDIAN INSTITUTE OF TECHNOLOGY INDORE

CANDIDATE'S DECLARATION

I hereby certify that the work which is being presented in the thesis entitled **Identification of Optimal PMU Locations and Synchrophasor Measurements Based Estimation of Electromechanical Modes in Power System** in the partial fulfillment of the requirements for the award of the degree of **DOCTOR OF PHILOSOPHY** and submitted in the **DISCIPLINE OF ELECTRICAL ENGINEERING, Indian Institute of Technology Indore,** is an authentic record of my own work carried out during the time period from July 2014 to July 2019 under the supervision of Dr. Amod C. Umarikar, Associate Professor, Indian Institute of Technology Indore, India and Dr. Trapti Jain, Associate Professor, Indian Institute of Technology Indore, India.

The matter presented in this thesis has not been submitted by me for the award of any other degree of this or any other institute.

Signature of the student with date
(JOICE G PHILIP)

This is to certify that the above statement made by the candidate is correct to the best of our knowledge.

Signature of Thesis Supervisor with date
(Dr. TRAPTI JAIN)

Joice G Philip has successfully given his Ph.D. Oral Examination held on

Signature of Chairperson (OEB)
Date:

Signature of External Examiner
Date:

Signature of Thesis Supervisor
Date:

Signature of PSPC Member #1
Date:

Signature of PSPC Member #2
Date:

Signature of Convener, DPGC
Date:

Signature of Head of Discipline
Date:

ACKNOWLEDGEMENTS

I take this opportunity to acknowledge my heartfelt gratitude to many people who have directly or indirectly helped me throughout my Ph.D. candidature.

I feel immense pleasure in expressing my deep sense of gratitude to my thesis supervisor **Dr. Trapti Jain** (Head, Discipline of Electrical Engineering, IIT Indore) for her inspiring guidance, precious supervision, excellent support and constant encouragement. Her constructive suggestions, positive criticism and philosophical mentoring helped me to complete this thesis in time.

I am grateful to the PSPC (Ph.D. Student Progress Committee) members **Dr. Amod C. Umarikar** and **Dr. Kapil Ahuja** for their precise observations and valuable suggestions to improve the quality of my doctoral work.

I am also very grateful to my fellow graduate students (Karthik, Prateek, Venkatesh, Raju, Ravindra, Vinay, Ajinkya, Suvamit, Arjun, Harisankar, Manu) for the technical discussions, unconditional support, and encouragement throughout my research. Also, for helping me in developing professionally and personally and making this period a very happy memory.

I would like to thank the Indian Institute of Technology Indore for providing me with an opportunity to carry out doctoral research in the Discipline of Electrical Engineering. Also, very thankful to the **Ministry of Human Resources Development (MHRD), India** for financially supporting me to carry out this research work successfully.

Last but not the least, I would like to thank my parents and my extended family, especially the members of my maternal home, who educated me, for always believing in my capabilities and encouraging me to pursue my dreams. Without them, I would not be in the position, where I am today.

JOICE G PHILIP

This thesis is dedicated to my family
who always believed in me

ABSTRACT

Phasor Measurement Units (PMU) are microprocessor-based devices used for real time monitoring of power system. PMU measures the voltage and current phasors of the buses in the power system and transfers the data to the control centre. This data is later used for various applications like stability assessment, adaptive relaying etc. However, due to the high installation cost of PMU and its related equipment, it is not economically viable to place the PMUs at every bus in the power system. Hence, this thesis aims to optimally place the PMUs maintaining complete observability of the power system during normal operating conditions and contingencies and develop algorithms using PMU data for identifying the poorly damped modes, which affect the small signal stability of the system. This thesis is divided into two sections. The first section deals with optimal placement of PMUs of different channel capacity along with maximization of measurement redundancy using an Integer programming technique. The effectiveness of the proposed model is tested on various IEEE test systems and a practical Indian power system for normal operating conditions as well as contingencies like single line outage and PMU outages.

The second part of the thesis is focussed on developing algorithms for analyzing the poorly damped modes in power system low frequency oscillations utilizing synchrophasor measurements. The low frequency oscillations occurring in power system can be broadly classified into ambient and ringdown type oscillations. The ringdown oscillations occur when the power systems are subjected to large-magnitude disturbances, whereas, ambient type oscillations occur due to random small changes in load or generation. The persistence of these oscillations in power system will cause cascaded tripping leading to blackouts. Hence, to prevent such unwanted occurrences, it is essential to identify these oscillations at the earliest. As the characteristics of these oscillations are not similar, different algorithms are needed for the proper analysis of these oscillating modes.

Algorithms based on Hankel's Total Least Square (HTLS) and Estimation of Signal Parameters using Rotational Invariance Technique (ESPRIT) have been developed for analysing ringdown oscillations. The model order which is a prerequisite for the proper implementation of HTLS and ESPRIT algorithms, are obtained through an FFT based technique and EMO algorithm respectively. A Stochastic Subspace Identification (SSI) based method is developed to analyse ambient type of oscillations. To improve the robustness of the proposed SSI based method, a Stationary Wavelet Transform (SWT) based denoising method is used. Further, the model order of the signal is estimated using EMO algorithm. Subsequently, in order to avoid the computation of model order, an Empirical Wavelet Transform (EWT)- ESPRIT algorithm has been developed for identifying the poorly damped modes in power system. In this algorithm, the EWT is used for splitting the multi-component signal into mono components and ESPRIT algorithm is used for estimating the modal parameters of these mono components. This algorithm can analyse stationary as well as non stationary signals, which occur during a transient condition.

The performance evaluation of these algorithms are conducted using synthetic signals with known modal parameters and real-time signals obtained from the PMUs installed in a practical system at different signal to noise ratios and PMU reporting rates. Results reveal that these algorithms perform better than the similar algorithms in literature.

Publications from the Thesis

Journal Papers:

1. Philip, Joice G., and Trapti Jain. , "Analysis of low frequency oscillations in power system using EMO ESPRIT," *International Journal of Electrical Power & Energy Systems*, vol. 95, no. 1, pp. 499-506, February 2018.

2. Philip, Joice G., and Trapti Jain. , "An improved Stochastic Subspace Identification based estimation of low frequency modes in power system using synchrophasors," *International Journal of Electrical Power & Energy Systems*, vol. 109, no. 1, pp. 495-503, July 2019.

3. Philip, Joice G., and Trapti Jain. , "An improved redundant observability model for optimal placement of PMUs with different channel capacities," *WSEAS Transactions on Power Systems*, vol. 13, no. 1, pp. 377-385, February 2018.

4. Philip, Joice G., and Trapti Jain. "An Empirical Wavelet Transform-ESPRIT approach for identifying the poorly damped modes in power system," *International Transactions of Electrical Energy Systems*, 2019 (To be submitted).

Conference Papers:

1. Philip, Joice G., and Trapti Jain, "Optimal placement of PMUs for power system observability with increased redundancy," *in Proc. of 2015 Conference on Power, Control, Communication and Computational Technologies for Sustainable Growth (PCC-CTSG).*, India, pp. 1-5, 18-20 December 2014.

2. Philip, Joice G., and Trapti Jain, "Estimation of modal parameters of low frequency oscillations in power system using Hankels total least square method," *in Proc. of 2018 IEEE Innovative Smart Grid Technologies-Asia (ISGT Asia)*, Singapore, pp. 764-769, 22-25 May 2018.

Contents

List of Figures

List of Tables

List of Abbreviations

AESOPS Analysis of Essentially Spontaneous Oscillations in Power System.

ARMA Auto Regressive Moving Average.

BILP Binary Integer Linear Programming.

BIP Binary Integer Programming.

BPSO Binary Particle Swarm Optimization.

CGA Cellular Genetic Algorithm.

CUF Channel Utilization Factor.

DWT Discrete Wavelet Transform.

EMD Empirical Mode Decomposition.

EMO Exact Model Order.

ESPRIT Estimation of Signal Parameters via Rotational Invariance Technique.

EWT Empirical Wavelet Transform.

FFT Fast Fourier Transform.

HHT Hilbert-Huang Transform.

HT Hilbert Transform.

HTLS Hankel's Total Least Square.

IGA Immunity Genetic Algorithm.

ILP Integer Linear Programming.

IQP Integer Quadratic Programming.

NRPG Northern Regional Power Grid.

PDC Phasor Data Concentrator.

PMU Phasor Measurement UNit.

RTU Remote Terminal Units.

SCADA Supervisory Control and Data Acquisition.

SNR Signal to Noise Ratio.

SSI Stochastic Subspace Identification.

TIC Total Installation Cost.

WAMS Wide-Area Measurement Systems.

Chapter 1

Introduction

1.1 Background

Low frequency oscillations occurring in power system is one of the major issues affecting its stability. If these oscillations are not monitored, it may lead to cascaded outages causing the blackout of entire power system. For instance, a serious power outage accident due to negatively damped inter-area oscillation caused the collapse of the West system in the U.S.A. on 10 August 1998 [1]. In China, similar incident occurred in 2005, where three system-wide low-frequency oscillation events occurred respectively in the South, Central and North China grids [1]. To prevent such incidents and to gain more information about these disturbances, it is necessary to monitor the power system at sufficiently many geographical locations using measurement equipments with sufficient bandwidth. The data collected should be accurately analyzed to avert incidents, which affect the security of the power system. This was conventionally done using Supervisory Control and Data Acquisition (SCADA) based systems. The schematic representation of a basic SCADA system for power system monitoring is shown in fig. 1.1 [2].

In this system, Remote Terminal Units (RTUs), which are placed at substations, collect the data and transmit it to the control centre through various communication links like fiber optics, microwave etc. The major types of data collected by RTU include generator outputs, bus voltages, line currents, loads and information on circuit beakers and transformer tap positions. The data received at the control centre is processed to filter out the measurement noise. The filtered data is then used for planning and analysis purposes. However, it is observed that the data rate of SCADA systems is quite low and the measurements taken

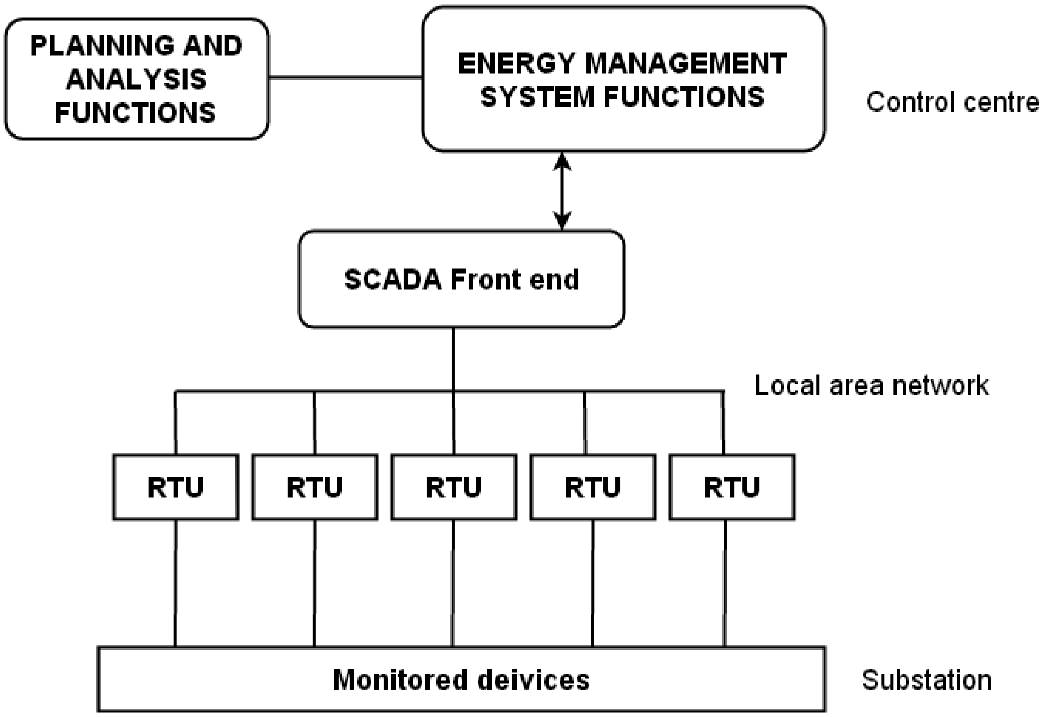

Figure 1.1: Block diagram of SCADA [2].

by the SCADA are not synchronized. Moreover, it cannot estimate the phase angle of bus voltages and line currents. Due to these drawbacks, SCADA based systems are increasingly replaced by PMU based monitoring systems in modern power networks [2].

1.2 Phasor Measurement Unit (PMU) and its Applications

PMU is a microprocessor based equipment, which estimates the voltage and current phasors of the host bus at high sampling rates and send this time stamped data over communication lines to Phasor Data Concentrator (PDC). The sampling rate of the PMU is between 30-120 samples per second. They are usually placed at substations and require three separate electrical connections to measure the voltage or current of each phase. PMUs time stamp their measured data using Global Positioning Satellite (GPS) clocks to synchronize the measurements made at different locations in the power system. The occurrence of major blackouts in many power systems around the world has accelerated the introduction of Wide-Area Measurement Systems (WAMS) based on PMUs. Data obtained from these PMUs helps the power system operators to accurately determine the exact sequence of events, which have led to the blackouts. Analysis of this sequence of events will help in finding the exact cause, which lead to catastrophic failure of the power system. The main advantage of the PMUs over SCADA based monitoring system is that PMUs can measure both the magnitude and phase angle of a quantity, whereas, the SCADA based system can measure only the magnitude. Moreover, the PMUs can accurately monitor the transient phenomenon occurring in the system as its data rate is high. Due to these reasons, PMUs are increasingly used for real time monitoring and control, power state system estimation and protection applications.

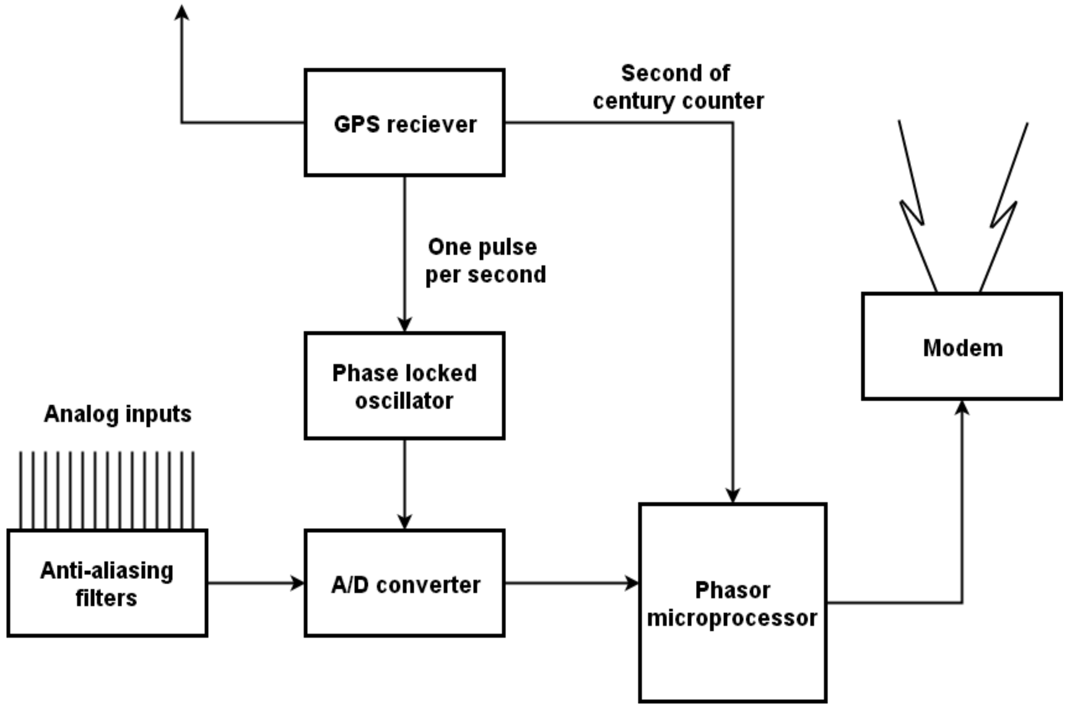

Figure 1.2: Block diagram of PMU [3].

The block diagram of a basic PMU is shown in fig. 1.2 [3]. The major components of the PMU are anti-aliasing filters, A/D converter, Phase locked oscillator, GPS receiver and Phasor Microprocessor. The signal under consideration is fed into the anti-aliasing filter of the PMU. Before this process, the signal is converted into its voltage equivalent (in range of +10V) with the help of instrument transformers or shunts. The anti-aliasing filter removes the frequency components other than the range of frequencies under consideration. The filtered signal is then digitized using an analog to digital converter. The microprocessor block calculates the phasors of this digitized signal through various signal processing techniques like Discrete Fourier Transform. The phase locked oscillator provides the synchronizing signal for time stamping the measured quantities with the help of the GPS clock [3]. The time stamped measurements from different PMUs placed across the power system is sent to Phasor Data Concentrator (PDC). A schematic representation of Wide Area Measurement system consisting of PMUs and PDCs is shown in fig. 1.3 [3].

Phasor Data Concentrator (PDC) receives the phasor data from multiple PMUs and time

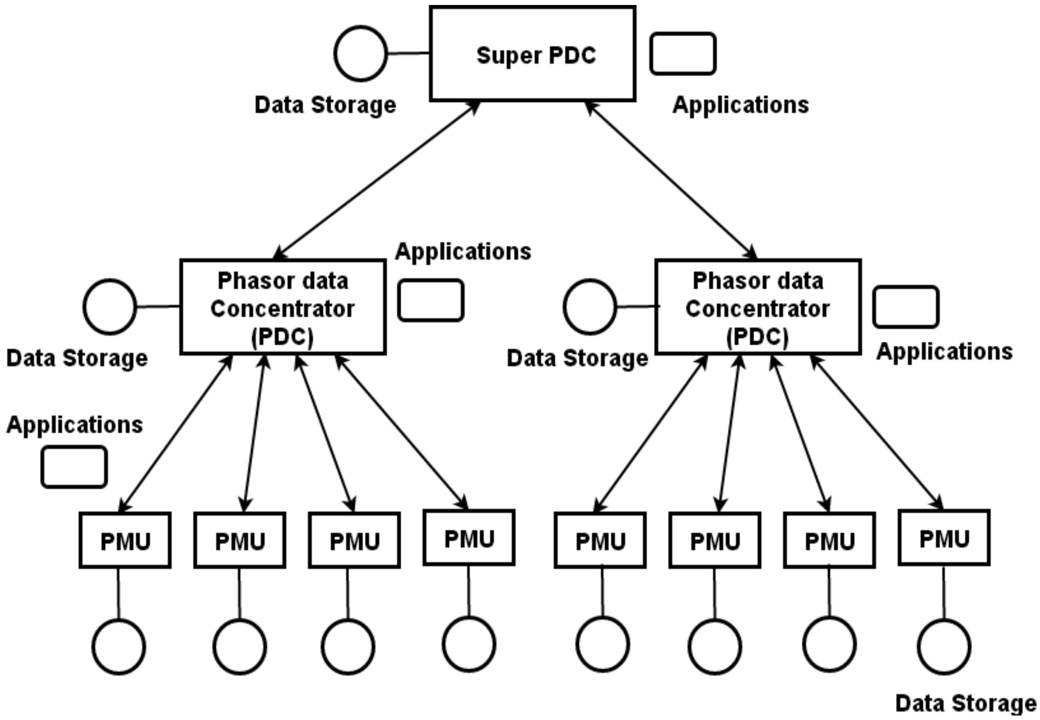

Figure 1.3: Block diagram of Wide Area Monitoring System (WAMS) [3].

synchronizes it to produce a real-time, time-aligned output data stream. A PDC can exchange phasor data with PDCs at other locations. Through use of multiple PDCs, multiple layers of concentrators can be implemented within an individual synchrophasor data system. PDCs also help in checking the dataset for completeness and finding errenous data, if any. They also make sure that the input and output data streams follow the IEEE C37.118 streaming protocol. Moreover, they buffer input data streams to accommodate the differing times of data delivery from individual PMUs. PDCs typically utilize threading and other parallel computing techniques available within modern operating systems to manage multiple connections at high speeds. A PDC based on its role or location can be classified as local PDC and super-PDC. Local PDCs are located closer to the PMUs for easier data collections. The data collected by local PDCs are sent to higher level concentrators or is stored locally for substation usage. Super PDCs operate on a regional scale and handle time synchronized data from multiple PDCs and several PMUs. It collects this data and makes them into a time synchronized data set, which can be later used in energy management systems and wide area monitoring using visualization softwares [3].

The major applications of PMU are

- State estimation

- Adaptive Relaying
- Power system control
- Instability prediction

State estimation: The power system operators use state estimators to monitor the state of the power system. The state of the power systems is calculated using voltage and current measurements received from different locations of the power system using an iterative nonlinear estimation technique. The state (vector) is a collection of all the positive sequence voltage phasors of the network. In SCADA based systems, state estimators available in present-day control centers are restricted to steady-state applications only due to low reporting rates and the time skew in data acquisition. On the other hand, the PMUs have high reporting rates and their measurements are synchronized due to which a dynamic state vector, which can follow the power system dynamics, can be constructed. This helps the operators to monitor the real-time power system dynamic phenomena with high fidelity at the control center. Apart from this application, the directly measured dynamic phenomena can be utilized for validating the power system models used in transient stability studies [4].

Adaptive Relaying: In conventional systems, power swings are detected with the help of the apparent impedance seen by the distance relays. The apparent impedance changes when the power swing occurs. The outcome of the power swing is inferred based on the variation of the impedance and the time taken to cause this variation. The settings of these relays are usually based on several stability simulations for all reasonable contingencies. However, if the characteristics of the power swing are entirely different from the assumed contingencies, then it may cause instability in the system. On the other hand, if synchrophasors are placed in the system it will help the power system operators to predict the outcome of a power swing using the real time data provided by them. This helps in countering the power swing in a better way [4].

Power system control: Power system control elements, such as generation excitation systems, HVDC terminals, variable series capacitors, SVCs, etc., use local feedback to achieve the control objective. PMU data, which is synchronized at high reporting rates, is an excellent choice as feedback to improve the control performance [4].

Instability prediction: The operation of power system is directly or indirectly governed by the possibility of the system going into unstable condition. Moreover, the system loading limits, operating speeds of the primary and back-up protection systems and the settings of out-of step relays also depend on this possibility. Hence, any improvement made in quick determination of the instability has great benefits to modern power systems. The traditional method for power system stability analysis uses system dynamic equations. However, for large power systems, it is computationally very intensive and hence can be used for steady state stability analysis only. After the introduction of synchrophasors, it is possible to track the dynamic changes happening in the power system. With the help of this data, the outcome of a power swing for a future time interval can be predicted with a fair degree of accuracy. This predicting capability helps in making better protection and control decisions to counter the power swing occurring in the system [4].

Since this thesis concentrates on small signal stability analysis of the power system using the data from synchrophasors, a brief description about this is given in the next section.

1.3 Stability Analysis of Power Systems

Power system stability is defined as the ability of the power system due to which it can remain in a state of operating equilibrium under normal operating conditions and to reclaim this state after being subjected to a disturbance. Since the major part of the electrical power generation is through synchronous machines, maintaining the synchronism of these machines is of paramount importance for power system stability. This aspect of stability is influenced by the dynamics of generator rotor angles and power-angle relationships. Hence, it is known as rotor angle stability. Apart from rotor angle instability, voltage instability and frequency instability are the other major stability issues affecting the power system. Voltage stability is the ability of a power system to maintain steady acceptable voltages at all buses in the system under normal operating conditions and after being subjected to a disturbance. Voltage stability is further classified into large-disturbance and small-disturbance voltage stability. Large-disturbance voltage stability is defined as the ability of the system to maintain steady voltages following large disturbances like system faults, loss of generation, or circuit contingencies. On the other hand, the ability of a system to maintain steady voltages when

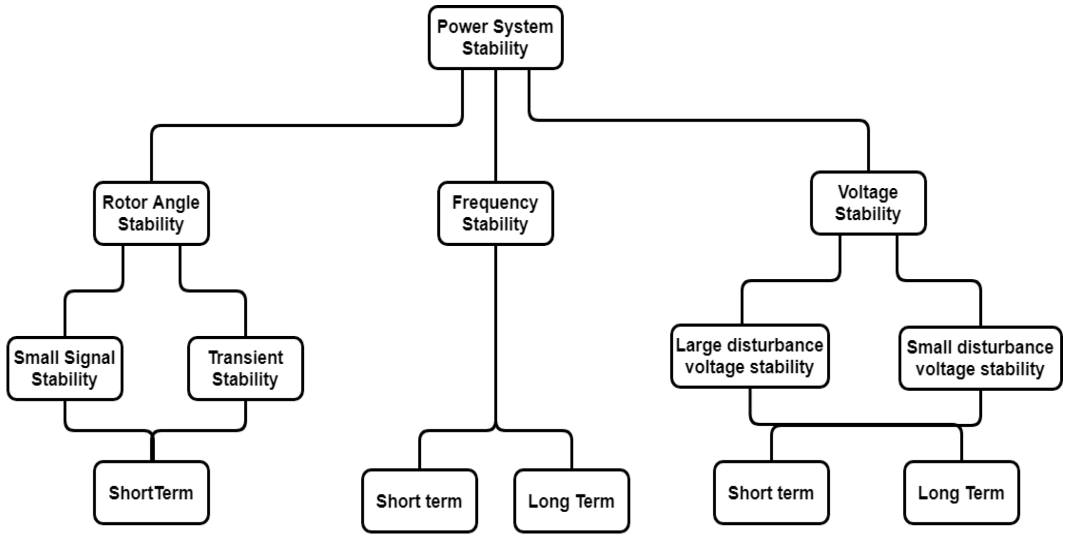

Figure 1.4: Classification of power system stability [5].

subjected to small perturbations such as incremental changes in system load is defined as small-disturbance voltage stability. Frequency stability is the ability of a power system to maintain steady frequency after a severe system upset resulting in a significant imbalance between generation and load. A schematic diagram showing the different classifications of power system stability is given in fig. 1.4 [5].

Small-signal stability is defined as the ability of the power system to maintain synchronism when subjected to small disturbances such as small variations in loads and generation. These disturbances are considered sufficiently small such that the system equations can be linearized for purposes of analysis. Small signal stability issues occur mainly when there is a steady increase in rotor angle due to lack of sufficient synchronizing torque or due to insufficient damping torque leading to rotor oscillations of increasing amplitude. In modern power systems, insufficient damping of oscillations is the major reason for small-signal stability issues. Large active power, large negative reactive power, long tie lines and large automatic voltage regulator gain with low time constant are some of the major reasons for insufficient damping in power systems. The major types of oscillations occurring in the power system as a result of small signal issues are local mode, inter area mode, control mode and torsional mode oscillations [6].

Intra plant mode oscillations ranges from $2-3$ Hz and occurs when some generators oscillate against its neighbours in the same power station. Local plant mode oscillations occurs when the units in a generating station oscillate against the rest of the power system. The frequency of these oscillations is in the range of 1-2 Hz. Inter-area mode oscillations have a frequency of $0.1-1$ Hz and are associated with two or more coherent generator groups swinging against each other in a power system. Torsional oscillations are associated with turbine generator shaft system and have their frequencies between $10-45$ Hz. These oscillations may cause reduction of shaft operative life or shaft failure. Control modes are associated with generating units and control equipment. Poorly tuned exciters, governors, high voltage DC converters and static VAR compensator controllers are the main reasons to initiate control mode oscillations [6, 7].

The persistence of these oscillations in power system network can cause blackouts. Hence, it should be detected at the earliest and suitable counter measures must be taken to damp out these oscillations. Conventionally, these oscillations are detected through Eigenvalue analysis. The state space equations of the power system linearized around an operating point are used for this purpose. The state space equations of the power system are developed from individual models of synchronous machines, transmission line, static and dynamic loads etc. The dynamics of machine rotor circuits, excitation systems, prime mover and other devices are represented by differential equations. The state space matrix of the power system generated from these state space equations, gives an idea about the small signal oscillations occurring in the power system. However, this method is not suitable for the analysis of large power system as the number of state variables required for its proper modelling will be very high and well outside the range of the conventional eigenvalue analysis methods. Hence, special techniques like Analysis of Essentially Spontaneous Oscillations in Power System (AESPOS) have therefore been developed to evaluate a selected subset of eigenvalues of such systems [6].

AESOPS is used for eigenvalue analysis of the oscillations associated with synchronizing power flow in large electric power systems. In this algorithm, eigenvalues associated only with rotor angle modes, one complex conjugate pair of eigenvalues at a time, is calculated. The AESOPS Program utilizes an overall system model formulated in terms of the incremental voltages at the terminal buses of synchronous machines and dc lines for this purpose. The overall system model is obtained by combining these partial system models:

- the network and generator stator equations
- the generator rotor motion and rotor flux linkage equations

The main disadvantage of this method is that unless the general characteristics of the critical modes are known beforehand, computational time required will be much higher. Moreover, there is no assurance that critical modes will be identified [6].

1.4 State of the art

After their invention in the mid-1980's, PMUs are widely used for monitoring and control of power system. The measurement data from the PMUs has a high data rate which makes them an ideal device for observing the power system under dynamic conditions. However, the installation cost of PMU and its associated equipment is very high. Hence, it cannot be installed at every bus of the power system. Moreover, PMU placed at a bus observes itself and all its interconnected buses provided it has sufficient channels. Therefore, the number of PMUs required to make the power system observable is always less than the total number of buses in that power system. Thus, identification of optimal locations for installation of PMU is considered as one of the research problems in this thesis.

After the PMUs are optimally placed in the power system, they will send the synchronized data to the phasor data concentrator as explained in the previous section. This data can be used for various purposes like small signal stability analysis, voltage stability analysis etc. This thesis focus mainly on techniques for online monitoring of small signal stability. The poorly damped low-frequency oscillations occurring in the power system is one of the major factors affecting its small signal stability. These oscillations have a range of $0.1-2$ Hz and occur mainly due to increased power demand, reduced generation reserve margins, physical limitation of the power system and deregulation. Identification of these oscillations is the other major research problem considered in this thesis. A literature survey of these issues relevant to the research work, carried out in this thesis is presented in the following sections.

1.4.1 Optimal PMU Placement

The algorithms used for determining optimal PMU placement can be broadly classified into Meta-heuristic and Deterministic algorithms. Metaheuristic algorithms use intelligent search techniques like Simulated Annealing [8], Binary search [9], Binary Particle Swarm Optimization (BPSO) [10], Genetic algorithm [11, 12] for finding the optimal PMU locations in the power system. The advantage of meta-heuristic algorithms is that it does not need a set of constraints to achieve a particular solution. In [8], optimal PMU problem was first solved using a combination of the bisecting search algorithm and simulated annealing. In this technique, the bisecting search algorithm was used to find the optimal number of PMUs needed for complete system observability whereas the simulated annealing technique was used for finding the optimal locations for placing the same. In [9], an exhaustive binary search based algorithm is used to find the optimal locations of the power system. In this approach, the solution with maximum measurement redundancy is selected in case of multiple solutions. This method provides the global optimal solution in most cases which is one of its main advantages. Tabu search based methods for optimal PMU placement are proposed in [13, 14]. In [13], a novel topological method based augment incidence matrix and Tabu search is proposed. This combination helps in obtaining the solution of the combinatorial OPP problem with less computational complexity. Moreover, it improves the robustness of the method. Optimal PMU placement using Recursive Tabu Search (RTS) method is introduced in [14]. In this method, the traditional Tabu search (TS) algorithm is executed multiple times and the best solution from the previous run is used for initialization. Particle swarm optimization based methods for optimal PMU placement are proposed in [10, 15–17]. In [15], a BPSO based model for simultaneously minimizing the number of PMUs for complete observability along with maximization of measurement redundancy is proposed. Optimal PMU placement through a combination of graph theoretical procedure and BPSO is proposed in [10]. The graph-theoretic procedure is used to provide the initial PMU placement which will improve the computation time of the proposed algorithm. A graph-based method using the concept of depth of unobservability is used in [18] for optimal PMU placement. Genetic Algorithm based methods are proposed in [11, 12, 19, 20]. Optimal PMU placement using Immunity Genetic Algorithm (IGA) was proposed in [19]. It incorporates the immune operator in the traditional genetic algorithm thereby alleviating the degeneration phenomenon present in it. This helps the IGA to obtain a convergence faster than the traditional GA algorithm. Non-dominated Sorting Genetic Algorithm (NSGA) is used in [11] for simultaneously finding the optimal PMU locations along with maximizing the measurement redundancy. Since, both these objectives are conflicting in nature, the NSGA algorithm is programmed to find the best trade off solution. The algorithm is combined with the graph-theoretical procedure and a simple GA to reduce the initial number of the PMU's candidate locations. A Non-dominated Sorting Differential Evolution (NSDE) algorithm using a combination of Pareto non-dominated sorting operation and differential evolution algorithm is utilized for obtaining the optimal PMU placement set along with maximization of measurement redundancy in

[21]. But the main disadvantage is that the computation time of these methods is quite high for large practical systems. Moreover, it fails to provide the global optimal solution in many cases.

Deterministic approaches use optimization algorithms like Integer Linear Programming (ILP) and Integer Quadratic Programming (IQP) for optimal PMU placement. In [22], optimal PMU placement considering the critical contingencies occurring in the power system is carried out using Integer Linear Programming (ILP). The critical contingencies are selected based on a voltage stability based contingency screening method. Another ILP based model for optimal PMU placement under different cases of redundant PMU placement, full observability and incomplete observability is proposed in [23]. An ILP based approach for multi-stage optimal PMU placement is proposed in [24]. In this approach, the placement of PMU is carried out in phases. It also introduces two indices namely bus observability index and system observability redundancy index for calculating the measurement redundancy of the optimal PMU placement set. Optimal PMU placement with improved measurement redundancy is proposed in [25]. In this method, the dual objectives of minimizing the number of PMUs and improving redundancy are combined into a single objective function in these models. An integer quadratic programming based approach for simultaneously minimizing the total number of PMUs required, for complete system observability and maximizing measurement redundancy is proposed in [26, 27]. This algorithm can accommodate existing conventional measurements in the proposed PMU placement method. Moreover, it ensures complete observability of the system under normal operating conditions as well as under the outage of a single transmission line or a single PMU. However, the computation time required for IQP based methods is higher than that of ILP. A new optimal PMU placement problem formulation taking into account the effect of DC lines on network observability is considered in [28]. The effect of limited channel capacity is also discussed and an installation cost formula based on the number and type of measurement channels is also proposed. In [29], an integer programming model for optimal PMU placement considering the stochastic nature of components and their outage probabilities is proposed. The PMU placement problem is considered as a multistage problem and the average probability of observability is maximized in the initial planning stages in this model. Reference [30] proposes a model for improving the network observability by considering random component outages. Conventional bus injection and line flow measurements and the effect of zero-injection buses are considered in this model. A model for optimal placement of PMUs depending on the cost and benefit facets is presented in [31]. The benefits associated with the PMU based WAMS system is quantified through probabilistic analysis. The effect of malfunctioning of the monitoring and control infrastructures on power system reliability assessment is analyzed in [32].

In the aforementioned literature, it was assumed that a PMU placed on a bus can observe all its interconnected buses. However, in reality, the channel capacity of PMU is limited. Hence, some of the buses connected to the PMU placed bus may not be observable when the number of interconnections is higher than the total channel capacity of the PMU. This problem is taken into account in few works [33–40]. In [33], a Binary Integer Linear Programming (BILP) approach for optimally placing the PMU is proposed. The effect of limited channel capacity of PMU is incorporated into this model. Similar models using ILP was formulated in [34, 35]. Reference [37] proposed an integer programming model for studying the effect of limited channel capacity during normal operations and contingencies like single line outage and PMU outages. Apart from ILP, metaheuristic algorithm like GA has also been used to solve the limited channel capacity problem. In [38], a cellular genetic algorithm based model is used for solving the optimal PMU placement problem with limited channel capacity during normal operation and power system contingencies. The model in [39] uses a combination of ILP and genetic algorithm to optimize the PMU placement considering the number of analog channels. A four stepped algorithm based on GA for simultaneously minimizing the number of PMUs along with the number of channels is proposed in [40].

Once the PMU are optimally placed in the power system through either meta-heuristic or deterministic algorithms, it will transmit the measured data to the PDC. This data is used for various applications like state estimation, stability analysis, adaptive relaying etc. In this thesis, the author focusses on utilizing the PMU data for analysing the small signal stability of the power system.

1.4.2 Identification of Electromechanical Modes using PMU Data

After the introduction of Phasor Measurement Unit (PMU) and Wide Area Measurement System (WAMS), measurement-based methods are increasingly used for estimating the poorly damped modes in these low frequency oscillations. In this approach, the poorly damped modes are estimated from the measured data using digital signal processing techniques. The commonly used measured data are generator rotor angle velocity, transmission line power and interconnected bus voltages. Prony analysis [41–46] , ESPRIT[47–51], Stochastic subspace identification (SSI) [52–54], Wavelet Transform (CWT) [7, 55–57], Hilbert-Huang transform [58], ARMA [59], and Fast Fourier Transform (FFT) [60] are some of the commonly sought out signal processing techniques used for identifying the poorly damped modes. Among these techniques, Prony algorithm [41–46] is one of the oldest and widely used measurement technique for identifying the modal parameters of power system oscillations. Prony algorithm is essentially a curve fitting technique and can accurately estimate the frequency, damping factor, amplitude and phase angle of modes of power system oscillations under normal operating conditions. However, when the measured data is highly noisy, the accuracy of the Prony algorithm decreases substantially. Moreover, the estimated results of the Prony algorithm will have real and fictitious modes. In such cases, separate techniques are required for filtering the real modes in the estimated results from the fictitious modes. Advanced versions of Prony algorithm are proposed in [44, 45]. In [44], the proposed method applies the Prony method to multiple windows generated from the same signal. The true modes of the signal are estimated by comparing the estimated results of these windows and selecting the common modes present in the estimated results of these windows. Prony algorithm with a robust autocorrelation matrix is proposed in [45]. The robust covariance matrix is generated using minimum covariance determinant technique to mitigate the effect of bad data. It is observed that the noise resistance of the Prony algorithm is marginally improved in these new models but the issue is not fully solved.

Estimation of modal parameters of low-frequency modes in the power system through the ESPRIT method is proposed in [47–51, 61]. ESPRIT based algorithms provide accurate estimates of signal parameters even under highly noisy conditions. However, they need an accurate estimate of the model order or the number of frequency components present in the signal for its smooth operation. In [48], a total least square ESPRIT method is used for estimating the modal parameters of the power system oscillation. However, the model order estimation algorithm used is not accurate especially when the signal is highly noisy which may lead to non- identification of one or more modes in the signal. Identification of poorly damped modes in the power system using a combination of Total Least Square (TLS)-ESPRIT and fourth-order mixed mean cumulant is proposed in [61]. In this approach, the fourth order mixed mean cumulant is used to suppress the effect of Gaussian coloured noise and TLS-ESPRIT is used for identifying the poorly damped modes in power system oscillations. However, the usage of the former technique makes this algorithm computationally intensive.

Stochastic subspace identification based methods for estimating the parameters of the low-frequency oscillations are proposed in [52–54, 62]. These methods are a better option for analyzing ambient oscillations as they can handle large amounts of data and system dynamic changes. Moreover, they accurately estimate the closely spaced modes occurring in the power system. However, these methods have only limited noise resistance. The main issue while using the SSI based methods is the estimation of model order, which is used for separating the signal and noise subspace. Few works [52, 53] selected the model order based on the dominant singular values. In [52], the model order is estimated based on the large reduction in singular values of the weighted projection matrix. However, both these methods may not work properly when the noise content of the signal is high. A method based on the mean of singular values is proposed in [52] but it causes overestimation of model order resulting in the presence of trivial modes. Estimation of the model order based on stabilization diagram is proposed in [63] but the complexity of the algorithm limits its application. A combination of model based analysis and Numerical Algorithms for Subspace State Space System Identification (N4SID) is proposed in [62] for the identification of critical modes in a power system.

Wavelet-based methods for estimating the poorly damped modes of power system low-frequency oscillations is proposed in [7, 55–57]. They are based on multi-resolution analysis where wavelets of variable sizes are used to extract the modal information present in the signal. These methods are easy to implement and can extract modal information of non-stationary signals effectively. A Continuous Wavelet Transform (CWT) based method which uses a Morlet wavelet is proposed in [55]. It uses a linear regression based technique to estimate the frequency and damping of the modes from wavelet coefficients. In [7], a CWTFT (FFT based CWT approach) based method is used for the same purpose. However, it is noticed that the accuracy of the estimated results changes depending upon the mother wavelet chosen. The wavelet transform technique is also used for denoising the signal in [64] before feeding it to the modal estimation algorithm. However, it increases the computation time of these proposed techniques.

Identification of poorly damped modes in power system through Kalman filter and extended Kalman filter is proposed in [65–67]. In these works, the signal is used to generate the state space model whose states give an idea about the estimated parameters. After this process, an Extended Kalman filter is designed using the state space model to estimate the modal parameters of the signal. In [65], Hankel Singular value decomposition is integrated into the Kalman filter to improve its initialization values. In [66], stability analysis of the model is carried out after the modal parameter estimation to prove the convergence of the parameters. The main disadvantage of Kalman filter based model is that its performance degrades with increase in noise.

HHT, FFT and ARMA based algorithms for identifying the poorly damped modes in the power system are proposed in [58–60]. HHT based methods [58] use a combination of Empirical Mode Decomposition (EMD) and Hilbert's transform for estimating the modes in the low-frequency oscillations. However, this method is computationally intensive and the estimated results suffer from mode mixing problem. Low-frequency oscillation monitoring using FFT based algorithms are proposed in [60]. These algorithms are computationally less complex and less sensitive to noise. However, their accuracy is limited due to spectral leakage with a finite length of the signal. ARMA methods are used in [59] for estimating the modes of ambient data but these methods are very sensitive to noise. Signal decomposition algorithms like Cosine modulated filter banks [68] and Zolotarev polynomial based filter [69] are also used for identifying the low-frequency modes in the power system. These algorithms decompose the multi-component signal into monocomponent and the modal parameters of the monocomponent are estimated using parametric techniques like Eigen Realization algorithm. These algorithms effectively deal with non-stationary signals but their computational complexity limits its application. Moreover, the performance of these methods degrades when the signal has closely spaced modes. Analysis of abnormal oscillations in the power system using wide area measurement data is proposed in [70].

1.5 Motivation and objectives

Phasor Measurement Units are increasingly used in modern power systems for dynamic monitoring and control purposes. However, the high cost of PMU and its related equipment limits its installation at every bus in the system. Moreover, PMU placed at a bus observes itself and all its interconnected buses, provided it has sufficient channels. Therefore, the number of PMUs required to make the power system observable is always less than the total number of buses in that power system. Hence, optimal placement of PMUs ensuring complete observability is one of the major research problems in this area.

It is observed that a considerable amount of work is already done on this topic through metaheuristic and deterministic approaches. Metaheuristic algorithms use intelligent search techniques like Simulated Annealing, Binary Particle Swarm Optimization, Genetic Algorithm for finding the optimal PMU locations of the power system, whereas, deterministic approaches use optimization algorithms like Integer Linear Programming (ILP) and Integer Quadratic Programming (IQP) for this purpose. It is also observed that along with optimal PMU placement, other objectives like maximization of measurement redundancy is also introduced in few of these models. However, in most of these works, it is assumed that the PMU has enough channels to measure the voltage of the host bus and the current phasor of the interconnected buses. But, in reality, the channel capacity of PMU is limited. Therefore, PMU placed at a bus may not observe all its interconnected buses if the number of interconnections is higher than the total channel capacity of the PMU. Optimal PMU placement including this effect was proposed in few works but they used PMUs of fixed channel capacity for this purpose. Further, other objectives like maximization of measurement redundancy were also not included in the models which considered the optimal placement of PMUs including the effect of channel limits. However, the usage of PMUs of different channel capacities helps in reducing the total installation costs and maximization of measurement redundancy ensures that there are multiple measurements of the same quantity ensuring increased reliability. Therefore, it is important to have an optimal placement model utilizing PMUs of different channel capacity ensuring complete observability of the system along with maximum measurement redundancy.

Small signal stability of power systems is one of the major concerns of power system engineers as they are operated near their stability limit due to the increased load growth and deregulation. Conventionally, the small signal stability assessment is conducted through eigenvalue analysis and it involves the identification of poorly damped modes in the low frequency oscillations occurring in the power system. The low frequency oscillation in the power system can be broadly classified as ringdown and ambient oscillations. Ambient oscillations occur when there is a random small change in the load or generation, whereas, ringdown oscillations occur when there is a large magnitude disturbance like line tripping or generator tripping in the system. Conventionally, the poorly damped modes in these oscillations were identified through Eigenvalue analysis. The main disadvantage of this method is that its computational burden increases with an increase in the number of buses, hence this method is mainly used for the analysis of smaller systems. Due to this reason, after the introduction of PMU and WAMS, several signal processing based algorithms have been proposed for identifying the poorly damped modes in these oscillations.

It is observed from past works that parametric methods like Estimation of Signal Parameters using Rotational Invariance Technique (ESPRIT), Hankel's Total Least Square (HTLS) are a better choice for the analysis of ringdown oscillations. However, these algorithms require an accurate estimate of model order for its proper implementation. Overestimation of model order leads to the presence of fictitious modes, whereas, one or more true modes present in the signal will not be identified in case of under estimation of model order. Hence, it can be inferred that the ringdown oscillations can be better analysed if these parametric techniques are coupled with a good model order estimation algorithm.

Similarly, Stochastic Subspace Identification (SSI) based methods are a good choice for the analysis of ambient oscillations as it can handle a large amount of data with dynamic changes in the system. However, the performance of the SSI based algorithms deteriorates when the signal under consideration contain moderate to high noise content. Therefore, it is necessary to denoise the signal before passing into the SSI algorithm. Moreover, SSI being a parametric method requires an accurate model order estimate to prevent the occurrence of fictitious modes in its estimated results. Hence, an accurate model order algorithm is essential for avoiding the presence of fictitious modes in the estimated results of the SSI method.

It is noticed from the literature review on signal processing techniques used for small signal stability analysis that parametric methods are better at identifying the poorly damped modes in power system. However, these methods need an accurate estimate of model order for its proper implementation, which increases the computational complexity. However, if the mono components which are extracted from the signal is fed into the parametric techniques, then the estimation of model order is not required. This is an alternate way for identifying the poorly damped modes in the low frequency oscillations.

In view of the above findings, the major objectives of the thesis can thus be summarised below

- To develop a methodology for optimally placing the PMUs of different channel capacity in order to achieve complete observability along with maximization of measurement redundancy.

- To develop an efficient algorithm for analyzing the ringdown oscillations occurring in the power system and find the poorly damped modes accurately using synchrophasor measurements.

- To develop a method for accurate estimation of modal parameters of ambient oscillations using PMU data.

- To estimate poorly damped modes in low frequency oscillations using parametric methods without model order estimation.

1.6 Thesis organization

This thesis is organized into seven chapters. Chapter 1 discusses the SCADA based monitoring system, Phasor measurement unit and its applications. A detailed literature review on optimal placement of PMUs and identification of electromechanical modes using PMU data is also presented in this chapter along with the motivation behind this research work.

In chapter 2, a new redundant observability model for determining the optimal placement of PMUs with varying channel capacity is presented. In this model, the channel capacity of the PMU placed at a bus is determined by its interconnections. Thus, the placement of a higher channel capacity PMU at a bus with fewer interconnections will be avoided thereby reducing the number of channels required for complete system observability during normal operations and contingencies like single line outage and PMU outages. Further, the objective function is modified such that the measurement redundancy is maximized and the number of PMUs is minimized even when PMUs with varying channel capacity is used. Moreover, a new constraint is added to take care of the fact that a PMU placed at a bus measures the voltage phasor of that bus irrespective of its channel limits. The proposed model is tested on IEEE test systems and Northern Regional Power Grid (NRPG) 246 bus Indian system and the results are compared with that of the cost minimization model in terms of Total Installation Cost (TIC) and Channel Utilization Factor (CUF).

In chapter 3, a Hankel's Total Least Square (HTLS) based algorithm for estimating the low-frequency modes present in the power system oscillations is developed. This algorithm is mainly used for identifying the modal parameters of the ringdown oscillations. In this algorithm, the model order of the signal, which is a prerequisite for the proper implementation of the HTLS algorithm, is estimated through a Fast Fourier Transform (FFT) based technique. The fictitious modes present in the estimated results are filtered out by comparing the amplitude of the estimated modes as the amplitude of the true modes will be much higher than that of the fictitious modes. The HTLS based algorithm is compared with Fourier based and Prony based algorithms at different levels of noise contamination and sampling frequencies using synthetic signals and real-time signals from PMUs. The comparison reveals that the HTLS based algorithm is accurate and robust than the other two methods.

In chapter 4, an ESPRIT based algorithm is proposed for the estimation of modal parameters of the low-frequency modes in the power system. ESPRIT, being a parametric method, requires an accurate estimate of the model order for its successful implementation. This is obtained through the Exact Model Order (EMO) algorithm, which estimates the model order of even highly noisy signals accurately. The performance of the ESPRIT based algorithm is compared with a Modified Prony, ARMA and TLS ESPRIT based algorithm in the literature using real and synthetic signals.

In chapter 5, a Stochastic Subspace Identification (SSI) based algorithm for identifying the poorly damped modes is presented. SSI is also a parametric method which is mainly used for estimating the modal parameters of ambient oscillations. However, SSI based algorithms perform poorly while analyzing signals with high noise content. Due to this reason, the signal under consideration is filtered using a Stationary Wavelet Transform (SWT) based filter before passing it to the SSI algorithm. Moreover, EMO algorithm is used for the accurate estimation of the model order in the proposed SSI method so that the presence of fictitious modes in the estimated results is eliminated. The effectiveness of the proposed method is proved by comparing it with similar methods in the literature.

In chapter 6, an Empirical Wavelet Transform (EWT)- ESPRIT method for identifying the poorly damped modes of low frequency oscillations occurring in the power system is proposed. In this method, the EWT act as a wavelet filter and decomposes the multi-component signal into its mono component. The ESPRIT algorithm is then used to estimate the modal parameters of these mono components. Model order estimation, which is a prerequisite for the proper working of the ESPRIT algorithm, is not required for these mono-components as they have only one frequency component present in them. This is one of the main advantages of using the EWT algorithm along with ESPRIT. The proposed method is capable of accurately extracting the modal parameters of even highly noisy non-stationary signals. This is proven with the help of test signals and real-time signals obtained from an actual power system.

Finally, Chapter 7 concludes the main findings of the thesis and suggests few possible areas of research.

Chapter 2

Optimal placement of PMUs with varying channel capacity

2.1 Introduction

Accurate monitoring of states of the power system is essential for maintaining its reliability and security. Conventionally, monitoring is carried out using SCADA systems. However, the measurements obtained using SCADA based systems are time skewed and has low reporting rates. Therefore, the probability of error in bus voltage phasor estimates obtained from these measurements is quite high. Moreover, the dynamic properties of the power system cannot be accurately represented by SCADA based systems due to its low reporting rates. The introduction of PMUs solved both these issues as they provide synchronous measurements of voltage and current phasors across the power system at high reporting rates. However, the high installation cost of PMU and its associated equipment makes it infeasible and uneconomical to place it at every bus. Moreover, the PMU placed at a bus can observe all the interconnected buses provided it has enough measurement channels. Therefore, obtaining a PMU placement set such that the complete observability is attained with a minimum number of PMUs is one of the main research problems in this area.

Literature review on optimal placement of PMU shows that many algorithms based on meta-heuristic [8–12] and deterministic methods [24–27] have been proposed on this topic. Meta-heuristic algorithms use artificial intelligence techniques like Binary Particle Swarm Optimization (BPSO) [10], Genetic algorithm [11, 12] to find the optimal PMU locations whereas deterministic algorithms use Integer Linear Programming (ILP) [24, 25] and Integer Quadratic Programming (IQP) [26, 27] for the same purpose. Additional constraints such as the effect of zero injection bus [24], improvement of measurement redundancy [25], contingencies like PMU outage and line outages are also considered in many of the above works.

In all the above works, it is assumed that the PMU placed at a bus can monitor all its interconnected buses through its voltage and current channels irrespective of the number of interconnections. However, in reality, the number of measurement channels of the PMU is limited. Therefore, the incorporation of this constraint into the optimal placement problem is essential for improving its chances of application in real scenarios. Few works [33–40] have considered this effect on optimal placement. However, the usage of PMUs of different channel capacity is not considered in any of these works. Moreover, other objectives like maximization of measurement redundancy are not considered along with this constraint.

Keeping these facts in mind, a new redundant observability model for determining the optimal placement of PMUs with varying channel capacity is presented in this chapter. In this model, the channel capacity of the PMU placed at a bus is determined based on the number of interconnections it has with neighbouring buses. If the number of interconnections is less, a PMU with lesser channel capacity is installed there. On the other hand, a PMU with higher channel capacity is installed at a bus with more interconnections. Thus, the placement of a higher channel capacity PMU at a bus with fewer interconnections will be avoided thereby reducing the number of channels required for complete system observability during normal operations and contingencies like single line outage and PMU outages. Further, the objective function is modified such that the measurement redundancy is maximized and the number of PMUs is minimized even when PMUs with varying channel capacity is used. Moreover, a new constraint is added to take care of the fact that a PMU placed at a bus measures the voltage phasor of that bus irrespective of the channel limits. The proposed model is tested on IEEE test systems and Northern Regional Power Grid (NRPG) 246 bus Indian system and the results are compared using two parameters viz. Total Installation Cost (TIC) and Channel Utilization Factor (CUF).

2.2 Basic PMU Placement Problem

The placement of PMUs across the power system will make the host buses and their interconnections observable. If PMUs are placed at every bus in the power system, then the voltage phasors of every bus and the current phasors of every line in the power system can be easily estimated. However, the high cost of PMU and its associated equipment makes it impossible to place PMU at every bus in the power system. Therefore, PMU should be placed at particular locations in the power system such that the overall cost of PMU installation is minimized without affecting the complete observability of the power system. This can be mathematically represented as

$$Min \quad \sum_{i=1}^{N} c_i x_i \tag{2.1}$$

here, x_i is a binary variable for indicating the presence of a PMU at i^{th} bus. If the value of x_i is one, then the PMU is placed at the i^{th} bus, otherwise not [37]. c_i denotes the cost of PMU placed at the i^{th} bus and N represents the number of buses present in the power system. This objective function is optimized according to certain observability constraints. These constraints are developed based on the observability rules mentioned below [24].

(1) PMU placed on a bus can measure the voltage phasor of that bus and the current phasors emanating from it making the host bus directly observable and all the connected buses observable using Kirchhoff's voltage law.

(2) If voltage phasors of the two interconnected buses are known then current phasor of the connected branch can be calculated through Ohm's law.

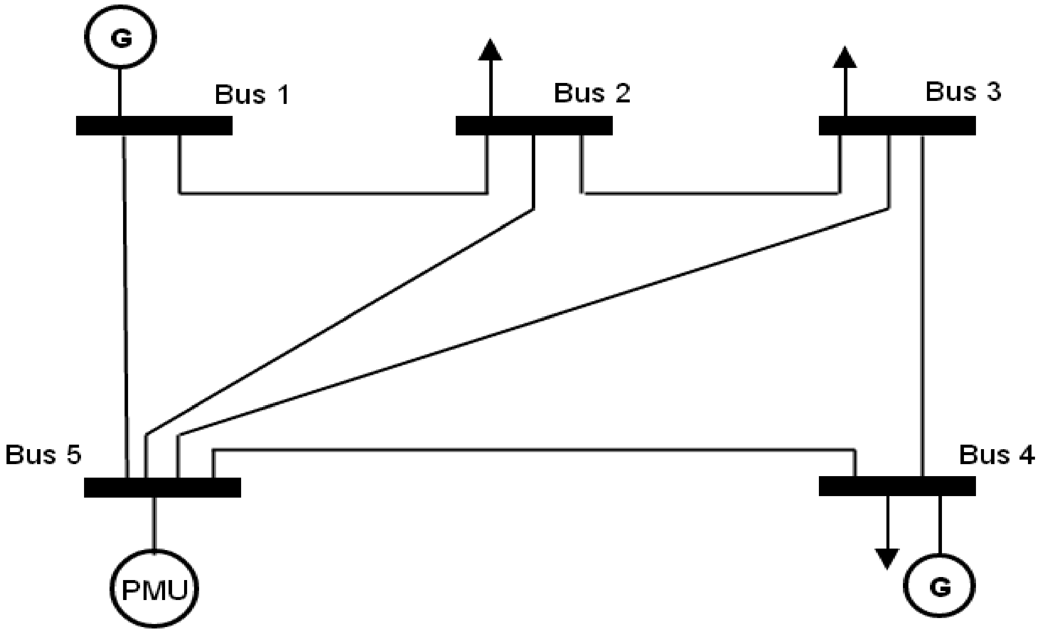

Figure 2.1: 5-bus system with PMU.

These rules are better explained with the 5-bus system shown in fig. 2.1. In this figure, it is noticed that the 5-bus system is made observable through the PMU placed at bus 5. The PMU through its voltage channel estimates the voltage phasor of the host bus i.e. bus 5. It also measures the current phasors flowing through the lines connecting buses 1-5, 2-5,3-5 and 4-5 through its current channels. The voltage phasors of buses 1,2,3 and 4 are then estimated from these current phasors using Kirchhoff's law. Once the voltage phasors of all the buses are calculated, the current flow in other lines is calculated through network equations [71].

For complete system observability, each bus should be observed at least once, which can be expressed mathematically as

$$\sum_{j=1}^{N} a_{ij}x_j \geq 1, \qquad \forall i \in I \tag{2.2}$$

where, a_{ij} is the binary connectivity parameter of buses i and j. It attains a value of one when the buses i and j are connected. I denote the set of buses in the power system.

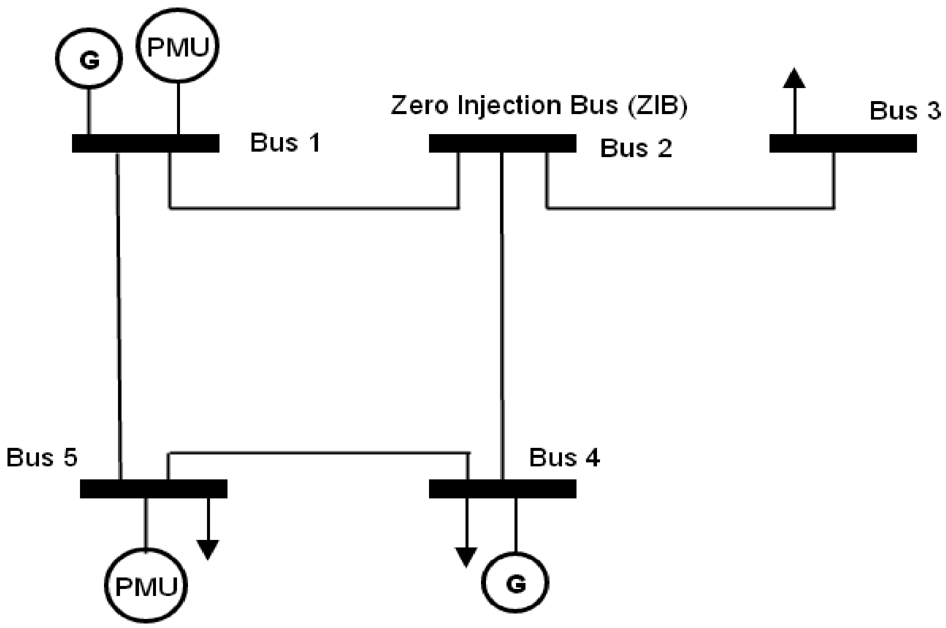

Figure 2.2: Zero injection effect - Rule 1.

There are some buses in the power system which are neither connected to any generators nor loads. These buses are used only for transferring the power from one point to another and are called zero injection buses. If zero injection buses are modelled in the observability constraints, then the total number of PMUs required for complete power system observability can be further decreased. They are modelled into the observability constraints subject to certain rules given below [71].

(1)When the buses incident to an observable zero injection bus, are all observable except

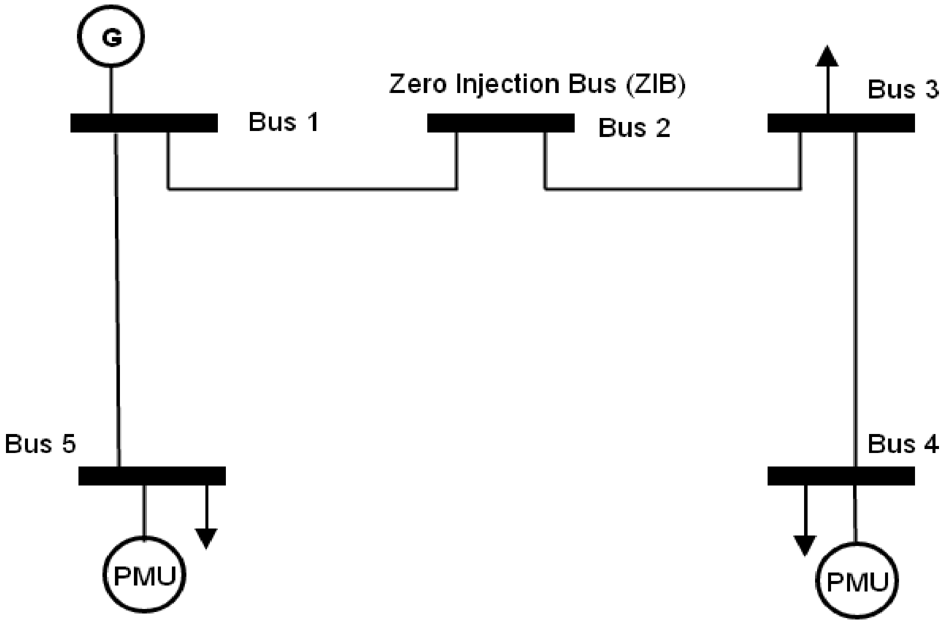

Figure 2.3: Zero injection effect - Rule 2.

one, then the unobservable bus is also identified as observable by applying KCL at the zero-injection bus. This rule is better explained with the help of fig. 2.2. In this figure, the zero injection bus (bus 2) is observed through the PMU placed on bus 1. All the buses connected to this zero injection bus are observable except bus 3. In such cases, according to this rule, bus 3 can be made observable by applying Kirchhoff's current law at bus 2.

(2)When all the buses incident to an unobservable zero injection bus are observable, then the zero-injection bus is also identified as observable by applying KCL at the incident node. For instance, bus 2 in fig. 2.3 is an unobserved zero injection bus. All the buses connected to bus 2 are observed through different PMUs placed in the system. Hence, according to this rule, the voltage phasor of the zero injection bus can be calculated through network equations.

These rules can be mathematically modelled as [71]

$$\sum_{j=1}^{N} a_{ij}x_j + \sum_{j \in ZIB} a_{ij}z_jy_{ij} \geq 1, \qquad \forall i \in I \tag{2.3}$$

$$\sum_{i=1}^{N} a_{ij}y_{ij} = z_j, \qquad \forall j \in ZIB \tag{2.4}$$

where, z_j and y_{ij} are binary variables used to include the zero injection effect into the observability constraints. If z_j is equal to one then the j^{th} bus is a zero injection bus, otherwise not. The value of y_{ij} indicates whether i^{th} bus is observed through the zero injection effect of bus j. If the value of y_{ij} is one, then it can be inferred that i^{th} bus is observed through the zero injection effect of bus j. ZIB denotes the set of zero injection buses in the system.

2.3 Proposed Formulation

It is noticed that while placing the PMUs, there may be more than one PMU placement set which gives complete observability of the power system using the same number of PMUs. The best placement set will be the one which can provide maximum measurements or the one with maximum measurement redundancy. For selecting the best placement set, a new criterion of maximizing measurement redundancy is added to the cost minimization making it a bi-objective optimization problem. Addition of this new objective will help in better utilization of the available channels of PMU. The modified objective function after including measurement redundancy is shown below.

$$\sum_{i=1}^{N} c_i x_i + \beta \sum_{i=1}^{N} (-f_i) \tag{2.5}$$

where,

$$f_i = \sum_{j=1}^{N} a_{ij} x_j, \qquad \forall i \in I \tag{2.6}$$

where, f_i is the observability constraint of the i^{th} bus which is developed based on the observability rules discussed in Section 2.2. The value of f_i indicates the number of times the bus is observed through different PMUs. Hence, the addition of f_i to the objective function will help in maximizing the number of times each bus in the power system is observed. However, the objective function is a minimization function. Therefore a negative sign is attached to f_i to convert the whole function into a minimization function. The parameter β is the normalization factor for the redundancy maximization function. If its value is low, then the measurement redundancy will not be properly maximized. On the other hand, if its value is high, then cost minimization part of the objective function will not work properly. Therefore, the value of β should be selected such that the cost minimization function is not affected. In [25], β is defined as the inverse of total times all the buses that can be ideally observed in a power system. But, for large practical systems, calculation of β using this equation will be tedious. Therefore, a new definition is proposed for β as shown in (2.7).

$$\beta = \frac{1}{N * C} \tag{2.7}$$

Here, C is the maximum number of connections of a bus in that system. Ideally, the value of β is always less than unity. The value of β derived through equation (2.7) is lesser than that of [25] which in turn helps in increasing the measurement redundancy of the system.

Phasor measurement units measure the voltage and current phasors using voltage and current channels. Voltage channels measure the voltage phasor of the bus at which it is placed whereas current channels measure line currents emanating from it [28]. In many of the previous works, it is assumed that the PMU has adequate number of measurement (voltage and current) channels. However, the number of channels of a PMU is limited and its number varies depending on the manufacturer. For instance, SEL and ABB are two famous PMU manufacturers. SEL 487E has 15 analog current channels for measuring five three-phase line current phasors whereas ABB RES521 has only six analog channels for measuring two three-phase line current phasors [34]. It is observed that, the maximum number of measurement channels in the PMU is usually not more than eight due to technical limitations and cost constraints [28].

Due to the limited number of channels, PMU placed at a bus cannot fully observe all the interconnected buses if the number of interconnections is higher than the number of current channels of the PMU. For instance, when a PMU having n current channels is placed on a bus which is connected to m other buses such that $m > n$, then $m - n$ buses will remain unobservable even though a PMU is placed at one of its interconnected buses. To overcome this problem, the observability constraints need to be modified to include the effects of channel limits. This is done by adding another binary variable to the observability constraint equation in (2.6) as shown below [71].

$$g_i = \sum_{j=1}^{N} a_{ij} w_{ij} x_j, \qquad \forall i \in I \tag{2.8}$$

The parameter w_{ij} denotes whether the bus i is observed using a PMU placed at bus j. The value of $w_{ij} = 1$ indicates that the PMU placed on j^{th} bus measures the current phasor between i^{th} and j^{th} buses using one of its current channels. The value of w_{ii} or $w_{jj} = 1$ indicates that the PMU placed on i^{th} bus measures the voltage phasors of the i^{th} bus using its voltage channel.

The modified objective function for improving the measurement redundancy along with cost minimization taking into account the limited channel capacity of PMU is

$$\sum_{i=1}^{N} c_i x_i + \beta \sum_{i=1}^{N} (-g_i) \tag{2.9}$$

The objective function mentioned above is optimized subject to the constraints formulated based on the observability rules explained in Section 2.2. However, the effect of zero injection bus is not modelled in these constraints. Since the effect of zero injection buses is independent of channel capacity of PMUs, this effect can be added into the constraints as in (2.3)-(2.4). The modified observability constraints can be written as

$$\sum_{j=1}^{N} a_{ij} w_{ij} x_j + \sum_{j \in ZIB} a_{ij} z_j y_{ij} \geq 1, \qquad \forall i \in I \tag{2.10}$$

$$\sum_{i=1}^{N} a_{ij} y_{ij} = z_j, \qquad \forall j \in ZIB \tag{2.11}$$

As explained earlier, the number of channels of the PMU is limited. Hence, the total number of measurements carried out by the PMU should be less than its total channel capacity. This is realized through the following constraint.

$$\sum_{i=1}^{N} a_{ij} w_{ij} \leq w_j^{max}, \qquad \forall j \in I \tag{2.12}$$

where, w_j^{max} is the channel capacity of the PMU placed at j^{th} bus [71].

The channel capacity of the PMU varies according to its manufacturer and cost. Generally, the higher the channel capacity of the PMU, the higher will be its total cost. Therefore, placement of a higher channel capacity PMU at a bus with lesser interconnection is uneconomical. However, usage of PMUs of different channel capacity is not considered in most of the works. Keeping this fact in mind, PMUs having varying channel capacities are used in this work. The channel capacity of the PMU at a particular bus is determined by the number of connections of the bus. To accommodate this, a new variable u_j, which represents the maximum observability of that bus is defined. It is determined by summing the j^{th} row of the binary connectivity matrix.

$$u_j = \sum_{i=1}^{N} a_{ij} \tag{2.13}$$

The value of u_j is compared with the channel capacities of the PMU available and the most appropriate channel capacity is selected for that particular bus. Thus the constraint

(2.12) is modified as given below.

$$\sum_{i=1}^{N} a_{ij}w_{ij} \leq \left\{ \begin{array}{ll} k1, & if \quad u_j \leq k1 \\ k2, & if \quad k1 < u_j \leq k2 \\ k3, & k2 < u_j \end{array} \right\}, \quad \forall j \in I \tag{2.14}$$

here, k1, k2 and k3 represents the channel capacities of PMU used in the system.

The buses connected to the PMU placed bus will be observed depending on the number of interconnections of the host bus and the number of measurement channels of the PMU. If the measurement channels of the PMU is higher than the interconnections, then all the interconnected buses will be observed. Otherwise, only a few of the buses will be observed. This is mathematically expressed in the following equation

$$w_{ij} \leq x_j, \qquad for\ i \neq j, \quad \forall i, j \in I \tag{2.15}$$

The PMU should measure the voltage phasor of the host bus using its voltage channel. This is realized through the following constraint. It is observed that this constraint is not implemented in [71]. The absence of this constraint causes the PMU placed bus to be observed through the current channel of some other PMU in the system. In such cases, the voltage channel of the host PMU is unutilized. The following constraint is formulated to prevent this situation [72].

$$w_{ij} = x_j, \qquad for\ i = j, \quad \forall i, j \in I \tag{2.16}$$

The objective function and the constraints used for optimal PMU placement with increased measurement redundancy using PMUs of varying channel capacities are summarized below.

$$Minimize \sum_{i=1}^{N} c_i x_i + \beta \sum_{i=1}^{N} (-g_i)$$

subject to

$$\sum_{j=1}^{N} a_{ij}w_{ij}x_j + \sum_{j=1}^{N} a_{ij}z_j y_{ij} \geq 1, \qquad \forall i \in I$$

$$\sum_{i=1}^{N} a_{ij}y_{ij} = z_j, \qquad \forall j \in ZIB$$

$$\sum_{i=1}^{N} a_{ij}w_{ij} \quad \leq \quad \left\{ \begin{array}{ll} k1, & if \quad u_j \leq k1 \\ k2, & if \quad k1 < u_j \leq k2 \\ k3, & k2 < u_j \end{array} \right\}, \quad \forall j \in I \tag{2.17}$$

$$w_{ij} \leq x_j, \qquad for\, i \neq j, \quad \forall i,j \in I$$

$$w_{ij} = x_j, \qquad for\, i = j, \quad \forall i,j \in I$$

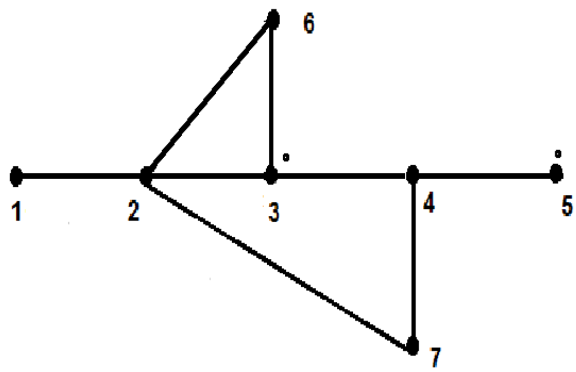

Figure 2.4: 7 bus system [73].

A flowchart of the proposed formulation using PMUs of varying channel capacities is shown in fig. 2.4. For better understanding, the proposed formulation is explained with the help of an example. Let us consider a 7-bus system having two zero injection buses 3 and 5 as shown in fig. 2.5. The objective function can be written as follows

$$Z = \sum_{i=1}^{7} X_i + \beta \sum_{i=1}^{7} (-g_i) \tag{2.18}$$

$$g_i = \sum_{j=1}^{7} a_{ij}w_{ij}x_j + \sum_{j \in 3,5} a_{ij}z_jy_{ij} \tag{2.19}$$

Here, g_i is the observability constraint of the i^{th} bus. The value of β is found to be 0.0357 using (2.7). The cost of the PMU is considered as 1 pu for simplicity. The observability constraints of the 7-bus system are given below.

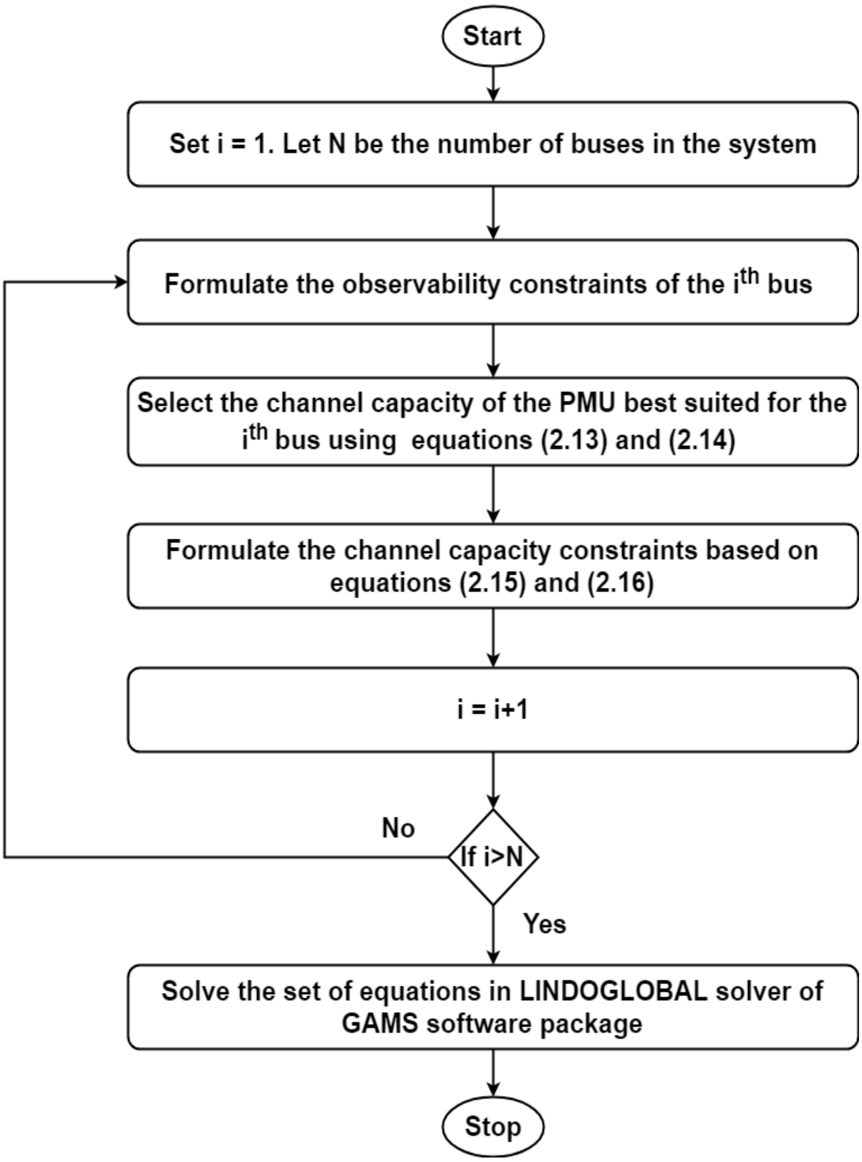

Figure 2.5: Flowchart of the proposed formulation.

$$
\begin{aligned}
& w_{11} * X_1 + w_{12} * X_2 \geq 1; \\
& w_{21} * X_1 + w_{22} * X_2 + w_{23} * X_3 + w_{26} * X_6 + w_{27} * X_7 + y_{23} \geq 1; \\
& w_{33} * X_3 + w_{32} * X_2 + w_{34} * X_4 + w_{36} * X_6 + y_{33} \geq 1; \\
& w_{44} * X_4 + w_{43} * X_3 + w_{45} * X_5 + w_{47} * X_7 + y_{43} + y_{45} \geq 1; \\
& w_{55} * X_5 + w_{54} * X_4 + y_{55} \geq 1; \\
& w_{66} * X_6 + w_{62} * X_2 + w_{63} * X_3 + y_{63} \geq 1; \\
& w_{77} * X_7 + w_{74} * X_4 + w_{72} * X_2 \geq 1; \\
& y_{23} + y_{33} + y_{43} + y_{63} = 1; \\
& y_{45} + y_{55} = 1;
\end{aligned}
\tag{2.20}
$$

In (2.20), the first seven equations represent the observability constraint of the seven buses in the system. The other two equations are used for representing the zero injection bus effect. The channel capacity of PMU placed at a particular bus is determined by (2.13) and (2.14). In this example, it is assumed that the channel capacities of PMU are 2 and 4 respectively. So $k1$ and $k2$ are set as 2 and 4 respectively. It is noticed from (2.20) that the maximum observability of all the buses except buses 1 and 5 is greater than 2. So these buses are suitable for the placement of PMU having $k2$ channels whereas PMU having $k1$ channels can be placed at buses 1 and 5. This is represented mathematically in (2.21)

$$\begin{aligned}
&w_{11}+w_{21}\leq 2;\\
&w_{12}+w_{22}+w_{32}+w_{62}+w_{72}\leq 4;\\
&w_{33}+w_{23}+w_{43}+w_{63}\leq 4;\\
&w_{44}+w_{34}+w_{54}+w_{74}\leq 4;\\
&w_{55}+w_{45}\leq 2;\\
&w_{66}+w_{26}+w_{36}\leq 4;\\
&w_{77}+w_{47}+w_{27}\leq 4;
\end{aligned}\tag{2.21}$$

In some cases, the PMU installed at a bus may not measure the voltage phasor of its own although it observes the other interconnected buses. For instance at bus 2, there may be a case when the value of w_{22} is 0 and all the other channels ($w_{12},w_{32},w_{62},w_{72}$) are 1. This means that the bus 2 is not self observed, which is contradictory to the principles of PMU placement. Moreover, the voltage channel of the PMU is remaining idle. The following set of equations are introduced to remove this limitation.

$$\begin{aligned}
&w_{11}=X_1;w_{22}=X_2;\\
&w_{33}=X_3;w_{44}=X_4;\\
&w_{55}=X_5;w_{66}=X_6;\\
&w_{77}=X_7;
\end{aligned}\tag{2.22}$$

The buses, which are connected to the PMU placed bus, will be observed depending on the channel capacity of the PMU. This is expressed in (2.23)

$$\begin{aligned}
&w_{21} \leq X_1; w_{12} \leq X_2;\\
&w_{32} \leq X_2; w_{62} \leq X_2; w_{72} \leq X_2;\\
&w_{23} \leq X_3; w_{43} \leq X_3; w_{63} \leq X_3;\\
&w_{34} \leq X_4; w_{54} \leq X_4; w_{74} \leq X_4;\\
&w_{45} \leq X_5;\\
&w_{26} \leq X_6; w_{36} \leq X_6;\\
&w_{47} \leq X_7; w_{27} \leq X_7;
\end{aligned} \tag{2.23}$$

The set of equations (2.18)-(2.23) are solved using LINDOGLOBAL solver in GAMS software package. The optimal PMU locations of the considered 7- bus system is found to be buses 2 and 3 when PMUs having channel capacities of 2 and 4 are used.

2.3.1 PMU Outage Scenario

The reliability of PMU and its associated equipment is quite high. However, in rare cases, it becomes faulty making one or more buses in the power system unobservable. To prevent this phenomenon, the observability of all the buses in the power system is increased from one to two. The reformulated constraints are [71]

$$g_i + \sum_{j=1}^{N} a_{ij} y_{ij} \geq 2, \qquad \forall i \in I \tag{2.24}$$

where g_i is the observability constraint of the i^{th} bus and the value of $a_{ij}y_{ij}$ denotes whether the i^{th} bus is observed through zero injection effect. If $\sum_{j=1}^{N} a_{ij}y_{ij} = 1$ then the i^{th} bus is observed through one of the zero injection buses connected to it. If i^{th} bus is not connected to any zero injection bus then $\sum_{j=1}^{N} a_{ij}y_{ij} = 0$.

2.3.2 Line Outage Scenario

Line outage in power system causes changes in the connectivity matrix. When a line connecting buses i and j is taken out, then the value of a_{ij} and a_{ji} in the connectivity matrix becomes zero making one or more buses unobservable. For making the system observable in this situation, new observability constraints which include the effect of line outage across line i-j should be formulated. They are formulated based on the following equations [71]

$$f_i^k \geq 1, \qquad \forall i \in I, \quad \forall k \in K \tag{2.25}$$

where

$$f_i^k = \sum_{j=1}^{N} a_{ij}^k w_{ij}^k x_j + \sum_{j \in ZIB}^{N} a_{ij}^k z_j y_{ij}^k, \quad \forall i \in I, \ \forall k \in K \tag{2.26}$$

$$\sum_{i=1}^{N} a_{ij}^k y_{ij}^k = z_j, \qquad \forall j \in ZIB, \ \forall k \in K \tag{2.27}$$

In the above equations, f_i^k is the post-contingency observability constraint of the i^{th} bus and K denotes the set of lines in a power system. Parameters a_{ij}^k and y_{ij}^k are the post-contingency values of a_{ij} and y_{ij}. If the line connecting buses i and j is taken out, then the values of both a_{ij}^k and y_{ij}^k will be 0.

2.4 Simulation Results and Discussion

The effectiveness of the proposed method in finding the optimal PMU locations during normal operating conditions and contingencies like single line outage and PMU outage is tested on different IEEE test systems viz. IEEE 14-bus, 30-bus, 57-bus, 118-bus systems and a Northern Regional Power Grid (NRPG) 246-bus Indian system [22, 74]. The required details about these test systems are given in Table 2.1. In these simulations, two different sets of PMUs having varying channel capacities are used. The channel capacities of the PMUs used in these sets are given below.

Set A - consists of PMUs with channel capacities of two, four and six.

Set B - consists of PMUs with channel capacities of three, five and seven.

Table 2.1: Test Systems

Test System	**Zero injection buses**	**Line outage considered**
IEEE 14 bus	7	1-2
IEEE 30 bus	6,9,22,25,27,28	10-17
IEEE 57 bus	4,7,11,21,22,24,26,34,36,37,39,40,45,46,48	41-42
IEEE 118 bus	5,9,30,37,38,63,64,68,71,81	101-102
NRPG 246 bus	54,56,59,61,62,63,69,70,71,72,73,74,75,80,81,86,102,103,104,107,122,126,129, 131,147,154,155,167,175,179,180,183,209,210,211,212,213,214,215,216,217, 221,222, 226,229,230,231,232,233,234,236,237,238,239,240,241,243,244	49-50

It is observed that the observability constraints of the PMU placement problem are non-linear in nature. Hence, the proposed model is solved through Mixed Integer Quadratic Constrained Programming (MIQCP) method in the GAMS software package as linear programming methods cannot effectively handle the non-linearity of the constraints. Prior to running the simulations, the relative stopping tolerance and absolute stopping tolerance of the LINDOGLOBAL solver in the GAMS are set to zero for obtaining the global optimal solution. The maximum iteration limit and tolerance for the gradient of non-linear functions of the solver is set as 40000 and $1e^{-7}$ respectively. Moreover, the maximum simulation time is set to 1000 seconds.

The advantages of using PMUs having varying channel capacities is proved by comparing the results of the simulations with the results when PMUs of fixed channel capacity are employed. In this comparison, the results obtained while using PMUs of set A are compared with that of PMUs having channel capacity of six. Similarly, results of set B are compared with that of PMUs having a channel capacity of seven. Two new parameters i.e. Channel Utilization Factor (CUF) and Total Installation Cost (TIC) are introduced for a fair comparison process. CUF is the ratio of Total Direct Observations (TDO) made by the set of PMUs to the Total number of PMU Channels (TPC) present in the system. As the value of TPC decreases, the CUF increases, which indicates that fewer channels are remaining idle.

$$CUF = \frac{TDO}{TPC} \tag{2.28}$$

Table 2.2: Fixed and variable charges of PMU [28]

Component	**Cost** ($)
PMU (Fixed Cost)	20k
Voltage channel	3k
Current channel	3k

TIC is the sum of the installation cost of all the PMUs in the system. Installation Cost (IC) of a PMU is broadly divided into fixed and variable costs. Fixed Costs (FC) includes the cost of the PMU panel and other associated equipment, Global Positioning System (GPS) installation etc whereas Variable Costs (VC) includes the cost of voltage and current channels[28].

$$IC_i = FC_i + VC_i \tag{2.29}$$

$$VC_i = (n_1 * CV_i + n_2 * CC_i) \tag{2.30}$$

$$TIC_i = \sum_{i \in PMUL} IC_i \tag{2.31}$$

Here, PMUL represents the set of PMU locations in the system. CV and CC denotes the cost of voltage channels and current channels respectively. n_1 and n_2 gives the number of voltage and current channels in the given PMU. The details about fixed cost, cost of voltage and current channels of a PMU are obtained from [28] and is shown in Table 2.2.

Table 2.3: TIC and CUF of the proposed model with PMUs of fixed and varying channel capacity during normal operation

Test System	No of PMUs for optimal placement with					No of channels needed		TIC of PMUs with ($)		CUF of PMUs with	
	FC	VC				FC	VC	FC	VC	FC	VC
		Two	Four	Six	Total						
					Set A						
IEEE 14 bus	3	0	1	2	3	18	16	114k	108k	0.833	0.9375
IEEE 30 bus	7	0	1	6	7	42	40	266k	260k	0.833	0.875
IEEE 57 bus	11	0	6	5	11	66	54	418k	382k	0.7121	0.8703
IEEE 118 bus	28	0	11	17	28	168	146	1064k	998k	0.8154	0 .9383
NRPG 246 bus	53	1	12	40	53	318	290	2014k	1930k	0.8551	0.9379
					Set B						
		Three	Five	Seven	Total						
IEEE 14 bus	3	0	3	0	3	21	15	123k	105k	0.7142	1
IEEE 30 bus	7	1	4	2	7	49	37	287k	251k	0.7346	0.9729
IEEE 57 bus	11	4	5	2	11	77	51	451k	373k	0.6233	0.9411
IEEE 118 bus	28	6	10	12	28	196	152	1148k	1016k	0.7193	0.9276
NRPG 246 bus	53	6	22	25	53	371	303	2173k	1969k	0.7574	0.9339

* FC: Fixed Channels
VC: Varying Channels

Table 2.3 compares the usage of PMUs of fixed and varying channel capacities for optimal placement during normal operation in terms of CUF and TIC. It is noticed that while using PMUs of varying channel capacity for optimal placement, the number of channels required for complete system observability is comparatively lesser than that when PMU of fixed channel capacity is used. For instance, 168 channels are required to fully observe the IEEE 118 bus system when PMUs with fixed channel capacity of six are used. However, the same system can be fully observed using just 146 channels when PMUs belonging to set A is used. Hence, there is a reduction of 22 channels when the PMUs of varying channel capacities are used for complete observability. This reduction in the number of channels causes an improvement in the CUF and reduction of TIC. It is observed that usage of PMUs of varying channel capacity for optimal placement in the IEEE 118 bus system reduces its TIC and improves the CUF of the system by 6.20% and 12% respectively.

Table 2.4: TIC and CUF of the proposed model with PMUs of fixed and varying channel capacity during single line outage

Test System	No of PMUs for optimal placement with					No of channels needed		TIC of PMUs with ($)		CUF of PMUs with	
	FC	VC				FC	VC	FC	VC	FC	VC
		Two	Four	Six	Total						
Set A											
IEEE 14 bus	4	0	0	4	4	24	24	152k	152k	.875	.875
IEEE 30 bus	8	0	2	6	8	48	44	304k	292k	.79166	.8636
IEEE 57 bus	11	0	6	5	11	66	54	418k	382k	.7121	.8703
IEEE 118 bus	29	0	8	21	29	174	158	1102k	1054k	.8505	.9367
NRPG 246 bus	54	1	12	41	54	324	296	2052k	1968k	.8611	.9425
Set B											
		Three	Five	Seven	Total						
IEEE 14 bus	4	0	3	1	4	28	22	164k	146k	.75	.9545
IEEE 30 bus	8	2	4	2	8	56	40	328k	280k	.6964	.975
IEEE 57 bus	11	4	5	2	11	77	51	451k	373k	.6233	.9411
IEEE 118 bus	29	5	9	15	29	203	165	1189k	1075k	.8177	.9454
NRPG 246 bus	54	4	23	27	54	378	316	2214k	2028k	.7698	.9208

Tables 2.4 and 2.5 compare the usage of PMUs of fixed and varying channel capacities during single line outage and PMU outage respectively in terms of CUF and TIC. It is ob-

Table 2.5: TIC and CUF of the proposed model with PMUs of fixed and varying channel capacity during PMU outage

Test System	No of PMUs for optimal placement with					No of channels needed		TIC of PMUs with ($)		CUF of PMUs with	
	FC	VC				FC	VC	FC	VC	FC	VC
		Two	Four	Six	Total						
Set A											
IEEE 14 bus	7	0	3	5	8	42	42	266k	286k	.7857	.8809
IEEE 30 bus	15	1	11	4	16	90	70	570k	530k	.622	.8571
IEEE 57 bus	26	1	18	8	27	156	122	988k	906k	.666	.8606
IEEE 118 bus	63	4	29	31	64	378	310	2394k	2210k	.7026	.896
NRPG 246 bus	125	20	49	57	126	750	578	4750k	4254k	.732	.9117
Set B											
		Three	Five	Seven	Total						
IEEE 14 bus	7	1	6	1	8	49	40	287k	280k	.6734	.9250
IEEE 30 bus	15	9	5	2	16	105	66	615k	518k	.5428	.9242
IEEE 57 bus	26	13	11	3	27	162	115	1006k	885k	.6481	.9217
IEEE 118 bus	63	24	21	19	64	441	310	2583k	2210k	.6485	.9137
NRPG 246 bus	125	46	49	31	126	875	600	5125k	4320k	.6171	.8983

served that, during single line outages, the proposed method gave better CUF and lesser TIC when PMUs of varying channel capacity were used for optimal placement irrespective of the test system under consideration. It is also observed that during single line outages, the number of measurement channels required for complete system observability is usually higher than that of normal operating conditions. This happens due to the usage of extra PMU for complete system observability during single line outages. Hence, CUF of the proposed model during single line outages is lesser than that of normal operating conditions irrespective of the type of PMU (fixed channel capacity or varying channel capacity) used.

From Table 2.5, it can be observed that the proposed model with PMUs of varying channel capacities needs an extra PMU as compared to that with fixed channel capacities for maintaining complete observability during PMU outages. However, extra channels are required if PMUs with fixed channel capacities are used. Therefore, both cases are compared using TIC. It is noticed that, except for the IEEE 14 bus system, the TIC of the proposed model with PMUs of varying channel capacity is lesser than that with fixed channel capacities. The savings in the TIC increases with the system size. It is highest for NRPG 246 bus system where the TIC with varying channel capacities is almost 10.4% less than that of with fixed channels.

Table 2.6: Optimal PMU locations of the proposed model using PMUs belonging to set A and B

System	Optimal PMU locations common for set A and set B	Set A	Set B
	Normal operation		
IEEE 14 bus	2,6,9		
IEEE 30 bus	2,4,10,12,15,27	20	19
IEEE 57 bus	1,4,13,20,25,29,32,38,51,54,56		
IEEE 118 bus	3,8,11,12,17,21,27,31,32,34,37,40,45,49,52,56,62,72,75,77,80,85,86, 91,94,105,110	101	102
IEEE 246 bus	6,11,15,21,24,27,29,34,40,44,48,49,56,65,66,70,82,83,88,89,91,96,97,106, 109,117,121,125,129,132,134, 140,141,142,157,158,160,165,166, 168, 181,185,187,190,191,194,199,202,203,219,235,245	128	183
	Line outage		
IEEE 14 bus	4,5,6,9		
IEEE 30 bus	2,4,10,12,15,17,20,27		
IEEE 57 bus	1,4,13,20,25,29,32,38,51,54,56		
IEEE 118 bus	3,8,11,12,17,21,27,31,32,34,37,40,45,49,52,56,62,72,75,77,80,85,86,89, 92,96,100,105,110		
IEEE 246 bus	6,11,15,21,24,27,29,34,40,44,48,54,55,56,65,66,70,82,83,88,89,91,96,97,106, 109,117,121,125,128,129,132,134,140,141,142,157,158,160,165,166,168,181, 185,187,190,191,194,199,202,203,219,235,245		
	PMU outage		
IEEE 14 bus	2,4,5,6,7,9,10,13		
IEEE 30 bus	1,3,5,7,9,10,12,13,15,17,19,20,24,25,27,30		
IEEE 57 bus	1,2,4,6,9,12,14,19,20,24,25,27,29,30,32,33,36,37,38,41,47,50,51,53,54,56	44	45
IEEE 118 bus	1,3,5,6,8,9,12,15,17,19,21,22,25,27,29,31,32,34,37,40,42,45,46,49,51,54,56, 57,59,61,62 ,66,68,70,71,72,75,77,79,80,83,85,86,87,89,91,92,94,96,100, 101,105,106,109,110,111,112,115,117	11,35,43, 52,76	13,36,44, 53,118
IEEE 246 bus	2,5,6,7,9,10,11,14,15,21,23,24,27,29,30,31,33,34,35,38,40,41,42,43, 44,47,48,50,54,55,56,57,61,62,63,64,65,66,70,74,75,77,80,82,83, 84,88,89,91,92,96, 97,100,101,105,106,109,111,113,118,119,121, 122,123,124,125,126,128,132,133,134,135,138,139,140,141,143, 145,147,149,152,156,157,158,159,160,163,165,166,168,169,172, 176,178,181,182,185,186,187,189,190,191,193,194,195,196,197, 199,201,202,203,205,207,208,216,219,223,224,234,235,243,245	103,108 148,174	68,85 146,173

Tables 2.6 shows the optimal PMU locations obtained with the proposed model using

PMUs of set A and set B respectively. The second column shows the optimal PMU locations common to set A and set B. The third and fourth columns show the optimal PMU locations obtained only in set A and set B, respectively. Thus, the total PMU locations obtained in set A is the locations given in second and third columns, while that in set B is the locations given in second and fourth columns. It is observed that for a particular test system, most of the optimal locations obtained are common to both the sets.

From Tables 2.3-2.5, it can be inferred that the proposed model can optimally place PMUs of varying channel capacity across the power system to make it completely observable during normal operation as well as contingencies like single line outage and PMU outages. The comparison of the proposed model using PMUs of fixed and varying channels reveals that usage of PMUs with varying channels improves the CUF and reduces the TIC. Apart from the usage of PMUs with varying channels, the proposed formulation also ensures increased measurement redundancy along with complete observability of the power system. The superiority of this formulation is proved by comparing it with the cost minimization model under similar operating conditions. The comparison is done in terms of System Observability Redundancy Index (SORI). The SORI of the test system for a particular channel capacity is the sum of the total number of direct and indirect observations made using the given set of PMUs. The indirect observations are made through zero injection effect. PMUs belonging to set A and B are only used in these models.

Table 2.7 shows the comparison of the number of PMUs for complete observability and the SORIs obtained with the proposed model against the cost minimization model under normal operating conditions as well as contingencies. It is noticed that irrespective of the operating condition, both the cost minimization model and the proposed model attain complete observability with the same number of PMUs. However, it is also noticed that the measurement redundancy of the proposed model is higher than that of the cost minimization model for all test systems. The difference in measurement redundancy of these two models is negligible for smaller systems. However, there is a considerable difference in the SORI for large practical systems. This is evident from the comparison of SORIs of NRPG system. It is observed that the measurement redundancy of the proposed model is around 10.36% higher than that of the cost minimization model while using PMUs of set A. It is also noted that the proposed model gives better measurement redundancy with PMUs of set B than set A due to the presence of additional channels in set B.

Table 2.7: Comparison of SORI of the proposed model against the cost minimization model

Test System	Set A				Set B			
	Cost Minimization Model		**Proposed Model**		**Cost Minimization Model**		**Proposed Model**	
	No. of PMUs	**SORI**	**No. of PMUs**	**SORI**	**No. of PMUs**	**SORI**	**No. of PMUs**	**SORI**
Normal operation								
IEEE 14 bus	3	16	3	16	3	16	3	16
IEEE 30 bus	7	35	7	41	7	37	7	42
IEEE 57 bus	11	61	11	62	11	63	11	63
IEEE 118 bus	28	137	28	147	28	143	28	151
NRPG 246 bus	53	299	53	330	53	311	53	341
Line outage								
IEEE 14 bus	4	19	4	22	4	19	4	22
IEEE 30 bus	8	37	8	44	8	36	8	45
IEEE 57 bus	11	61	11	62	11	63	11	63
IEEE 118 bus	29	150	29	158	29	153	29	165
NRPG 246 bus	54	298	54	337	54	315	54	349
PMU outage								
IEEE 14 bus	8	38	8	38	8	38	8	38
IEEE 30 bus	16	65	16	66	16	67	16	67
IEEE 57 bus	27	119	27	120	27	119	27	121
IEEE 118 bus	64	270	64	288	64	281	64	296
NRPG 246 bus	126	558	126	585	126	595	126	597

The effectiveness of the proposed model is further validated by comparing with existing models in Table 2.8. The proposed model uses PMUs belonging to set A and B whereas similar models in [33, 38, 71, 75, 76] uses PMUs having a fixed channel capacity of six for this comparison. It is noticed that the above mentioned works [33, 38, 71, 75, 76] have considered only cost minimization as their main objective function. Therefore, the objective function is modified such that the measurement redundancy maximization function is removed from the proposed model and the performance comparison is done in terms of optimal PMUs required for complete observability and TIC. It is evident from Table 2.8 that usage of PMUs with varying channels reduces the TIC of the proposed model in comparison to the models in [33, 38, 71, 75, 76] even though all these models use the same number of PMUs for obtaining complete observability. For instance, the TIC of the IEEE 57 bus system using the proposed model is 8.6% lesser than that of the model in [38]. So it can be inferred that the proposed model is more economical than the models in [33],[71],[38],[75] and [76].

Table 2.8: Comparison of the proposed model with other existing models

Model		IEEE 14 bus		IEEE 30 bus		IEEE 57 bus		IEEE 118 bus	
		No. of PMUs	TIC ($)	No. of PMUs	TIC ($)	No. of PMU	TIC ($)	No. of PMUs	TIC ($)
PM	Set A	3	108k	7	242k	11	382k	28	992k
	Set B	3	105k	7	239k	11	379k	28	1004k
Binary Integer Programming [33]		3	114k	7	266k	12	456k	28	1064k
Integer Linear Programming [71]		3	114k	7	266k	11	418k	28	1064k
Cellular Genetic Algorithm [38]		3	114k	7	266k	11	418k	29	1102k
Binary Integer Programming [75]		3	114k	7	266k	12	456k	28	1064k
Cellular Genetic Algorithm [76]		3	114k	7	266k	12	456k	28	1064k

⋆ PM: Proposed Model

2.5 Conclusion

A redundant observability model for optimally placing the PMUs of varying channel capacities is proposed in this chapter. In this model, the channel capacity of the PMU placed at a bus is determined by its number of interconnections. The observability constraints of this model are non-linear in nature. Hence, it is solved using Mixed Integer Quadratic Constrained Programming. The superiority of using PMUS of varying channel capacity is proved by comparing its performance with that of PMU with fixed channel capacity under normal operating conditions as well as contingencies like single line outage and PMU outages. The redundant observability formulation of the proposed model is tested by comparing it with cost minimization model using PMUs with varying channels. Results reveal that the proposed model provides better measurement redundancy than the cost minimization model using the same number of PMUs for complete system observability.

Chapter 3

Hankel's Total Least Square based algorithm for analyzing ringdown oscillations

3.1 Introduction

The identification of poorly damped oscillatory modes occurring in power system is critical for maintaining its small signal stability. Depending on the range of frequencies, these modes can be classified as inter-area (0.05 - 0.3 Hz), intra area (0.4 - 1.0 Hz), intra plant (1.5 - 3.0 Hz) and inter plant (1.0 - 2.0 Hz) respectively. If these poorly damped modes are not monitored, it may cause cascaded tripping in the power system leading to blackouts. Therefore, early identification of these modes is essential to prevent such unfortunate incidents [77].

Poorly damped modes in power system oscillations are determined through eigenvalue based and measurement based approaches. In the eigenvalue-based method, the power system is linearized around its operating point to generate the state space equations. The eigenvalues of the power system are calculated from these equations. The modal parameters of the oscillations are extracted from these eigenvalues. The main disadvantage of this method is that its computational burden increases with an increase in the number of buses, hence this method cannot be used for large practical power systems. Measurement-based methods extract the modal parameters of the power system oscillations using digital signal processing techniques. Power system signals like active power variation, frequency variation is used as the input for these measurement based methods. With the advent of PMU and Wide Area

Measurement System (WAMS), measurement-based methods utilizing Fast Fourier Transform (FFT) [78], Wavelet transform [7, 55, 56], Prony algorithm [41–45, 79], Estimation of Signal Parameters using Rotational Invariance Technique (ESPRIT) [48, 50], Matrix Pencil method [80], Stochastic Subspace Identification (SSI) [52] are increasingly used for identifying the poorly damped modes in power system oscillations.

Among these methods, FFT based methods are simple and easy to implement but they cannot detect closely spaced modes, which is one of their main drawbacks. Moreover, the damping coefficient of the modes cannot be estimated directly in this method. Wavelet transform based methods are proposed in [7, 55, 56]. These methods can analyse non-stationary signals efficiently compared to other methods. However, their accuracy is dependent on the type of wavelet used for analysis. Prony algorithm [41–43, 79] based methods are one of the oldest measurement techniques used for estimating the parameters of low-frequency oscillation. However, it performs poorly under high levels of noise. Improved versions of the Prony algorithm are proposed in [44, 45] but the above limitations are not fully solved. Parametric methods like ESPRIT [48, 50], Matrix Pencil [80], SSI [52, 53], Hankels Total Least Square method (HTLS) [81] are also used to find the dominant modes present in the low frequency oscillations. These methods normally provide better estimates of modal parameters than the Prony algorithm and perform well even under high levels of noise contamination. However, parametric methods need an accurate estimate of the model order or the number of modes present in the signal for its successful performance. In [48], the ESPRIT based method uses a technique based on the ratio of eigenvalues of the autocorrelation matrix developed from the signal data to estimate the number of modes present in the signal. Although this method is simple, the model order is either underestimated or overestimated in cases where the signal has closely spaced modes. In [52], the initial model order is estimated using a technique based on the average of singular values of the Hankel matrix developed from signal data and subsequently, the SSI based method is used to compute the modes.

From the above literature, it can be concluded that a parametric method combined with an efficient model order algorithm can accurately identify the poorly damped modes. However, if the model order is not accurately estimated, it will lead to the presence of fictitious modes or non-identification of real modes present in the signal. When the model order is overestimated, it leads to the presence of fictitious modes in the estimated results whereas real modes present in the signal are not identified in case of underestimation of model order. Therefore,

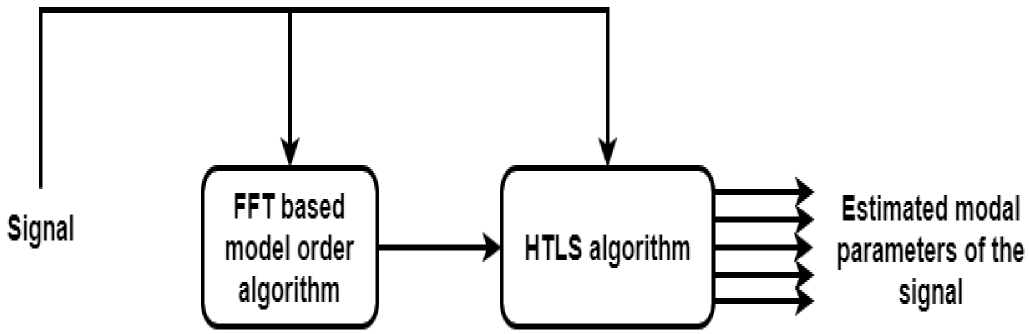

Figure 3.1: Block diagram of the proposed method.

accurately estimating the model order of the signal is essential for identifying the real modes present in the signal. Conventional model order algorithms like Akaike Information Criterion (AIC) [82] can estimate the model order but the computational burden associated with them is very high. However, a near accurate estimate of the model order of the same signal can be obtained through simpler techniques like FFT.

Therefore, this chapter proposes an HTLS based algorithm for identifying the low-frequency oscillation modes occurring in the power system in which an FFT based technique is used for model order estimation. In this technique, the number of peaks in the FFT plot of the signal represents a near accurate estimate of the model order. This estimate is slightly incremented and is fed into the HTLS algorithm. The incrementing is done to make model order estimate higher than its actual value so that all the modes present in the signal is identified. The drawback of this incrementing operation is that fictitious modes will be present in the estimated results. The true modes of the signal are separated from these fictitious modes by comparing their amplitudes as the amplitude of the true modes will be much higher compared to the fictitious modes. The proposed algorithm is compared with Fourier based and Prony based algorithms at different levels of noise contamination and sampling frequencies using synthetic signal and real-time signals from PMUs. Results reveal that the proposed method provides accurate estimates of modal parameters of low-frequency oscillations even in the presence of noise and low PMU reporting rates.

3.2 Proposed Methodology

The proposed method utilizes an HTLS based algorithm for finding the modal parameters of low frequency oscillations. The block diagram of the proposed method is shown in fig. 3.1. In this method, the signal is split into a sum of exponentially decaying sinusoids. It can be mathematically represented as

$$x(t) = \sum_{i=1}^{K} A_i e^{-\sigma_i t} \cos(2\pi * f_i t + \phi_i) + s_t \tag{3.1}$$

Here, $x(t)$ is the signal under consideration. It is split into K exponentially damped sinusoids having a frequency of f_i and phase of ϕ_i. A_i is the amplitude of the mode i and σ_i is its attenuation factor. s_t is the noise present in the signal. In case of power systems, $x(t)$ is obtained from the PMUs present in the power system. The HTLS algorithm being a parametric method requires an accurate estimate of the model order or the number of frequency components present in the system for its proper implementation. The FFT based model order algorithm used in the proposed method is explained in the next subsection.

3.2.1 Determination of Initial Model Order

Model order estimation is the process of accurately estimating the number of frequency components or modes present in the signal. A Fourier based algorithm for estimating the model order is used in the proposed method. This technique is easy to implement and the computational complexity associated with it is quite low unlike AIC. The main steps of this algorithm are given below.

Step 1: Obtain the FFT of the signal and plot the same.

Step 2: Find the highest peak in the FFT plot.

Step 3: Calculate the number of peaks, which has at least 10% amplitude of the highest peak. This value is set as the initial model order of the signal. The amplitude cutoff is used to exclude the peaks corresponding to the noise present in the signal as their amplitudes will be much lesser than that of the modes present in the signal.

This technique estimates the model order of the signal accurately in most cases. However, precise estimation of the model order is practically not possible when the signal is highly noisy or when the energy of one or more modes of the signal is very low. In such cases, the model order is underestimated causing non identification of one or more modes in the system. To prevent this phenomenon, the initial model order estimated is incremented by a small number before sending it to the HTLS algorithm for separating the dominant singular values. The increased model order will help in identifying all the modes present in the signal. However, in some cases, the estimated model order is higher than the actual value after the increment operation leading to fictitious modes in the estimated results. In such cases, the real modes present in the signal are identified from these fictitious modes by comparing the amplitude of modes as the amplitude of these fictitious modes will be very low when compared to the real modes.

3.2.2 HTLS Algorithm

The main steps for estimating the modal parameters of the low-frequency oscillation using the HTLS algorithm are as follows [81, 83].

1. Generate the Hankel matrix H from the given signal data.

$$\mathbf{H} = \begin{bmatrix} x(0) & x(1) & x(2) & .... & x(M-1) \\ x(1) & x(2) & x(3) & .... & x(M) \\ .. & .. & x(3) & & .. \\ x(L-1) & .. & .. & .. & x(N-1) \end{bmatrix}$$

Here, $x(0)$, $x(1)$ .... $x(N-1)$ represent the signal data. $x(0)$ and $x(N-1)$ are the first and last samples of the signal. N and M represent the length of the signal and the order of the Hankel matrix respectively.

2. Calculate the Singular Value Decomposition (SVD) of H and obtain its singular values.

$$\mathbf{H} = \mathbf{USV^t} \tag{3.2}$$

Here, $\mathbf{U}$ and $\mathbf{V}$ are the left and right singular vectors. The singular values of the Hankel matrix are present in $\mathbf{S}$.

3. Arrange the singular values of the Hankel matrix in the descending order. Select the first $2n$ singular values where n is the model order of the system. The reason for selecting $2n$ singular values is due to the fact that each mode is represented by two singular values. These singular values correspond to the signal subspace and are known as dominant singular values.

4. Separate the dominant singular values from S and its corresponding left singular vectors as shown below.

$$\mathbf{H} = \begin{pmatrix} \mathbf{U_1} & \mathbf{U_0} \end{pmatrix} \begin{pmatrix} \mathbf{S_1} & \mathbf{0} \\ \mathbf{0} & \mathbf{S_0} \end{pmatrix} \begin{pmatrix} \mathbf{V_1^t} \\ \mathbf{V_0^t} \end{pmatrix} \tag{3.3}$$

Here, $\mathbf{S_1}$ is a submatrix of the dominant singular values and $\mathbf{U_1}$ is its corresponding left singular vectors. S_0 is a submatrix of singular values corresponding to the noise subspace and $\mathbf{U_0}$ and $\mathbf{V_0}$ represent its corresponding left and right singular vectors,

5. Obtain $\mathbf{U_1^+}$ and $\mathbf{U_1^-}$ matrices from $\mathbf{U_1}$ by deleting the first and last rows of the $\mathbf{U_1}$ matrix.

$$\mathbf{U_1^+} = \mathbf{U_1}(\mathbf{2} : \mathbf{end}) \tag{3.4}$$

$$\mathbf{U_1^-} = \mathbf{U_1}(\mathbf{1} : \mathbf{end} - \mathbf{1}) \tag{3.5}$$

6. Compute $\mathbf{Z}$ such that $\mathbf{U_1^+} = \mathbf{U_1^-} * \mathbf{Z}$ through total least square method.

7. The frequency (f_k), attenuation factor (AF_k) and damping coefficient (ζ_k) of the modes present in the low frequency oscillations are determined from the eigenvalues of $\mathbf{Z}$ using the following equation.

$$f_k = f_s * \frac{imag(log(\lambda_k))}{2\pi} \tag{3.6}$$

$$AF_k = f_s * real(log(\lambda_k)) \tag{3.7}$$

$$\zeta_k = -\frac{AF_k}{\sqrt{(AF_k)^2 + (2\pi * f_k)^2}} \tag{3.8}$$

8. The amplitude (AM) of the modes are obtained from the basis vectors using the following equations.

$$\mathbf{basis} = \mathbf{e}^{([\mathbf{t}]^{\mathbf{T}} * ([\mathbf{AF_k}]^{\mathbf{T}} + \mathbf{j} * \mathbf{2}\pi * [\mathbf{f_k}]^{\mathbf{T}}))} \tag{3.9}$$

$$\mathbf{AM} = (\mathbf{basis}(\mathbf{1} : \mathbf{N}), :)^{\dagger} * \mathbf{x^T} \tag{3.10}$$

Here, t denotes the time interval for which signal is present in steps of sampling time and $(basis(1 : N), :)$ denotes the first N rows of basis matrix. † represent the pseudo inverse of a matrix.

The proposed HTLS based algorithm is explained using the two mode signal $x(t)$ given below.

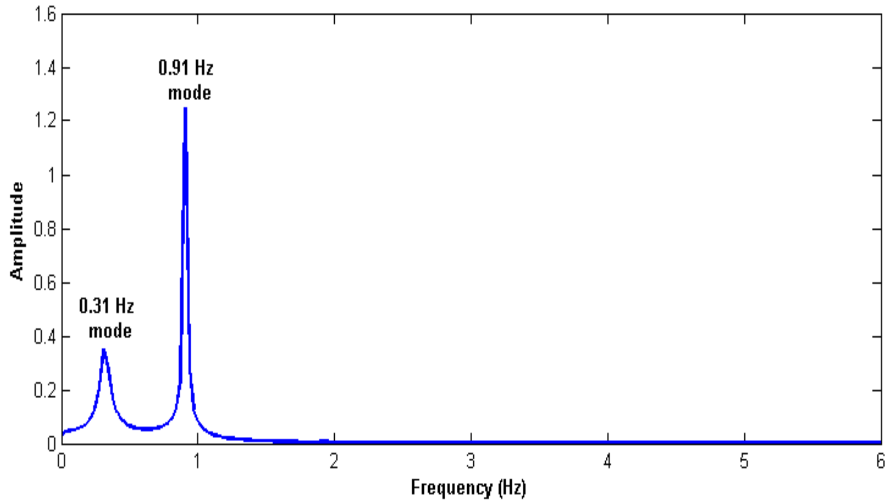

Figure 3.2: FFT plot of $x(t)$.

$$x(t) = \cos(2\pi * 0.31t + (1.5\pi))\exp(-0.17t) + (\cos(2\pi * 0.91t + (4.5\pi))\exp(-0.03t))); \quad (3.11)$$

$x(t)$ is corrupted by adding white Gaussian noise such that the SNR value after the addition is 40 dB. The FFT plot of the corrupted signal is given in fig. 3.2.

It is observed that the FFT plot in fig. 3.2 has two peaks corresponding to 0.31 Hz and 0.91 Hz modes. So, the initial model order is set as 2. This value is slightly incremented by adding a small number and the incremented model order estimate is fed into the HTLS algorithm, which estimates the modal parameters present in it. In this example, the model order is incremented by 2. The estimated modal parameters and its amplitudes are listed in Table 3.1.

Table 3.1: Modal parameters of $x(t)$

Frequency	**Damping**	**Amplitude**
0.9100	***-0.03***	***1.0013***
0.3096	***-0.1709***	***1.0052***
1.5760	0.0354	0.003
1.2713	0.0168	0.0078

It is observed that the proposed method estimated four modes of which two modes has an amplitude of 1 unit whereas the other two modes have an amplitude of less than 0.01 unit. The modes with lesser amplitude (1.576 Hz mode and 1.2713 Hz mode) are the fictitious modes while the other two modes (0.3096 Hz and 0.9100 Hz mode) are the true modes.

3.3 Simulation Results and Discussion

The applicability of the proposed method to accurately estimate the modal parameters of the low-frequency oscillations occurring in the power system is demonstrated using synthetic signals with known modal parameters and a real-time signal obtained from Western Electricity Coordinating Council (WECC) system. The results obtained through the estimation of these signals are compared with that of the Modified Prony based and Fourier based methods proposed in [44] and [60] respectively at various SNRs and PMU reporting rates. Prior to these simulations, the length of the window used and the distance between the successive windows of the Fourier method is set as 500 and 50 respectively. Similarly, the value of M which is used for generating the Hankel matrix in the proposed method is set as 200.

3.3.1 Synthetic Signals

In this subsection, three synthetic signals with known modal parameters are used to inspect the accuracy of estimation of the proposed method by comparing it with the Modified Prony [44] and Fourier [60] based methods in the literature. The synthetic signals used for this analysis are

$$\begin{aligned} Signal\ \ 1 = &(\cos(2\pi * 0.45t + (1.3\pi))\exp(-0.07t)) \\ &+ (cos(2\pi * 0.85t + (4.5\pi))\exp(-0.13t))); \end{aligned} \tag{3.12}$$

$$\begin{aligned} Signal\ \ 2 = &(\cos(2\pi * 0.45t + (1.3\pi))\exp(-0.06t)) \\ &+ (\cos(2\pi * 0.79t + (0.6pi))\exp(-0.09t)) \\ &+ (cos(2\pi * 0.85t + (4.5\pi))\exp(-0.11t))); \end{aligned} \tag{3.13}$$

$$\begin{aligned} Signal\ \ 3 = & (\cos(2\pi * 0.32t + (1.5\pi))\exp(-0.1t)) \\ & + (\cos(2\pi * 0.39t + (1.5pi))\exp(-0.05t)) \\ & + (cos(2\pi * 0.81t + (0.5\pi))\exp(-0.03t)) \\ & + (cos(2\pi * 0.91t + (0.5\pi))\exp(-0.0702t))); \end{aligned} \tag{3.14}$$

White Gaussian noise is added to these signals such that their SNR is between 5 dB to 15 dB. These corrupted signals are analyzed using the proposed method, Fourier based method [60] and Modified Prony based method at different signal to noise ratios and PMU reporting rates. The results obtained are tabulated in Tables 3.2 and 3.3.

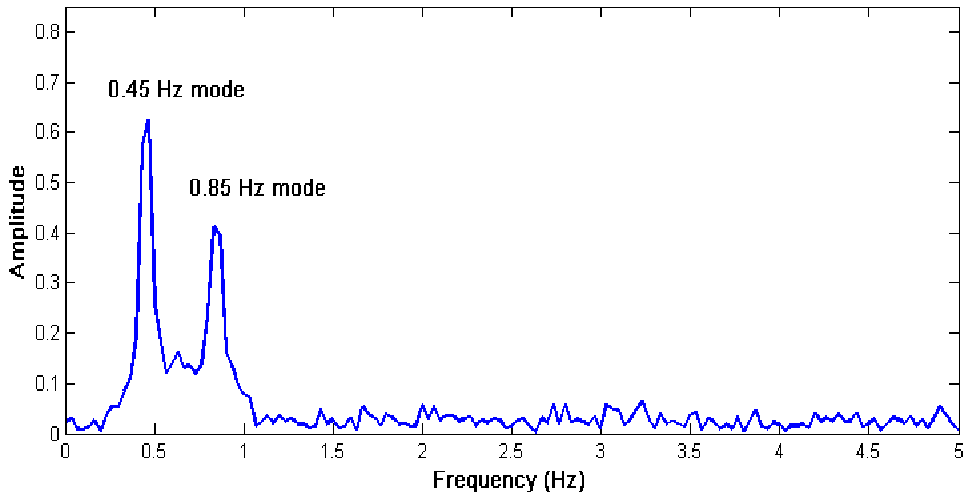

Figure 3.3: FFT plot of Signal 1 at 5 dB SNR.

Table 3.2 shows the estimated modal parameters of the three synthetic signals obtained using the three modal estimation algorithms under consideration at SNRs of 5 dB, 10 dB and 15 dB. The modal parameters listed in this table are obtained by taking an average of 50 independent simulations. As explained in Section 3.2.1, the modal order estimate of the proposed method is obtained through an FFT based technique. Figs. 3.3, 3.4 and 3.5 show the FFT plots of these three synthetic signals at SNR of 5 dB. It is observed from these plots that the FFT based technique accurately estimates the number of frequency components in both these signals even though closely spaced modes are present in them. This eventually helps the HTLS algorithm to identify all the modes in the signal even when its SNR value is 5 dB. On the other hand, it is noticed that the Modified Prony and Fourier models fail to

Table 3.2: Modal parameters of the synthetic signal estimated using the proposed method, Modified Prony method[44] and Fourier method [60]

Method	SNR = 5 dB				SNR = 10 dB				SNR = 15 dB			
	Estimated		*Std (%)*		*Estimated*		*Std (%)*		*Estimated*		*Std (%)*	
	Freq (Hz)	**AF**	**Freq (Hz)**	**AF**	**Freq (Hz)**	**AF**	**Freq (Hz)**	**AF**	**Freq (Hz)**	**AF**	**Freq (Hz)**	**AF**
					Signal 1							
True	0.4500	0.070			0.3200	0.070			0.3200	0.070		
value	0.8500	0.130			0.8500	0.030			0.8500	0.030		
HTLS	0.4501	0.0687	0.10	0.55	0.4500	0.0703	0.02	0.12	0.4501	0.0699	0.01	0.13
method	0.8494	0.1277	0.13	0.96	0.8502	0.1301	0.06	0.34	0.8498	0.0298	0.02	0.24
Fourier	-	-	-	-	0.4660	0.1766	$< 10^{-5}$	0.54	0.4660	0.0670	$< 10^{-5}$	0.24
	-	-	-	-	0.8348	0.1201	$< 10^{-5}$	0.98	0.8335	0.1267	$< 10^{-5}$	0.59
Prony	0.4468	0.0.0865	1.37	0.21	0.4502	0.728	0.24	0.08	0.4429	0.0710	0.24	3.69
	0.8528	0.1579	2.38	0.31	0.8502	0.1371	0.48	0.16	0.8593	0.1337	0.49	3.33
					Signal 2							
True	0.4500	0.0600			0.4500	0.0600			0.4500	0.0600		
value	0.790	0.090			0.790	0.090			0.790	0.090		
	0.850	0.11			0.850	0.11			0.850	0.11		
HTLS	0.4502	0.0613	0.11	0.81	0.4500	0.0595	0.04	0.41	0.4501	0.0599	0.02	0.17
method	0.790	0.0864	0.23	0.95	0.7903	0.0880	0.39	0.83	0.790	0.0906	0.16	0.48
	0.8496	0.1174	0.32	1.38	0.8493	0.1122	0.45	1.22	0.8505	0.1087	0.15	0.74
Modified	-	-	-	-	0.4503	0.0616	6.97	0.62	0.4493	0.0591	0.06	0.65
Prony	-	-	-	-	0.7899	0.1378	1.63	3.5	0.7895	0.1036	1.38	5.83
method	-	-	-	-	0.8586	0.1620	2.23	2.63	0.8502	0.1404	3.46	4.76
	-	-	-	-	0.4500	0.0600	$< 10^{-5}$	0.48	0.4500	0.0600	$< 10^{-5}$	0.15
Fourier	-	-	-	-	0.790	0.050	$< 10^{-5}$	0.61	0.790	0.050	$< 10^{-5}$	0.27
method	-	-	-	-	0.850	0.11	$< 10^{-5}$	0.67	0.850	0.11	$< 10^{-5}$	0.28
					Signal 3							
True	0.3200	0.100			0.3200	0.100			0.3200	0.100		
value	0.390	0.050			0.390	0.050			0.390	0.050		
	0.810	0.03			0.810	0.03			0.810	0.03		
	0.910	0.0702			0.910	0.0702			0.910	0.0702		
	0.3248	0.0911	1.78	1.68	0.3248	0.0911	1.78	1.68	0.3248	0.0911	1.78	1.68
HTLS	0.3856	0.0558	1.78	1.38	0.3902	0501	0.08	0.55	0.3886	0.0512	0.98	0.69
	0.8099	0.0280	0.06	0.39	0.8100	0.0297	0.04	0.27	0.8099	0.0299	0.02	0.14
	0.9102	0.0716	0.17	0.79	0.9101	0.0704	0.07	0.43	0.9102	0.0701	0.04	0.27
Fourier	-	-	-	-	0.2842	0.0905	$< 10^{-5}$	1.27	0.2996	0.1093	$< 10^{-5}$	0.52
	-	-	-	-	0.3879	0.0535	$< 10^{-5}$	1.72	0.3995	0.0458	$< 10^{-5}$	0.12
	-	-	-	-	0.7989	0.0300	$< 10^{-5}$	0.16	0.7989	0.0279	$< 10^{-5}$	0.09
	-	-	-	-	0.8988	0.0642	$< 10^{-5}$	0.35	0.8988	0.0612	$< 10^{-5}$	0.14
Prony	-	-	-	-	0.3188	0.1222	0.17	1.48	0.3196	0.1061	0.09	0.082
	-	-	-	-	0.3914	0.0588	0.09	0.58	0.3903	0.0543	0.0525	0.2
	-	-	-	-	0.8098	0.0329	0.06	0.23	0.8100	0.0309	0.024	0.2
	-	-	-	-	0.9105	0.0712	0.11	0.39	0.9102	0.0720	0.05	0.2

* Modified Prony and Fourier methods fails to estimate the modal parameters of the synthetic signal at 5 dB SNR. So the columns are left blank.

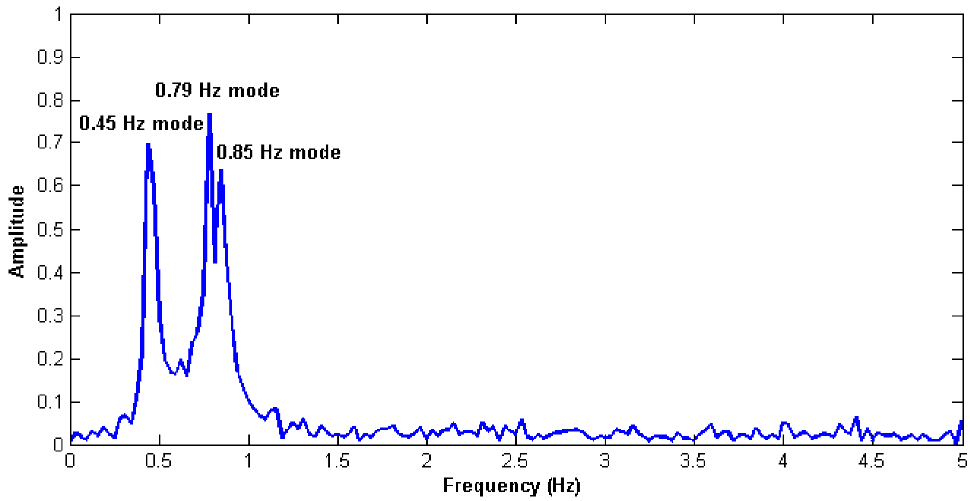

Figure 3.4: FFT plot of Signal 2 at 5 dB SNR.

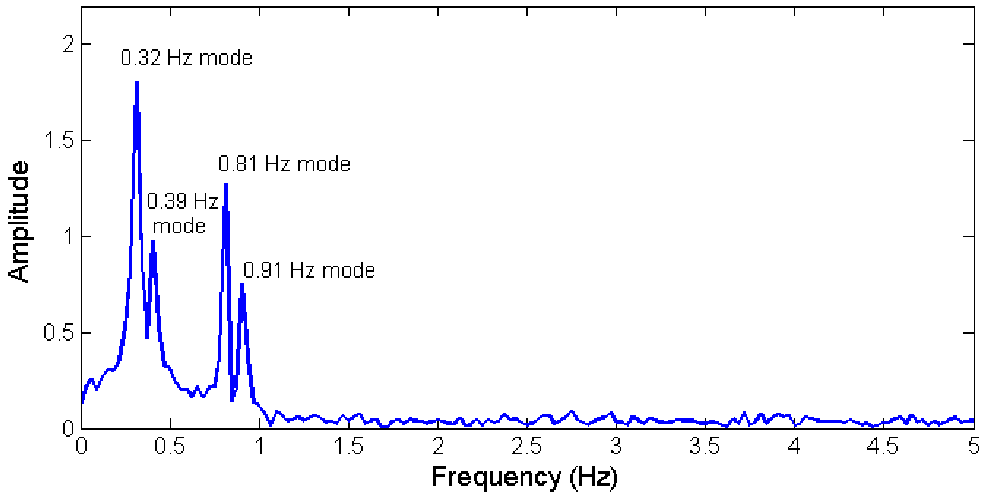

Figure 3.5: FFT plot of Signal 3 at 5 dB SNR.

identify all the modes when the SNR value of the signal is 5 dB. However, at SNR values of 10 dB and 15 dB, both these methods identify all the modes present in the signal but their accuracy of estimation is quite poor when compared to that of the proposed method. This is noticeable from three-dimensional bar graphs in figs. 3.6 and 3.7 where the error in attenuation factor estimation of different modes in Signal 2 and Signal 3 are plotted at different SNRs. From these graphs, it is evident that the attenuation factor estimation error is highest for the Modified Prony method, followed by the Fourier method and is least for the proposed method. Hence, it is inferred that the proposed method performs better than the Fourier and Modified Prony based methods while estimating the modal parameters of noise contaminated signals.

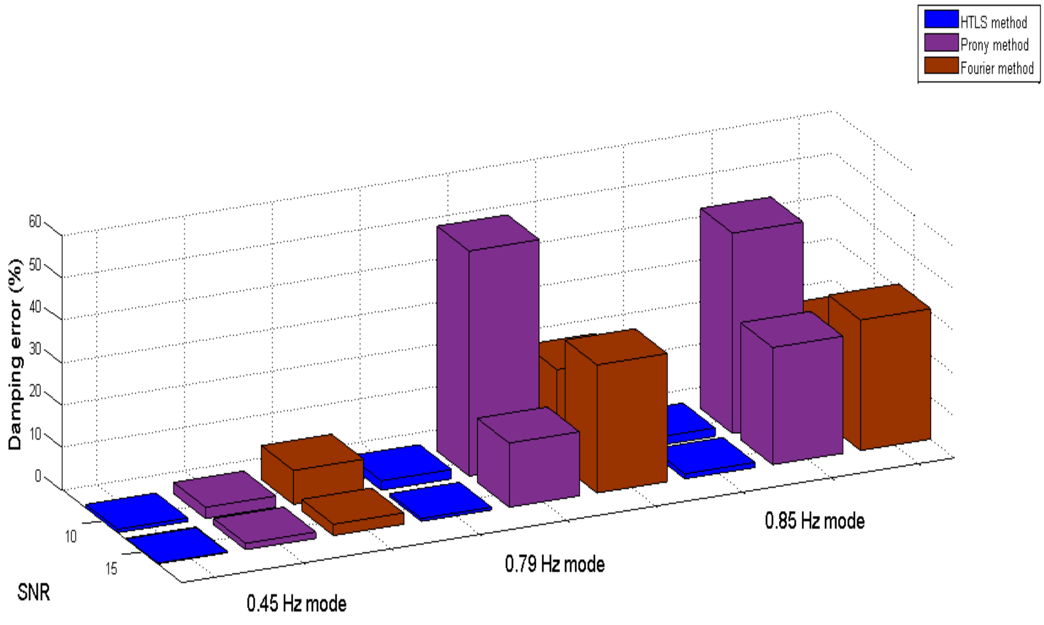

Figure 3.6: Absolute error in the estimation of attenuation factor of the Signal 2.

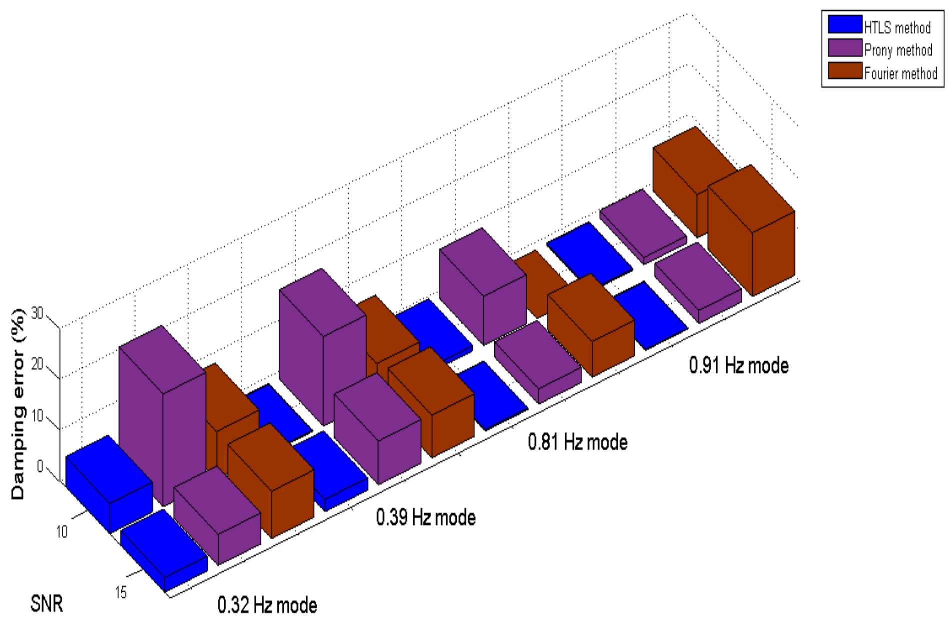

Figure 3.7: Absolute error in the estimation of attenuation factor of the Signal 3.

The reporting rates of the PMU ranges from 10 Hz to 120 Hz. For a modal estimation technique to be effective, it should provide satisfactory results irrespective of the PMU reporting rate. Hence, the modal parameters of the signal, sampled at different PMU reporting rates are estimated using the proposed method and the results are tabulated in Table 3.3. It

Table 3.3: Performance of the proposed method for synthetic signal with change in PMU reporting rate

PMU reporting rate	γ_1	γ_2	**Estimated**		**Standard deviation**		**Absolute percentage Error**	
			Freq (Hz)	***AF***	***Freq (Hz)***	***AF***	***Freq (Hz)***	***AF***
10	50	0	0.3204	0.0992	0.0012	0.0065	0.125	0.8
			0.3900	0.0499	0.0007	0.0133	0	0.2
			0.8099	0.0301	0.0003	0.0116	0.0123	0.33
			0.9101	0.0694	0.0005	-	0.0109	1.11
20	50	0	0.3199	0.0989	0.0013	0 .0062	0.03125	1.1
			0.3899	0.0502	0.0004	0.0026	0.0256	0.4
			0.8100	0.0301	0.0002	0.0013	0	0.33
			0.9100	0.0701	0.0003	0.0024	0	0.142
30	50	0	3201	0.1002	0.00063	0.0043	0.03125	0.2
			0.3900	0.0499	0.00031	0.0022	0	0.2
			0.8100	0.0300	0.00013	0.0003	0	0
			0.9100	0.0705	0.00027	0.0016	0	0.42
40	50	0	0.3200	0.0998	0.0006	0.0025	0	0.2
			0.3900	0.0500	0.00029	0.0012	0	0
			0.8100	0.0300	0.00012	0.0008	0	0
			0.9100	0.0700	0.00022	0.0015	0	0.28
60	50	0	0.3200	0.0997	0.00046	0.0022	0	0.3
			0.3900	0.0500	0.00019	0.0012	0	0
			0.8100	0.0300	0.00011	0.0008	0	0
			0.9100	0 .0700	0.00022	0.0012	0	0.28
120	50	0	0.3199	0.1002	0.00027	0.0016	0.03125	0.2
			0.3900	0.0499	0.00015	0.0009	0	0.2
			0.8100	0.0301	0.00006	0.0005	0	0.33
			0.9100	0 .0701	0.00017	0.0009	0	0.14

is observed that the proposed method is highly accurate even at low PMU reporting rates as evident from the percentage error in modal parameter estimation of the signal having a PMU reporting rate of 10 Hz. The maximum absolute error in frequency and attenuation factor estimation at this reporting rate is 0.125% and 1.11% respectively. It is also observed that the standard deviation of the estimated modal parameters at this reporting rate is very low proving that the estimated results are almost the same during successive simulations.

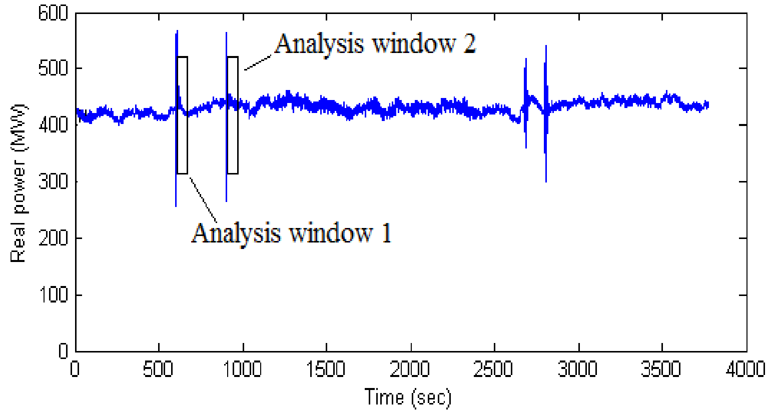

Figure 3.8: Variation of power in WECC system on 14^{th} September 2005 [84].

3.3.2 Real Time PMU Data

The effectiveness of the proposed method in accurately estimating the modal parameters of real-time signals obtained from the PMUs installed across the power systems is tested in this subsection. The signals are generated from the probe test data of the Western Electricity Coordinating Council (WECC) system on 14^{th} September 2005 [84, 85]. It represents the variation in the active power flow of the MALN - Round Mountain 1 line of the WECC system as shown in fig. 3.8. Three signals with window lengths of 8.6 sec as shown in fig. 3.8 are extracted from the active power flow data for this purpose. Analysis window 1 (20:10:11.993 - 20:10:20.526 UTC) and 2 (20:15:13.324 - 20:15:21.857 UTC) corresponds to data acquired after first and second sequential probing of $\pm$125 MW respectively whereas analysis window 3 (20:00:03.333 - 20:00:11.866 UTC) corresponds to ambient data [84, 85]. The modal parameters of these signals are estimated through the proposed method, Modified Prony and Fourier methods and the results are tabulated in Table 3.4.

Table 3.4: Frequencies and damping ratios of WECC system probe data

Window	Estimated value from [84]		Proposed method		Fourier		Modified Prony	
	Frequency (Hz)	ζ (%)	***Frequency*** (Hz)	ζ (%)	***Frequency*** (Hz)	ζ (%)	***Frequency*** (Hz)	ζ (%)
Window 1	0.318	8.3	0.3183	8.39	0.3497	7.7	0.3204	8.94
	-	-	0.6962	11.83	0.6993	3.86	0.7065	15.20
Window 2	-	-	0.316	8.11	0.3512	8.05	0.3217	8.19
	-	-	0.6642	10.51	0.6993	4.03	0.7184	5.74

The FFT plots of the signal corresponding to these analysis windows are given in figs. 3.9 and 3.10. It is noticed that, while analysing the signal corresponding to analysis window 1, all the three methods identified both the modes present in it. The dominant among them

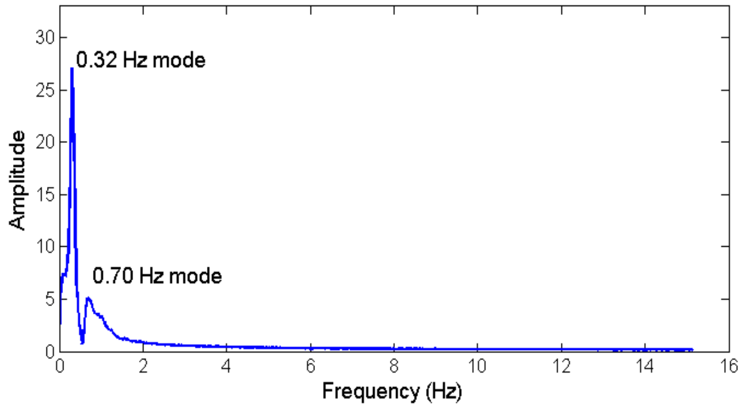

Figure 3.9: FFT plot of signal corresponding to analysis window 1.

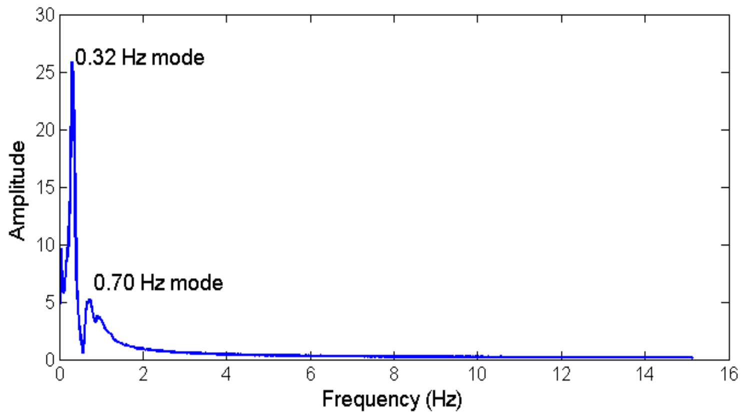

Figure 3.10: FFT plot of signal corresponding to analysis window 2.

Table 3.5: Frequencies and damping ratios of WECC system probe data under different noise levels

Window	**SNR=5 dB**		**SNR=10 dB**		**SNR=15 dB**		**SNR=20 dB**	
	Frequency (Hz)	ζ (%)	***Frequency*** (Hz)	ζ (%)	***Frequency*** (Hz)	ζ (%)	***Frequency*** (Hz)	ζ (%)
Window 1	0.3188	8.53	0.3183	8.39	0.3188	8.41	0.3188	8.35
	0.6970	11.73	0.6969	11.75	0.6966	11.63	0.0.6972	11.68
Window 2	0.3161	8.17	0.3161	8.19	0.3143	8.22	0.3146	8.20
	0.6648	10.54	0.6647	10.55	0.6641	10.51	0.664	10.52

is the 0.32 Hz mode. It is also noticed that the estimates of the proposed method were closer to the actual value reported in the WECC probe report in [84]. On the other hand, the Modified Prony method and the Fourier method gave less accurate estimates of the damping coefficient although the frequency of the dominant mode is estimated accurately in all these methods. Similarly, the estimated modal parameters of analysis window 2 are also closer to the reported values in [48]. The modal parameters of the proposed method are almost constant even under varying levels of noise as evident from the estimated values tabulated in Table 3.5. Hence, it can be inferred that, when compared to the Modified Prony and Fourier methods, the proposed method is better suited for the analysis of real-time signals.

3.4 Conclusion

This work has proposed an HTLS based method for identifying poorly damped modes of low-frequency oscillation in the power system. The model order of the signal, which is a prerequisite for analysing through HTLS method, is obtained using an FFT based technique. The estimated model order is incremented to ensure the identification of all the modes present in the signal before feeding it into the HTLS algorithm. The fictitious modes, if any, present in the estimated results is filtered out by comparing the amplitudes of the modes as the amplitude of the true modes will be much higher compared to the fictitious modes. The effectiveness of the proposed method is proven by testing it using real and synthetic signals and the results are compared with that of Modified Prony and Fourier based methods proposed in the literature. Test results reveal that the proposed method outperforms the other two methods irrespective of noise contamination and sampling rate of the signal.

Chapter 4

EMO ESPRIT based algorithm for analyzing ringdown oscillations

4.1 Introduction

The HTLS technique explained in Chapter 3 can accurately estimate the modal parameters of the signal in most cases. However, when the signal has closely spaced modes or when amplitude of the poorly damped modes is quite low, the FFT based model order algorithm fails to accurately estimate the model order. In most cases, the model order is underestimated as the FFT based method fails to distinguish closely spaced modes as separate modes. Due to this underestimation, one or more modes present in the signal are not identified. To prevent such phenomenon, an ESPRIT based modal parameter estimation method is explained in this chapter.

ESPRIT [47, 48, 50, 51] is a measurement based method which can accurately identify the modal parameters of low frequency oscillations, especially ring down oscillations. ESPRIT based methods have the ability to detect close modes and provide accurate estimates during modal estimation. They use correlation matrix for generating the signal subspace. Due to this reason, ESPRIT based methods have higher noise immunity although the usage of correlation matrix makes it slightly more computationally intensive. However, they require precise information about model order or the number of modes present in the signal for successful modal estimation, which is one of their drawbacks. In [48, 50], a Total Least Square ESPRIT (TLS-ESPRIT) based method is used for estimating the modal parameters of low frequency oscillations. It uses a method based on singular value of autocorrelation matrix

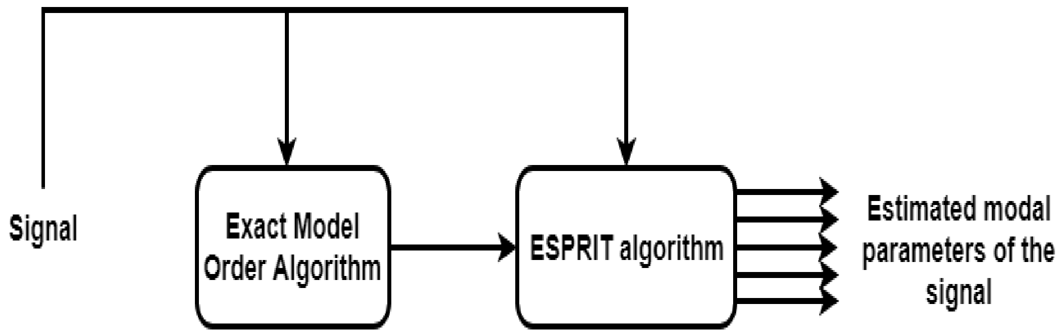

Figure 4.1: Block diagram of the proposed method.

for estimating the model order. The main limitation of this model order estimation method is that it provides inaccurate estimates of model order when the number of modes present in the signal is less or modes are closely spaced. Due to this reason, the proposed ESPRIT based model for modal parameter estimation of low frequency oscillations uses Exact Model Order (EMO) algorithm [86] for accurately identifying its model order. The effectiveness of the proposed EMO ESPRIT method is tested using synthetic test signals and the results are compared with modified Prony method [44], ARMA based method [59] and TLS-ESPRIT [48] method. Further, the proposed method is used to estimate the modes of a practical probing test data of the WECC system.

4.2 Proposed Methodology

The proposed method uses an ESPRIT based algorithm for estimating the modal parameters of the low frequency oscillations present in the power system. The schematic diagram of this method is given in fig. 4.1. ESPRIT is a signal processing technique, which decomposes complex signals into sum of sinusoids using a subspace based approach. It can be mathematically represented as

$$x(t) = \sum_{i=1}^{K} A_i e^{-\sigma_i t} \cos(2\pi * f_i t + \phi_i) + s_t \tag{4.1}$$

Here, $x(t)$ is the multimode signal to be decomposed. In this chapter, it is assumed that $x(t)$ is obtained from different PMUs placed in the power system. f_i, σ_i and ϕ_i are the frequency, attenuation factor and phase of the i^{th} sinusoidal component decomposed from $x(t)$. s_t represents the white Gaussian noise present in the signal and K is the total number of frequency components present in the signal. For the proper implementation of the ESPRIT algorithm, prior knowledge of the number of frequency components present in the signal is necessary. This is obtained through the model order estimation algorithm explained below.

4.2.1 Model Order Estimation

Conventionally, the model order of a signal is estimated using the dominant singular values of its autocorrelation matrix. A commonly used method for model order estimation was proposed in [48]. In this algorithm, the singular values of the autocorrelation matrix generated from the signal data are arranged in the descending order as shown below

$$D(i) = \rho_1 > \rho_2 > \rho_3 > ...\rho_i > ... > \rho_l \tag{4.2}$$

Here, ρ_i is the i^{th} singular value of the auto correlation matrix and l is the total number of singular values of the autocorrelation matrix. The $D(i)$ index corresponding to these singular values are calculated using the following equation

$$D(i) = \frac{\rho_1^2 + \rho_2^2 + \rho_3^2 + ...\rho_i^2}{\rho_1^2 + \rho_2^2 + \rho_3^2 + ...\rho_l^2} \tag{4.3}$$

The value of i for which $D(i)$ is closest to one is selected as the model order of the system. Although this method works perfectly for most signals, it fails to accurately estimate the model order when the number of modes present in the signal is less or modes are closely spaced. This can be explained with the help of an example.

Let us consider a power system signal x_1 as in the following equation.

$$\begin{aligned} x_1 = ((1\cos(2\pi*0.4t)\exp(-0.0909t)) \\ +(0.9\cos(2\pi*0.5t)\exp(-0.35t)) \\ +(0.7\cos(2\pi*0.6t+(\pi/6))\exp(-0.2001t)) \\ +(0.4\cos(2\pi*1.1t+(\pi/4)).*\exp(-0.666t))); \end{aligned} \tag{4.4}$$

This signal is sampled at 50 Hz and is corrupted by adding white Gaussian noise at 40 dB. The autocorrelation matrix of x_1 is created using the signal data and $D(i)$ index corresponding to the singular values of the autocorrelation matrix is also calculated. The $D(i)$ vs i graph of x_1 is shown in fig. 4.2.

It is observed that the value of $D(i)$ is closest to one at $i = 6$. So the model order is esti-

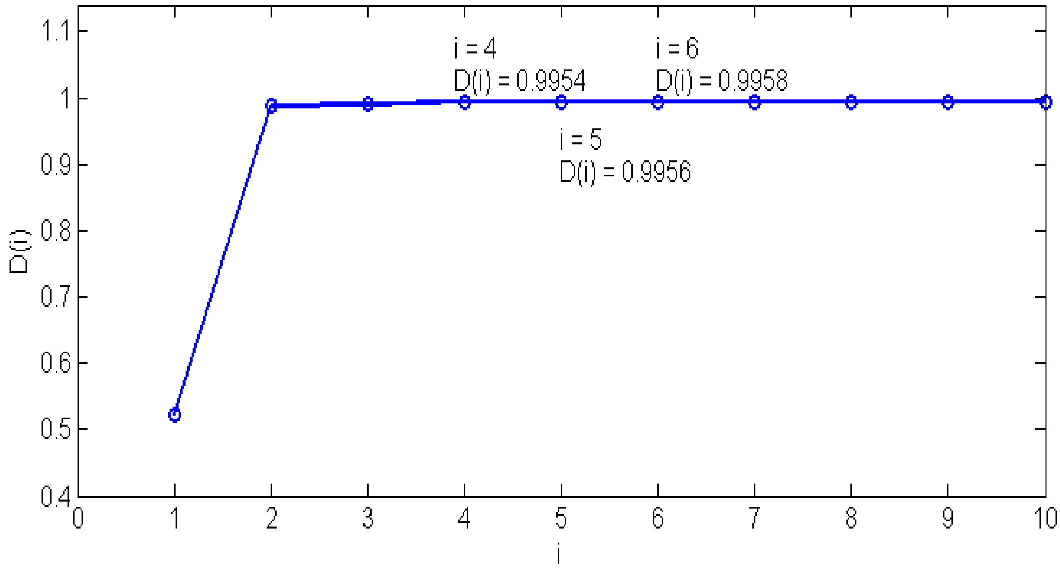

Figure 4.2: D(i) vs i plot.

mated as 6. But this estimation is incorrect as x_1 has only four frequency components. Also the estimate further deviates if the signal is highly noise contaminated and contains close frequency components. Therefore, this chapter employs the Exact Model Order algorithm proposed in [86] for precise estimation of number of modes.

Exact Model Order (EMO) Algorithm

EMO algorithm estimates the model order based on the fact that there will be considerable difference between the eigen values of the signal and noise subspace. This property is used for effectively separating the autocorrelation matrix into signal and noise subspaces. This algorithm can be summarized in the following steps.

1. Generate the autocorrelation matrix from the signal data and find its eigenvalues.
2. Arrange the eigenvalues (λ_i) in the ascending order.
3. Calculate the Relative Difference vector (RD) using the following equation

$$RD = \frac{\lambda_i - \lambda_{i-1}}{\lambda_{i-1}} \quad for \;\; i = 2,3,4...T \tag{4.5}$$

Here, T is the total number of Eigenvalues of the autocorrelation matrix.

4. Plot the RD vs i (RD index or RDI) graph and select five of its highest peaks.

5.The largest value of RDI among the five peaks is selected as the preliminary estimate of model order.

6. Check whether the eigenvalue corresponding to the selected RDI has more energy than

the noise subspace. This is done using the following equation.

$$\lambda_{\$} \geq \alpha * \frac{\lambda_{\$+1} + \lambda_{\$+2} + \lambda_{\$+3} + \ldots \lambda_T}{T - \$} \tag{4.6}$$

Here \$ represent the preliminary estimate of the model order. The value of α is between two and five.

5. If the above equation is satisfied, then model order is estimated as $RDI/2$. Else, the next lower value of RDI among the five peaks is selected as the next estimate. The process continues till the above equation is satisfied.

Each frequency component present in the signal is represented by two dominant eigenvalues. Hence, the total number of dominant eigenvalues corresponding to the signal will be twice its model order [87]. The eigenvalues other than the dominant ones are of very small value and represent the noise subspace. It is observed that the value of $RD(i)$ shoots up as the value of i reaches twice the model order. The reason for this sudden increase in the value of $RD(i)$ is that, as the value of i reaches twice the model order, λ_i is a dominant eigenvalue and belongs to the signal subspace whereas λ_{i+1} is considerably lower as it belongs to the noise subspace. This logic is utilized in the EMO algorithm for finding the exact model order. To confirm whether the estimated model order is accurate, (4.6) is used. If the estimated model order is accurate, then the average of successive eigenvalues after λ_i till λ_M is much lesser than λ_i.

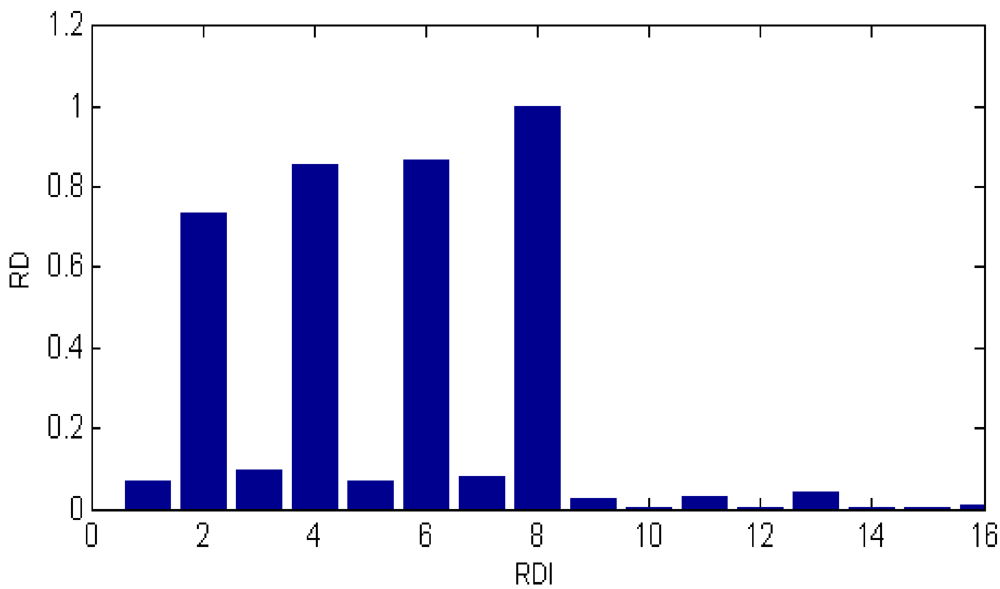

Figure 4.3: RD vs RDI plot.

To prove the effectiveness of this method, the signal in (4.4) is chosen for testing this method. The RD vs RDI graph of this signal is shown in fig. 4.3. It is observed that peaks of RD occurs at RDI values of $2,4,6$ and 8. Therefore, according to step 5, the $RDI = 8$ is selected as the preliminary model order estimate and verified using (4.6). This value satisfies (4.6) and thereby the obtained model order is $RDI/2 = 4$ which is the true value.

The reason for selecting five highest peaks in Step 4 of the EMO algorithm is explained using x_2 below.

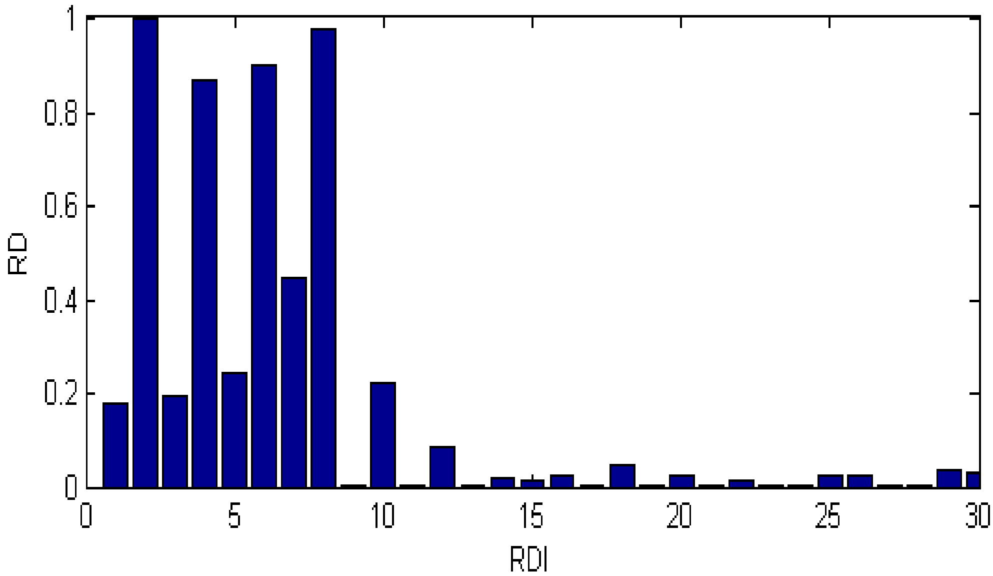

Figure 4.4: RD vs RDI plot of x_2.

$$\begin{aligned} x_2 = ((100\cos(2\pi * 0.4t)\exp(-0.0909t)) \\ +(0.9\cos(2\pi * 0.5t)\exp(-0.35t)) \\ +(0.7\cos(2\pi * 0.6t+(\pi/6))\exp(-0.2001t)) \\ +(0.4\cos(2\pi * 1.1t+(\pi/4)).*\exp(-0.666t))); \end{aligned} \quad (4.7)$$

While estimating the model order of a signal using the EMO method, it is noticed that the highest peak of the RD vs RDI plot usually occurs at RDI value $= 2 * model\ order$. In such cases, the model order can be accurately estimated by selecting the RDI value corresponding to its highest peak. However, if one of the modes of the signal has very high amplitude compared to others as in x_2, the highest peak occurs at an RDI value $< 2 * model\ order$.

For instance, 0.2 Hz mode of signal x_2 has much higher energy than other modes owing to its higher amplitude. The RD vs RDI plot of this signal in fig. 4.4 shows that the highest peak of RD vs RDI plot occurs at $RDI = 2$ although the model order of the signal is 4. If only one peak is selected, then it will lead to erroneous estimation of model order for such signals. To prevent this scenario, five highest peaks are chosen in Step 4 of the EMO algorithm.

4.2.2 ESPRIT Algorithm

The main steps for estimation of frequency using ESPRIT algorithm is as follows [47, 86].

Step 1: Create an auto correlation matrix $\boldsymbol{R}_x$ from the data points received from the PMU.

$$\boldsymbol{R}_x = \frac{1}{N-M}\boldsymbol{X}^H.\boldsymbol{X} \tag{4.8}$$

Here, $\boldsymbol{X}$ is the Hankel matrix of order M and N is the length of the PMU data under consideration. It is constructed from the signal $x(t)$ as shown below

$$\boldsymbol{X} = \begin{bmatrix} x(0) & x(1) & x(2) & x(3) & ..... & x(M-1) \\ x(1) & x(2) & x(3) & x(4) & ..... & x(M) \\ . & . & . & . & ..... & . \\ x(N-M) & x(N-M+1) & x(N-M+2) & x(N-M+3) & ..... & x(N-1) \end{bmatrix}$$

Step 2: Apply Eigen Value Decomposition (EVD) on auto correlation matrix $\boldsymbol{R}_x$. The eigenvalues obtained from the EVD are arranged in the decreasing order and the first $2n$ eigenvalues are selected, where n is the model order of the signal obtained using EMO algorithm.

Step 3: Form the signal subspace $\boldsymbol{R}_{xs}$ using the eigenvectors corresponding to these eigenvalues.

Step 4: Construct two shifted submatrices $\boldsymbol{R}_1$ and $\boldsymbol{R}_2$ from the signal subspace $\boldsymbol{R}_{xs}$ using the following formula.

$$\boldsymbol{R}_i = \boldsymbol{S}_i * \boldsymbol{R}_{xs}, \quad i = 1,2 \tag{4.9}$$

Where $\boldsymbol{S}_1 = [\boldsymbol{I}_{N_s} \;\; 0_{d_s}]$ and $\boldsymbol{S}_2 = [0_{d_s} \;\; \boldsymbol{I}_{N_s}]$. $\boldsymbol{I}_{N_s}$ is an identity matrix of size $N_s \times N_s$, where $N_s = M - d_s$. d_s is the distance between two sub matrices which is usually kept as 1.

Step 5: The shifted submatrices $\boldsymbol{R}_1$ and $\boldsymbol{R}_2$ can be related through a matrix ψ using shift invariance property such that $\boldsymbol{R}_2$=$\boldsymbol{R}_1.\psi$. The matrix ψ is found out using the following least square estimate.

$$\psi = (\boldsymbol{R}_1^H \boldsymbol{R}_1)^{-1} \boldsymbol{R}_1^H \boldsymbol{R}_2 \tag{4.10}$$

Step 6: The frequency (f_k) and attenuation factor (AF_k) of the components of the signal is obtained from the eigen values of the matrix ψ.

$$f_k = f_s * \frac{imag(\log(\lambda_{\psi k}))}{(2\pi)} \quad \forall k = 1,2,3...2n \tag{4.11}$$

$$AF_k = f_s * real(\log(\lambda_{\psi k})) \quad \forall k = 1,2,3...2n \tag{4.12}$$

Here, f_s is the sampling frequency of the signal and $\lambda_{\psi k}$ is the eigen value of the matrix ψ. The damping coefficient (ζ) of a frequency component is obtained from its frequency and attenuation factor using the following equation [55].

$$\zeta_k = -\frac{AF_k}{\sqrt{(AF_k)^2 + (\omega_k)^2}} \tag{4.13}$$

4.3 Simulation Results and Discussion

To validate the performance of the proposed method, it is compared with an ARMA block processing [59], TLS-ESPRIT [48] and modified Prony methods [44] using synthetic signals with known modal parameters and real time signals obtained from PMUs placed in an actual power system. The performance of the ARMA method [59] is poor under noisy conditions. So, a low pass filter is used to separate the low frequency modes of the signal and to reduce the effect of measurement noise. The specifications of this filter are (i) 2 Hz pass-band corner frequency, (ii) 5 Hz stop-band corner frequency,(iii) 0.2 dB ripple in the pass-band, and (iv) 20 dB ripple in the stop-band.

4.3.1 Synthetic Signals

The synthetic signals used for the analysis are given below.

$$
\begin{aligned}
Signal\ \ 1 = &(2\cos(2\pi * 0.2t + 1.5\pi))\exp(-0.17t) \\
&+ 2\cos(2\pi * 0.75t + (0.5\pi))\exp(-0.13t)
\end{aligned} \tag{4.14}
$$

$$
\begin{aligned}
Signal\ \ 2 = &2\cos(2\pi * 0.2t + (1.5\pi))\exp(-0.17t) \\
&+ 2\cos(2\pi * 0.28t + (0.5\pi))\exp(-0.05t) \\
&+ (2\cos(2\pi * 0.75t + (4.5\pi))\exp(-0.13t)));
\end{aligned} \tag{4.15}
$$

$$
\begin{aligned}
Signal\ \ 3 = &(2\cos(2\pi * 0.25t + (1.5\pi))\exp(-0.17t)) \\
&+ (2\cos(2\pi * 0.33t + (1.5pi))\exp(-0.12t)) \\
&+ (2cos(2\pi * 0.78t + (0.5\pi))\exp(-0.13t)) \\
&+ (2cos(2\pi * 0.87t + (0.5\pi))\exp(-0.0702t)));
\end{aligned} \tag{4.16}
$$

These signals are simulated in MATLAB and white Gaussian noise is added to them. The modal parameters of these corrupted signals are estimated using the proposed method, ARMA, TLS-ESPRIT, and modified Prony methods. The results obtained are tabulated in Tables 4.1, 4.2, 4.3 and 4.4.

Table 4.1 shows the estimated modal parameters of the synthetic signals using the proposed method, ARMA [59] and modified Prony methods [44] at SNR ranging from 5 dB to 15 dB. In this table, *freq* and *AF* denotes the frequency and attenuation factor of the mode of the test signal whereas *Std* refers to their standard deviation. The frequencies and attenuation factors of a signal at a particular SNR is obtained by taking the mean of the estimated values obtained from 50 independent simulations. It is noticed that, while analysing simple signals like Signal 1 which do not have closely spaced modes, all the methods under consideration gave accurate frequency estimates. However, when compared to Modified Prony and ARMA methods, the proposed method gave the best estimates of attenuation factor of Signal 1. For instance, while analysing the modal parameters of Signal 1 at 5 dB SNR using the proposed

Table 4.1: Modal parameters of different signals estimated using the proposed method, modified Prony method[44] and ARMA method [59]

	SNR = 5 dB				SNR = 10 dB				SNR = 15 dB			
Method	Estimated		Std (%)		Estimated		Std (%)		Estimated		Std (%)	
	Freq (Hz)	AF	Freq (Hz)	AF	Freq (Hz)	AF	Freq (Hz)	AF	Freq (Hz)	AF	Freq (Hz)	AF
Signal 1												
True	0.200	0.170			0.200	0.170			0.200	0.170		
value	0.750	0.130			0.750	0.130			0.750	0.130		
EMO	0.199	0.171	0.24	1.53	0.200	0.171	0.15	0.63	0.199	0.169	0.06	0.42
ESPRIT	0.750	0.129	0.16	0.79	0.750	0.130	0.08	0.62	0.750	0.131	0.06	0.29
Modified	0.201	0.178	0.36	2.73	0.201	0.176	0.18	1.25	0.199	0.172	0.11	0.58
Prony	0.751	0.142	0.45	1.24	0.751	0.133	0.13	0.80	0.749	0.132	0.08	0.38
ARMA	0.201	0.184	0.34	2.8	0.199	0.178	0.12	0.37	0.201	0.175	0.08	0.72
	0.750	0.143	0.26	1.02	0.751	0.131	0.37	0.53	0.749	0.132	0.06	0.35
Signal 2												
True	0.200	0.170			0.200	0.170			0.200	0.170		
Value	0.280	0.050			0.280	0.050			0.280	0.050		
	0.750	0.130			0.750	0.130			0.750	0.130		
EMO	0.200	0.174	0.90	2.57	0.200	0.172	0.37	1.63	0.199	0.171	0.17	0.92
ESPRIT	0.280	0.052	0.23	0.95	0.280	0.052	0.08	0.46	0.280	0.050	0.04	0.26
	0.749	0.132	0.17	0.09	0.750	0.131	0.09	0.62	0.749	0.131	0.04	0.34
	0.211	0.266	0.57	5.59	0.209	0.202	1.73	1.5	0.202	0.170	0.15	3.98
Prony	0.278	0.079	0.58	1.98	0.309	0.059	10.57	0.95	0.279	0.059	0.38	2.30
	0.749	0.140	0.29	1.71	0.744	0.136	2.08	0.93	0.749	0.134	0.14	0.44
ARMA					0.216	0.202	0.86	3.66	0.214	0.206	1.8	2.51
					0.284	0.053	0.22	0.69	0.297	0.058	5.69	0.46
					0.749	0.135	0.11	1.29	0.749	0.135	0.10	0.61
Signal 3												
True	0.250	0.170			0.250	0.170			0.250	0.170		
value	0.330	0.120			0.330	0.120			0.330	0.120		
	0.780	0.130			0.780	0.130			0.780	0.130		
	0.870	0.070			0.870	0.070			0.870	0.070		
EMO	0.249	0.175	0.76	3.24	0.250	0.169	0.37	1.77	0.250	0.169	0.19	0.82
ESPRIT	0.330	0.119	0.42	2.57	0.330	0.122	0.24	1.18	0.330	0.119	0.24	1.18
	0.782	0.131	0.36	1.79	0.780	0.129	0.18	0.09	0.780	0.129	0.08	0.61
	0.870	0.071	0.19	0.09	0.869	0.071	0.11	0.49	0.870	0.070	0.07	0.29
Modified	0.252	0.162	0.19	2.29	0.249	0.177	0.26	0.15	0.248	0.172	0.24	1.36
Prony	0.330	0.123	0.17	1.14	0.331	0.122	0.25	1.00	0.324	0.126	0.11	0.73
	0.780	0.114	0.16	7.43	0.780	0.131	0.11	0.70	0.779	0.137	0.12	0.63
	0.869	0.070	0.04	0.63	0.870	0.069	0.05	0.18	0.871	0.071	0.04	0.30
ARMA					0.223	0.150	1.50	4.41	0.235	0.186	1.48	2.56
					0.341	0.152	0.85	3.77	0.337	0.122	0.66	2.51
					0.785	0.102	0.69	4.07	0.780	0.118	0.38	2.19
					0.868	0.081	0.32	2.27	0.870	0.078	0.13	0.86

ARMA method fails to estimate the modal parameters of Signals 2 and 3 with 5 dB SNR. So the columns are left blank.

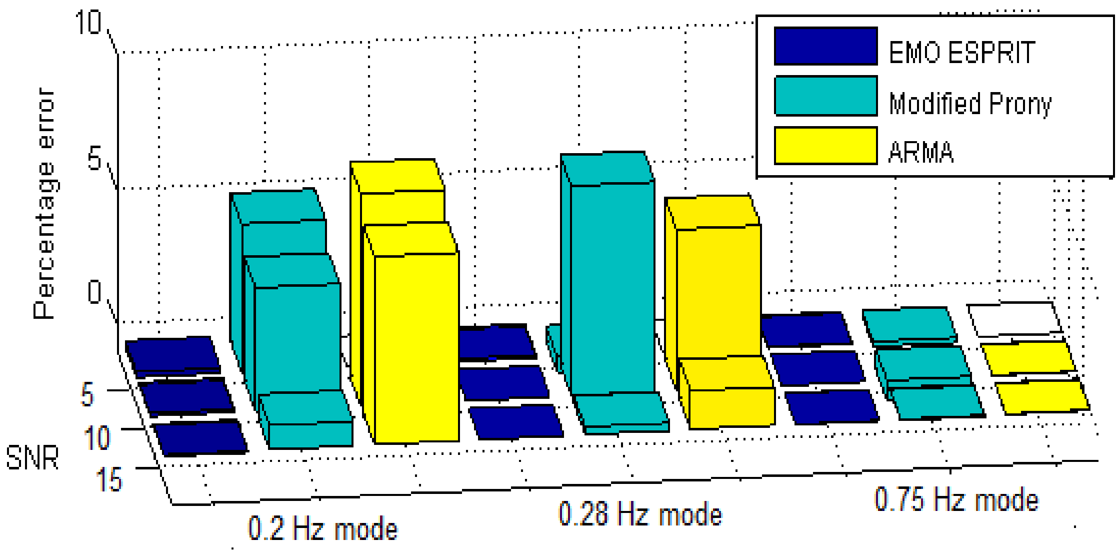

Figure 4.5: Absolute error in the frequency estimation of modes of Signal 2 with different methods at different SNR levels.

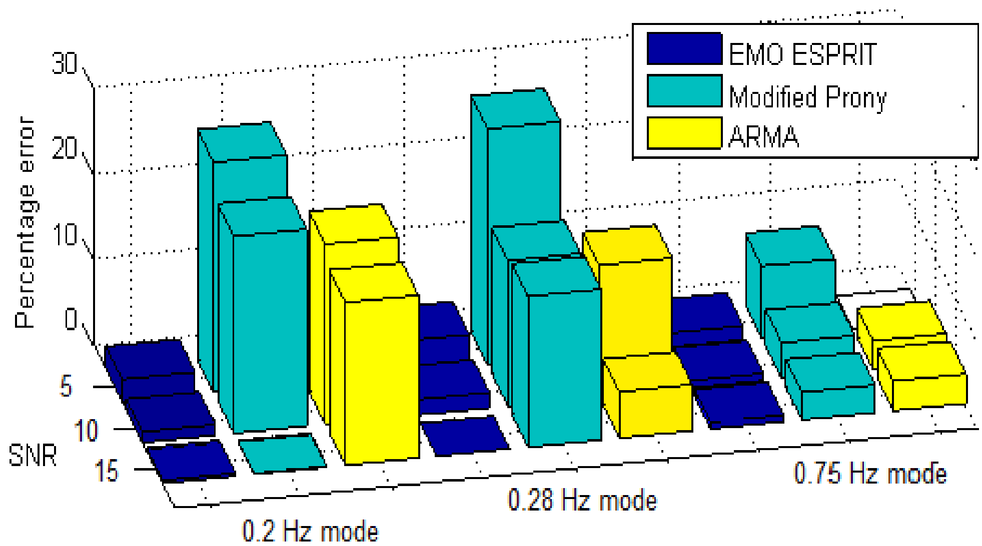

Figure 4.6: Absolute error in the attenuation factor estimation of modes of Signal 2 with different methods at different SNR levels.

method, the attenuation factor estimation error of 0.75 Hz mode is 0.23% whereas that of the ARMA and modified Prony methods, is approximately 9%.

It is also noted that, while analysing signals with closely spaced mode like Signal 2, the performance of the proposed method is much better than that of the modified Prony and ARMA methods. This is evident from figs. 4.5 and 4.6, which show the plots of absolute error in frequency and attenuation factor estimation of Signal 2 at different SNRs obtained

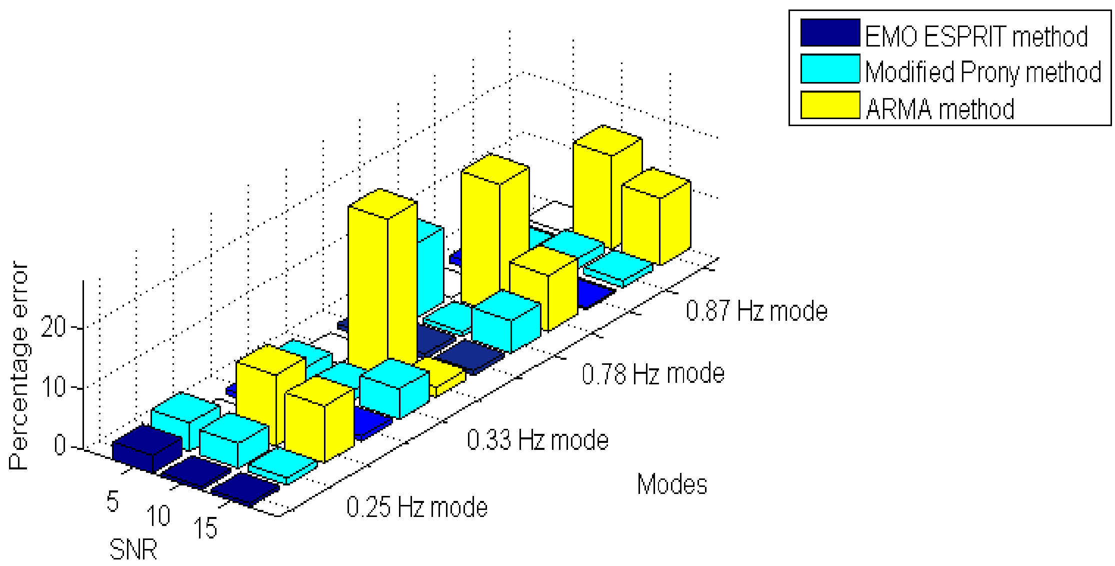

Figure 4.7: Absolute error in the attenuation factor estimation of modes of Signal 3 with different methods at different SNR levels.

through ARMA, modified Prony and proposed methods. It is noticed that, the absolute error in frequency and attenuation factor estimation is comparatively lesser for the proposed method when compared to that of other two methods. The maximum absolute error in the frequency and attenuation factor estimation of Signal 2 with 5 dB SNR is 7.7% and 27.6% for modified Prony method whereas that of the proposed model is only 0.2% and 3.8%. ARMA method fails to detect all the modes present in Signal 2, therefore it is not considered in this comparison. Moreover, the standard deviation of the proposed method is very small which implies that almost all the estimations are similar. Similar inferences can be drawn from fig. 4.7, which shows the plot of absolute error in attenuation factor estimation of Signal 3 at different SNRs obtained through ARMA, modified Prony and proposed methods. Hence, it can be inferred that, when compared to the modified Prony and ARMA methods, the proposed method is better suited for estimating the signal parameters especially when the signal has high noise contamination.

Table 4.2 shows the comparison of modes estimated by TLS ESPRIT and EMO ESPRIT methods. The main difference between these methods is that the proposed method uses EMO based algorithm for model order estimation whereas the TLS ESPRIT based method uses a D(i) index based method for the same purpose. Both these model order algorithms are explained earlier in Section 4.2.1. The main disadvantage of the D(i) index based method in [48] is that optimum D(i) value used for selecting the model order varies depending upon the modes present in the signal. For signals having large number of modes, the optimum D(i) value will be very close to one whereas for signals with less number of modes, it will be further away. Hence, using a common D(i) value for analysing all the signals will result in under estimation or over estimation of model order for most of the signals. This can be explained clearly using the following examples. While analysing Signal 1 at 5 dB SNR, TLS ESPRIT method identifies four modes of which two are fictitious (9.226 Hz and 17.847Hz) at D(i) = 0.935. The results are worse in case of D(i) = 0.99 and D(i) = 0.995 as the number of modes estimated are 46 and 90 respectively. The D(i) vs i plot for Signal 1 in fig. 4.8 reveals that the optimum value of D(i) for accurately estimating its model order is around 0.75. As the D(i) values used in this simulation are all higher than 0.75, it causes over estimation of the model order leading to the presence of fictitious modes in estimated results.

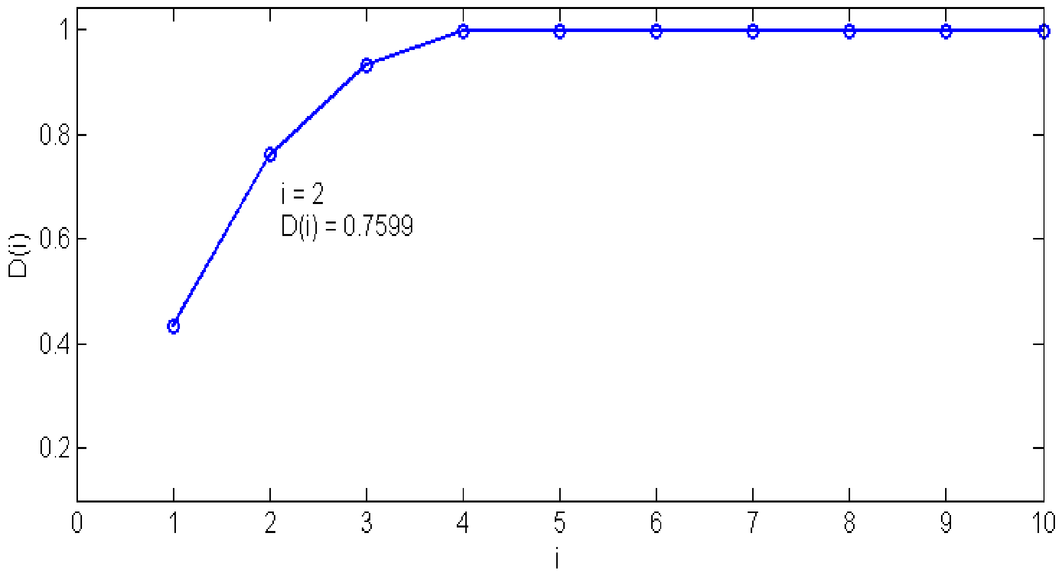

Figure 4.8: D(i) vs i plot of Signal 1 at 5 dB SNR.

Similarly, while analysing signals with higher number of frequency components, like Signal 3, using the TLS ESPRIT method, there are chances of under estimation of model order for the chosen value of D(i). Fig. 4.9 shows the D(i) vs i plots of Signal 3 with 15 dB SNR. From the graph, it can be concluded that the optimum value of D(i) for accurate estimation of the model order of this signal is around 0.99. If the value of D(i) used in the TLS ESPRIT method is less than this optimum value, then one or more modes present in the signal are not estimated. Moreover, the estimated modes are inaccurate with a high degree of error. This is evident from the estimated results of Signal 3 using TLS ESPRIT method

Table 4.2: Estimated model order and modal parameters of the proposed method and TLS-ESPRIT method for different signals [48]

SNR	**TLS-ESPRIT**									**EMO ESPRIT**		
(dB)	**D(i) = 0.935**			**D(i) = 0.99**			**D(i) = 0.995**					
	MO	**Freq**	**AF**	**MO**	**Freq**	**AF**	**MO**	**Freq**	**AF**	**MO**	**Freq**	**AF**
					Signal 1							
	4	0.1999	0.1683		0.1992	0.1763	90	0.1981	AF	2	0.1990	0.1743
5		0.7500	0.1304	46	0.7475	0.1279		0.7525	AF		0.7490	0.1281
		9.226	0.0122		+ 44 other			+ 88 other				
		17.847	0.0733		components			components				
	4	0.2004	0.1712	4	0.1999	0.1716	4	0.2000	0.1717	2	0.2001	0.1708
10		0.7419	0.1193		0.7462	0.1272		0.7500	0.1299		0.7500	0.1301
		14.6867	-.0002		10.312	0.0076		7.6169	0.0242			
					18.799	-.0321		16.9532	0.0499			
	3	0.1999	0.1701	4	0.2000	0.1693	4	0.2000	0.1689	2	0.1998	0.1698
15		0.7500	0.1301		0.7500	0.1301		0.7499	0.1301		0.7500	0.1311
		14.224	0.0063		10.7566	-0.0011		10.6568	0.0074			
					8.5599	0.0003		19.2177	-.0107			
					Signal 2							
	2	0.2613	0.0177	4	0.2007	0.1717	4	0.2015	0.1732	3	0.2004	0.1744
5		0.7374	0.0855		0.2805	0.0522		0.2804	0.0512		0.2803	0.0509
					0.7500	0.1313		0.7503	0.1324		0.7497	0.1322
					12.6422	0.0014		13.573	0.0014			
	2	0.2612	0.0177	4	0.2014	0.1687	4	0.2005	0.1697	3	0.2002	0.1721
10		0.7371	0.0830		0.2802	0.0512		0.2802	0.0504		0.2800	0.0509
					0.7499	0.1296		0.7501	0.1308		0.7500	0.1311
					14.217	0.0071		14.487	0.0182			
	2	0.2611	0.0177	4	0.2002	0.1726	4	0.2003	0.1694	3	0.1999	0.1706
15		0.7375	0.0834		0.2800	0.0508		0.2801	0.0500		0.2800	0.0500
					0.7500	0.1302		0.7500	0.1308		0.7499	0.1310
					13.886	-0.0006		15.103	-0.6663			
					Signal 3							
	3	0.3025	0.2699	4	0.2478	0.1714	6	0.2490	0.1771	4	0.2492	0.1745
5		.7224	0.0697		0.3314	0.1235		0.3311	0.1139		0.3300	0.1189
		.8641	0.1127		0.7810	0.1295		0.7803	0.1346		0.7817	0.1305
					0.8697	0.0714		0.8698	0.0701		0.8703	0.0706
								8.2821	0.0067			
								16.469	-0.0015			
	3	0.3025	0.2731	4	0.2504	0.1724	5	0.2496	0.1695	4	0.2503	.1694
10		0.7217	0.0696		0.3302	0.1174		0.3296	0.1234		0.3301	0.1216
		0.8643	0.1130		0.7799	0.1296		0.7802	0.1281		0.7801	0.1291
					0.8702	0.0710		0.8702	0.0707		0.8699	0.0707
								15.826	0.0071			
15	3	0.3027	0.2729	4	0.2497	0.1714	5	0.2503	0.1705	4	0.2501	0.1699
		0.7228	0.0680		0.3301	0.1201		0.3299	0.1191		0.3301	0.1193
		0.8642	0.1130		0.7800	0.1300		0.7798	0.1303		0.7801	0.1291
					0.8700	0.0705		0.8701	0.0700		0.8699	0.0703
								10.944	-0.002			

when D(i) is set as 0.935. In this case, only three modes out of four of Signal 3 are identified and the error in the frequency and damping estimation of these modes are quite high.

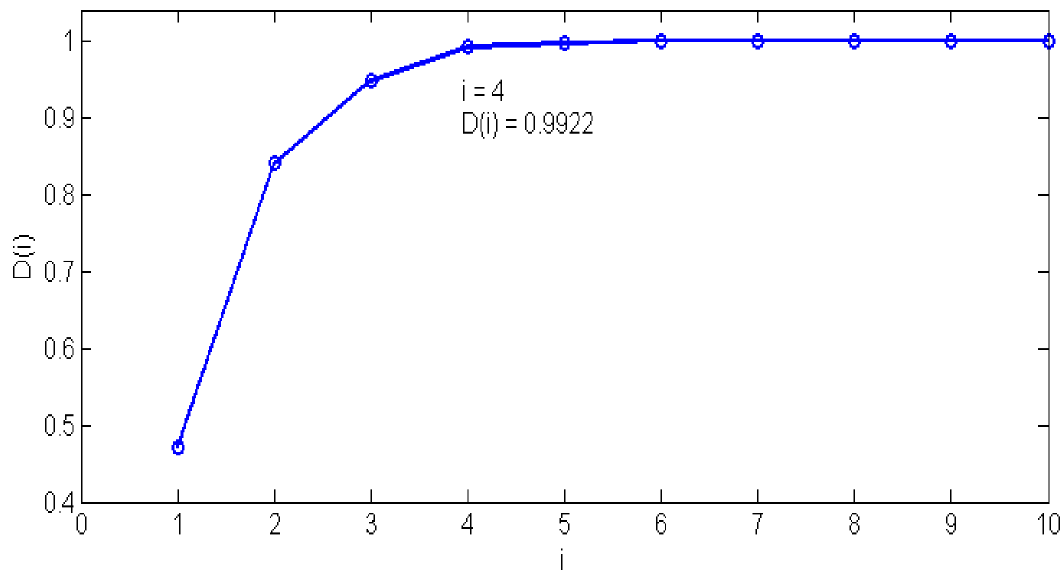

Figure 4.9: D(i) vs i plot of Signal 3 at 15 dB SNR.

Hence, it can be inferred that the model order estimation algorithm in [48] is not accurate and its results depend upon the D(i) value chosen. On the other hand, the proposed method uses EMO algorithm for estimating the model order. In this algorithm, the model order is estimated based on the Relative Difference (RD) vector generated from the eigenvalues of the autocorrelation matrix. It is observed that irrespective of the noise contamination of the signal, EMO algorithm estimates the model order accurately making it best suited for analysing low frequency oscillations than TLS ESPRIT method.

Table 4.3: Comparison of the true mode extraction capability of the proposed method with ARMA [59], Modified Prony [44] and TLS ESPRIT [48] methods

SNR (dB)	**Signal 2**								**Signal 3**							
	TLS ESPRIT		**EMO ESPRIT**		**PRONY**		**ARMA**		**TLS ESPRIT**		**EMO ESPRIT**		**PRONY**		**ARMA**	
	γ_1	γ_2	γ_1	γ_2	γ_1	γ_2	γ_1	γ_2	γ_1	γ_2	γ_1	γ_2	γ_1	γ_2	γ_1	γ_2
5	49	1	49	1	17	33	8	42	42	8	44	6	17	33	-	-
10	50	0	50	0	18	32	11	39	47	3	49	1	19	31	10	40
15	50	0	50	0	20	30	12	38	50	0	50	0	22	28	11	39
20	50	0	50	0	25	25	14	36	50	0	50	0	24	26	13	37

γ_1 Number of times all the modes in the signal are estimated.
γ_2 Number of times only some modes in the signal are estimated.

Table 4.3 compares the true mode extraction capability of the proposed method with that of the TLS-ESPRIT method [48], modified Prony method [44] and ARMA method [59]. Fifty independent simulations of Signal 2 and Signal 3 are carried out at SNRs of 5 dB, 10 dB, 15 dB and 20 dB for this purpose. For effective comparison of these methods, two new terms, γ_1 and γ_2 are introduced. γ_1 of a particular method refers to the number of times, out of fifty simulations, all the modes present in the signal are identified by that method whereas γ_2 refers to the number of times, only some modes are identified. It is noticed that irrespective of the noise content present in the signal, the proposed EMO ESPRIT based method and TLS ESPRIT based method in [48] identifies all the modes present in the signal consistently during successive simulations whereas the performance of the ARMA and Modified Prony based methods is quite poor. For instance, while estimating the modal parameters of the Signal 3 with 5 dB SNR, the percentage of successful estimation of all modes in the signal is 88% for the proposed method while that of the modified Prony method is only 34%. The ARMA method is not able to detect all the modes in this case. It is also noticed that the estimated results of the ARMA, Modified Prony and TLS ESPRIT methods contain fictitious modes whereas that of the proposed method contains true modes only. If prior information is not available about the modes of the signal being estimated, then accurate estimation of these modes may not be possible. So it can be inferred that the proposed model has better true mode extraction capability than the models in [44], [48] and [59].

In practical scenario, the PMU reporting rate vary from 10 Hz to 120 Hz. Therefore, simulations have been carried out to verify the performance of the proposed method with change in PMU reporting rate and the results obtained are listed in Table 4.4. Fifty independent simulation of signal 3 at each reporting rate is performed for this purpose and the frequency and damping is estimated by taking the means of these 50 simulations. It is observed that irrespective of the reporting rates of the PMU, all the modes were accurately estimated even though the signal has close modes. It is also noted that the error in the frequency estimation is negligible even at low reporting rates. For instance, when the PMU reporting rate is 10 Hz, the absolute error in the frequency and damping estimation is only 0.28% and 2% respectively. It is also observed that, at higher reporting rates, the results of the estimation are better than that of low rates. The standard deviation of the measurements of the modal parameters is also quite small as expected. Therefore, it can be concluded that the proposed method is quite robust even under low reporting rate conditions and high noise levels.

Table 4.4: Performance of the proposed method for Signal 3 with change in PMU reporting rate

PMU reporting rate (Hz)	γ_1	γ_2	**Estimated**		**Standard deviation**		**Absolute percentage Error**	
			Freq (Hz)	**AF**	**Freq (Hz)**	**AF**	**Freq (Hz)**	**AF**
10	50	0	0.2507	0.1729	0.0054	0.0207	0.2800	1.712
			0.3300	0.1187	0.0027	0.0133	0	1.086
			0.7798	0.1303	0.0024	0.0116	0.0256	0.238
			0.8700	0.0699	0.0012	0.0057	0	0.7112
20	50	0	0.2496	0.1708	0.0032	0 .0157	0.0112	0.47
			0.3308	0.1193	0.0021	0.0112	0.2446	0.58
			0.7800	0.1294	0.0016	0.0071	0	0.46
			0.8700	0.0707	0.00068	0.0043	0	0.426
30	50	0	0.2508	.1725	0 .0027	0.0117	0.32	1.47
			0.3298	0.1182	0.0018	0.00085	0.0606	1.5
			0.7797	0.1293	0.0014	0.0073	0.0384	0.53
			0.8701	0.0708	0.00061	0.0040	0.011	.56
60	50	0	0.2499	0.1703	0.0017	0.0080	0.04	0.1764
			0.3302	0.1197	0.0011	0.0060	0.0606	0.2546
			0.7801	0.1300	0.00071	0.0049	0.0128	0
			0.8700	0.0708	0.00046	0.0022	0	0.5612
100	50	0	0.2500	0.1703	0.0014	0.0065	0	0.171
			0.3300	0.1210	0.00086	0.0046	0	0.833
			0.7801	0.1296	0 .00065	0.0038	0.0128	0.3243
			0.8700	0 .0703	0.00038	0.0016	0	0.1412
120	50	0	0.2500	0.1699	0.0009	0.0047	0	0.058
			0.3300	0.1200	0.0006	0.0028	0	0
			0.7800	0.1299	0 .0005	0.0008	0	0.081
			0.8700	0.0703	0.0002	0.0009	0	0.1412

4.3.2 Real time PMU data

To further validate the ability of the proposed method to estimate the modal parameters of real time signals, it is tested using the PMU data from WECC system obtained on 14^{th} September 2005. The details about the WECC system and the analysis windows used are explained in Section 3.3.2. The modal estimation of the signals corresponding to these analysis windows are carried out using the proposed method, TLS-ESPRIT method [48], modified Prony method [44] and ARMA method [59] at different SNRs and the estimated results are tabulated in Tables 4.5 and 4.6.

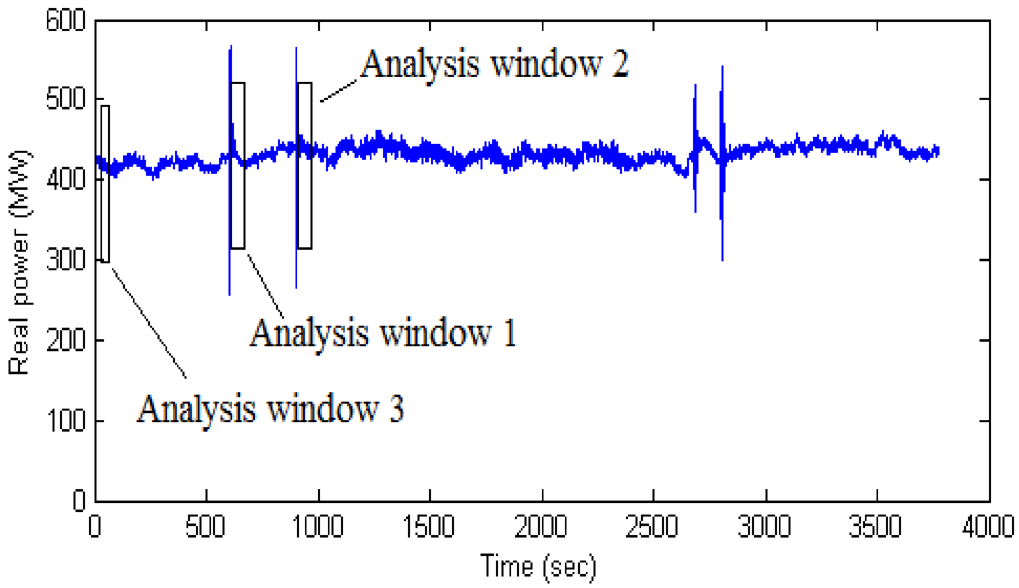

Figure 4.10: Probing data corresponding to flow of real power MALN-Round Mountain 1 line of the WECC system [85]

Table 4.5: Frequencies and damping ratios of WECC system probe data

Window	Estimated value from [84]		TLS-ESPRIT		EMO ESPRIT		Modified Prony		ARMA	
	Frequency (Hz)	ζ	Frequency (Hz)	ζ	Frequency (Hz)	ζ	Frequency (Hz)	ζ	Frequency (Hz)	ζ
Window 1	0.318	8.30	0.3259	6.86	0.3207	8.30	0.3167	8.87	0.3626	12.54
Window 2	-	-	0.3151	7.78	.3149	7.88	0.3143	8.25	0.4010	6.78
Window 3	-	-	0.2991	2.43	0.2720	2.81	0.2635	2.74	.02826	3.49

Table 4.6: Frequencies and damping ratios of WECC system probe data under different noise levels

Window	SNR=5 dB		SNR=10 dB		SNR=15 dB		SNR=20 dB	
	Frequency (Hz)	ζ	Frequency (Hz)	ζ	Frequency (Hz)	ζ	Frequency (Hz)	ζ
Window 1	0.3207	8.28	0.3208	8.32	0.3207	8.30	0.3207	8.29
Window 2	0.3157	7.95	0.3149	7.97	0.3143	8.00	0.3146	8.00
Window 3	0.2747	2.78	0.2799	2.83	0.2722	3.07	0.2719	2.84

It is noticed from Table 4.5 that the modal parameter estimates of the signal corresponding to analysis window 1 obtained through the proposed method (0.3207 Hz mode with 8.3% damping) are closest to the reported values in [84] whereas ARMA, the modified Prony and the TLS-ESPRIT methods gave less accurate estimation of this mode. Similar observation are made for analysis window 2 and 3 where the proposed method gave a good estimate of the frequency and damping of the modes present in these windows.

Table 4.6 shows that the proposed method can accurately estimate the modal parameters accurately irrespective of the noise content present in the signal under consideration. Thus, it can be inferred that, the proposed method is better suited for the estimation of real time signals. However, this algorithm is slightly more computationally intensive than similar methods and hence, its implementation requires a powerful processor.

4.4 Conclusion

An ESPRIT based technique for estimating the poorly damped modes in the ringdown oscillations occurring in the power system is proposed in this chapter. ESPRIT being a parametric method requires accurate estimate of the model order for its proper implementation, which is provided through Exact Model Order algorithm. It is observed that the proposed method estimates the modal parameters of the signals accurately even under high levels of noise and low PMU reporting rates. The effectiveness of the proposed method is compared with an ARMA, the TLS-ESPRIT and the modified Prony based methods in the literature using synthetic signals as well as test probe data from WECC system. Simulation results prove that the proposed method consistently provides accurate estimation of modal parameters of the signal under consideration without the presence of fictitious modes irrespective of the noise contamination, presence of close modes in the signal and low PMU reporting rates.

Chapter 5

An improved Stochastic Subspace Identification based algorithm for analyzing ambient oscillations

5.1 Introduction

The modal estimation algorithms for ringdown type oscillations is already proposed in Chapters 3 and 4. However, it is observed that these methods are not a suitable choice for the analysis of ambient type of oscillations. Ambient type oscillations occur due to small level disturbances in the power system and they exist for a longer period than ringdown oscillations. Therefore, the data associated with ambient oscillations is considerably larger than ringdown oscillations. SSI is a parametric technique which can handle large amounts of data and dynamic changes in the system. This makes SSI one of the best choices for analyzing the ambient oscillations.

Few SSI based works [88, 89] selected the model order based on the dominant singular values. In [54], the model order is estimated based on the large reduction in singular values of the weighted projection matrix. However, when the signal under consideration is highly noisy, the accuracy of model order estimate of these methods is quite poor. A method based on the mean of singular values is proposed in [52] but it causes overestimation of model order resulting in the presence of trivial modes. Estimation of the model order based on stabilization diagram is proposed in [63] but the complexity of the algorithm limits its application. Hence, it can be inferred that the model order algorithms in [52, 63, 88, 89] may not give the accurate results. If the model order is not accurately estimated, it will cause trivial modes in the estimated results. Separate clustering and refinement algorithms will be required to remove these trivial modes from the true modes of the signal. However, if the model order is accurately estimated, the true modes of the signal can be identified directly without the use of separate refinement algorithms.

Therefore, this work proposes an SSI based method for power system modal identification where the model order of the signal is accurately estimated using Exact Model Order (EMO) algorithm [86] explained in Section 4.2.1. Further, Stationary Wavelet Transform (SWT) based denoising technique is included in the proposed SSI based method to improve its noise resistance. The robustness of the proposed method is verified by comparing it with an SSI based method [52], Teager Kaiser based method [68] and a Fourier based method [60] using synthetic signals. Finally, the proposed method is used to estimate the dominant modes of real time PMU data obtained from Western Electricity Coordinating Council (WECC) system.

5.2 Proposed Methodology

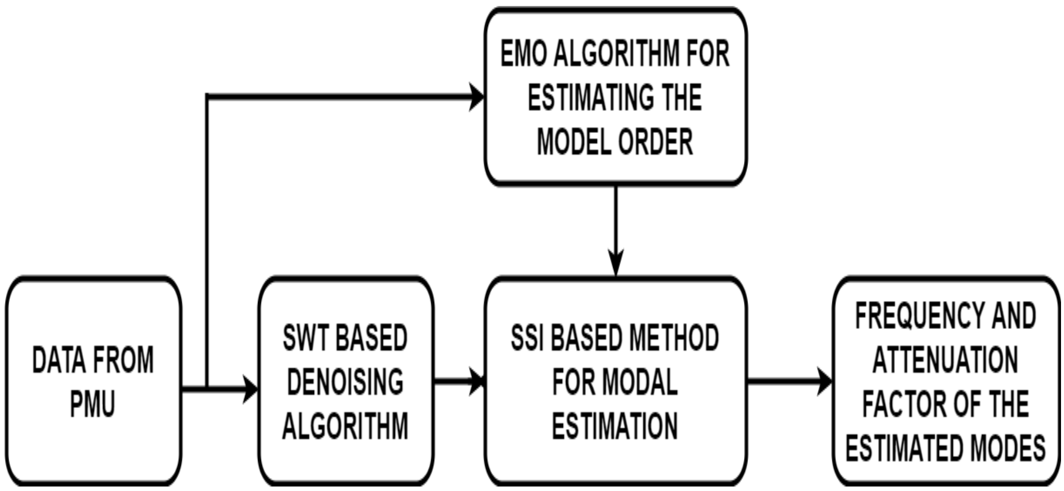

Figure 5.1: Block diagram of the proposed method.

The schematic representation of the proposed SSI based method for estimating the modal parameter estimates of low frequency electromechanical oscillations is shown in fig. 5.1. In this method, the data obtained from PMUs placed across the power system is filtered using an SWT based filter for removing the noise contamination before passing it into the SSI based algorithm. The modal parameters of this filtered data is then identified using the SSI algorithm and the results are passed to the control centre for further action. SSI being a parametric method requires an initial estimate of model order for its successful implementation. However, similar SSI based algorithms [52, 53] proposed recently, overestimated the model order leading to the presence of fictitious modes in their estimated results. Separate filtering algorithms are required for identifying the true modes from these fictitious modes. However, these filtering algorithms increases the computational complexity of the whole method and makes its real time implementation difficult. A detailed explanation of this problem is given in subsection 5.2.2. Hence, to prevent the above issues, the model order estimation of the proposed method is carried out using Exact Model Order (EMO) algorithm. EMO algorithm estimates the model order of the signal accurately irrespective of its noise contamination. Hence the limitations in [52, 53] are not present in the proposed method. A detailed explanation of all the components of the proposed method is given in the following subsections.

5.2.1 Stationary Wavelet Transform (SWT) Based Denoising

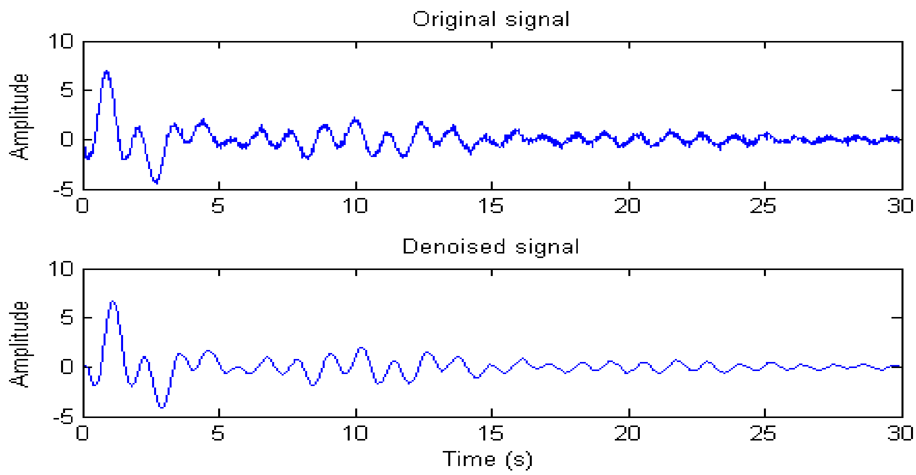

Figure 5.2: Original and denoised signal using SWT algorithm.

The data from the PMU will have noise present in it. The accuracy of modal parameter estimates of the proposed method can be improved if the noise contamination present in the PMU data is removed. Therefore, an SWT based denoising technique is employed in the proposed method for this purpose. SWT is a wavelet transform algorithm, which is similar to Discrete Wavelet Transform (DWT). However, the lack of translation invariance, which is one of the main drawbacks of DWT, is not present in SWT. The SWT based denoising provides enhanced signal to noise ratio and less mean and peak errors compared to other denoising methods [90, 91]. In the proposed method, the SWT based denoising algorithm uses symlet wavelet with three decomposition levels for denoising the PMU data. The ability of the SWT based technique to effectively denoise the noisy signal is shown in fig. 5.2 using a two mode signal having an SNR of 15 dB. From the figure, it is evident that the distortions present in the original signal are not present in its denoised version. Hence, it can be inferred that the noise content in the signal is substantially reduced in the denoised version.

5.2.2 Model Order Estimation

SSI being a parametric method requires an accurate estimate of the model order or number of frequency components present in the signal for its proper implementation. In most of the SSI based methods, the model order is estimated based on the dominant singular values of the weighted projection matrix. The recently published SSI based methods use an algorithm based on the average of singular values. If $\beta_1, \beta_2, ...\beta_k$ are the singular values obtained by the Singular Value Decomposition of the weighted projection matrix, then their β_{avg} is calculated as

$$\beta_{avg} = \frac{1}{k}\sum_{i=1}^{k}\beta_i \tag{5.1}$$

The model order r is estimated as

$$r = \left\{ \begin{array}{ll} a, & \beta_{a+1} \leq \beta_{avg} \leq \beta_a,\ int(a/2) = a/2 \\ a+1, & \beta_{a+1} \leq \beta_{avg} \leq \beta_a,\ int(a/2) < a/2 \end{array} \right\} \tag{5.2}$$

This technique accurately estimates the model order of signals with less noise content. However, when the signal is highly noisy, the model order of the signal is grossly overestimated. The main reason for this overestimation is that when the signal is highly noisy, there is little difference between the singular values of the signal and noise subspace. This is proved with the help of an example.

Let x_1 be a power system signal with four frequency components as shown below [92].

$$\begin{aligned} x_1 = ((1\cos(2\pi * 0.4t)\exp(-0.0909t)) \\ + (0.9\cos(2\pi * 0.5t)\exp(-0.35t)) \\ + (0.7\cos(2\pi * 0.6t + (\pi/6))\exp(-0.2001t)) \\ + (0.4\cos(2\pi * 1.1t + (\pi/4)).*\exp(-0.666t))); \end{aligned} \tag{5.3}$$

x_1 has a length of 30 seconds and it is sampled at 50 Hz. It is contaminated by adding white Gaussian noise at 50 dB SNR. The value of i and j which are used for generating the Hankel matrices Y_f and Y_p of the SSI method are set as 200 and 1000 respectively.

The block Hankel matrix of x_1 is obtained from the signal data which is used to generate the weighted projection matrix. The following S matrix is obtained from the SVD of this weighted projection. The singular values of the S matrix and its row location are given in Table 5.1.

Table 5.1: Singular values of x_1

Row no.	**1**	**2**	..	**7**	**8**	**9**	**10**	**11**	**12**	..	**35**	..	**70**	..	**200**
							without noise								
Singular value	2.36	2.36	..	2.35	2.32	$8.5e^{-7}$	$2.0e^{-7}$	$1.7e^{-7}$	..	..	$8.3e^{-7}$	..	$76.9e^{-8}$	..	$7.1e^{-9}$
							with 50 dB noise								
Singular value	2.23	2.23	..	2.02	1.92	1.72	1.72	1.67	..	..	1.36	..	1.08	..	0.002

It is noticed from Table 5.1 that, when the noise content is not present in the signal, the first eight singular values of the weighted projection are high and rest of the singular values are very low. These eight singular values represent the four dominant modes present in x_1 as each mode is represented by two singular values. Rest of the singular values represent the trivial modes. However, when the signal is highly noisy, the dominant modes cannot be distinguished easily as the difference between consecutive singular values is less.

The mean of the singular values of the corrupted signal is found to be 0.8720 and the model order of the signal having only four frequency components is estimated as 98 using (5.2). The true modes present in the signal are identified from the 94 other fictitious modes using separate filtering algorithms. In this algorithm, the model order is varied from an initial value to a higher value and separate discrete system state matrices are calculated corresponding to each model order. The eigenvalues which are present in all these discrete system state matrices represent the dominant modes of the signal. After running this algorithm, the four dominant modes of the x_1 are identified . However, the construction of numerous discrete system state matrices and its eigen decomposition (for finding the eigenvalues) increases the computational complexity of this method limiting its real time implementation. Hence, EMO algorithm is used in the proposed method for estimating the model order accurately. The details about the EMO algorithm is given in Section 4.2.1.

To prove the effectiveness of the EMO algorithm, it is used to estimate the model order

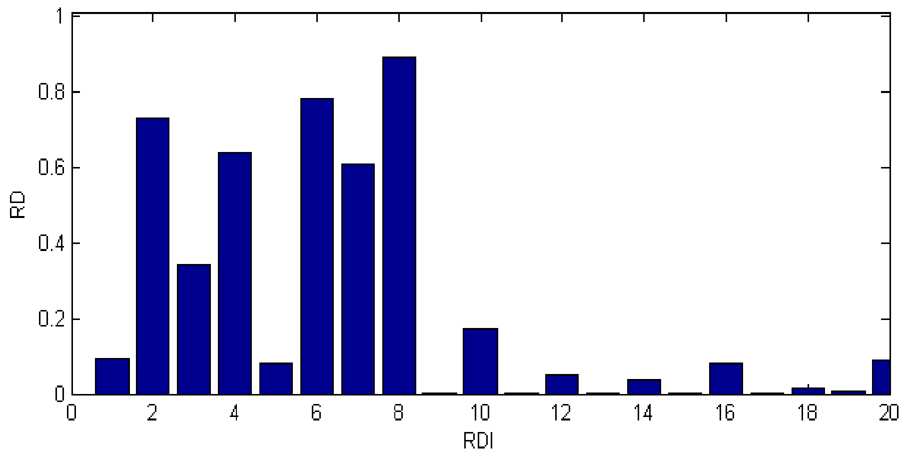

Figure 5.3: RD vs RDI plot of signal x_1.

of the signal in (5.3). The autocorrelation matrix is created using the signal data and vector RD obtained from its eigenvalues is calculated for this purpose. Fig. 5.3 shows the RD vs RDI plot of this signal corresponding to the first 20 eigenvalues. It is observed that RD has peaks at RDI values of $2,4,6,7$ and 8. The preliminary model order estimate is 8 as it is the highest RDI value. The eigenvalue corresponding to this model order estimate satisfies (4.6). So, the estimated value of the model order is $RDI/2 = 4$, which is the correct value.

5.2.3 Stochastic Subspace Identification [53, 54]

The power system data obtained from the PMUs is discrete in nature. It can be represented as

$$\mathbf{x}((\mathbf{k}+\mathbf{1})\mathbf{T}) = \mathbf{A}\mathbf{x}(\mathbf{kT}) + \mathbf{w}(\mathbf{kT}) \tag{5.4}$$

$$\mathbf{y}(\mathbf{kT}) = \mathbf{C}\mathbf{x}(\mathbf{kT}) + \mathbf{v}(\mathbf{kT}) \tag{5.5}$$

where, T is the sampling time, k is the sampling number, $\mathbf{x}\varepsilon\mathbf{R}^{\mathbf{n}}$ is the discrete time state vector, $\mathbf{y}\varepsilon\mathbf{R}^{\mathbf{l}}$ is the output vector and $\mathbf{A}\varepsilon\mathbf{R}^{\mathbf{n}\times\mathbf{n}}$ is the discrete system state matrix. $\mathbf{w}\varepsilon\mathbf{R}^{\mathbf{n}}$ and $\mathbf{v}\varepsilon\mathbf{R}^{\mathbf{l}}$ represent process disturbance and measurement noise respectively. The dominant modes of the power system are estimated from the eigenvalues of discrete system state matrix. In this method, the discrete system state matrix $\mathbf{A}$ is generated from the PMU data using Canonical Variate Algorithm (CVA).

The key steps of CVA are given below.

Step 1: Create a block Hankel matrix $Y_{0|2i-1}$ from the PMU data.

$$\mathbf{Y_{0|2i-1}} = \begin{pmatrix} y_0 & y_1 & .. & y_{j-1} \\ y_1 & y_2 & .. & y_j \\ .. & .. & .. & .. \\ y_{i-1} & y_i & .. & y_{i+j-2} \\ .. & .. & .. & .. \\ y_{2i-1} & y_{2i} & .. & y_{2i+j-2} \end{pmatrix} \tag{5.6}$$

Here, the subscript $0|2i-1$ represents the first and last element of the first column of block Hankel matrix $Y_{0|2i-1}$. The value of i is set as $2Q/l$, where, Q and l denotes the expected maximum order of the system and the number of its output channels respectively. The value of Q is selected such that it is higher than the actual model order of the system.

Step 2: Form past matrices Y_p, Y_p^+, and the future matrices Y_f and Y_f^- from $Y_{0|2i-1}$.

$$\mathbf{Y_p} = \begin{pmatrix} y_0 & y_1 & .. & y_{j-1} \\ y_1 & y_2 & .. & y_j \\ .. & .. & .. & .. \\ y_{i-1} & y_i & .. & y_{i+j-2} \end{pmatrix} = \mathbf{Y_{0|i-1}} \tag{5.7}$$

$$\mathbf{Y_f} = \begin{pmatrix} y_i & y_{i+1} & .. & y_{i+j-1} \\ y_{i+1} & y_{i+2} & .. & y_{i+j} \\ .. & .. & .. & .. \\ y_{2i-1} & y_{2i} & .. & y_{2i+j-2} \end{pmatrix} = \mathbf{Y_{i|2i-1}} \tag{5.8}$$

$\mathbf{Y_f^-} = \mathbf{Y_{i+1|2i-1}}$ and $\mathbf{Y_p^+} = \mathbf{Y_{0|i}}$

Here $\mathbf{Y_f^-}$ is generated from $\mathbf{Y_f}$ by deleting its first row whereas $\mathbf{Y_p^+}$ is obtained from $\mathbf{Y_p}$ by adding one more row to its end.

Step 3: Obtain the projection matrices $\mathbf{O_i}$ and $\mathbf{O_{i-1}}$ from $\mathbf{Y_f}$, $\mathbf{Y_f^-}$, $\mathbf{Y_p}$ and $\mathbf{Y_p^+}$.

$$\mathbf{O_i} = \mathbf{Y_f}/\mathbf{Y_p} \tag{5.9}$$

$$\mathbf{O_{i-1}} = \mathbf{Y_f^-}/\mathbf{Y_p^+} \tag{5.10}$$

Here, $\mathbf{Y_f}/\mathbf{Y_p} = \mathbf{Y_f}\mathbf{Y_p^t}(\mathbf{Y_p}\mathbf{Y_p^t})^{\dagger}\mathbf{Y_p}$. † denotes pseudo inverse of the matrix.

Step 4: Compute the weighting matrices $\mathbf{W_1}$ and $\mathbf{W_2}$ using the following equation

$$\mathbf{W_1} = ((1/j)\mathbf{Y_f}\mathbf{Y_f^t})^{(-1/2)} \tag{5.11}$$

$$\mathbf{W_2} = \mathbf{I_j} \tag{5.12}$$

here, $\mathbf{I_j}$ represent an identity matrix of size $j \times j$.

Step 5: Perform Singular Value Decomposition of the weighted projection $\mathbf{W_1 O_i W_2}$

$$\mathbf{W_1 O_i W_2} = \mathbf{USV^t} = \begin{pmatrix} \mathbf{U_1} & \mathbf{U_2} \end{pmatrix} \begin{pmatrix} \mathbf{S_1} & \mathbf{0} \\ \mathbf{0} & \mathbf{0} \end{pmatrix} \begin{pmatrix} \mathbf{V_1^t} \\ \mathbf{V_2^t} \end{pmatrix} \tag{5.13}$$

here, $\mathbf{U}$ and $\mathbf{V}$ are the matrices containing the left and right singular vectors of the weighted projection $\mathbf{W_1 O_i W_2}$ obtained through the Singular Value Decomposition whereas the matrix $\mathbf{S}$ contains its singular values. $\mathbf{S_1}$ is a $q \times q$ submatrix of $\mathbf{S}$, which contains all the singular values corresponding the signal subspace, where q is twice the actual model order of the system.

Step 6: Obtain the extended observability matrices $\mathbf{T_i}$ and $\mathbf{T_{i-1}}$ using the following equation.

$$\mathbf{T_i} = \mathbf{W_1^{-1} U_1 S_1^{1/2}} \tag{5.14}$$

$\mathbf{T_{i-1}}$ is obtained from $\mathbf{T_i}$ by removing its last l rows.

Step 7: Calculate the Kalman filter state sequences $\mathbf{X_i}$ and $\mathbf{X_{i+1}}$.

$$\mathbf{X_i} = \mathbf{T_i^{\dagger} O_i} \tag{5.15}$$

$$\mathbf{X_{i+1}} = \mathbf{T_{i-1}^{\dagger} O_{i-1}} \tag{5.16}$$

Step 8: State space matrix A is determined as

$$\begin{pmatrix} \mathbf{A} \\ \mathbf{C} \end{pmatrix} = \begin{pmatrix} \mathbf{X_{i+1}} \\ \mathbf{Y_{i|i}} \end{pmatrix} \mathbf{X_i^{\dagger}} \tag{5.17}$$

Step 9: The frequency (f_k) and attenuation factor (AF_k) of the modes present in the signal is obtained from eigenvalues (λ_k) of **A**.

$$f_k = f_s * \frac{imag(log(\lambda_k))}{2\pi} \tag{5.18}$$

$$AF_k = f_s * real(log(\lambda_k)) \tag{5.19}$$

Here, f_s is the sampling frequency of the signal. The damping coefficient (ζ_k) of the mode is obtained using the following equation [55].

$$\zeta_k = -\frac{AF_k}{\sqrt{(AF_k)^2 + (2\pi * f_k)^2}} \tag{5.20}$$

5.3 Simulation Results and Discussion

The implementation of the proposed SSI based model depends on its ability to extract the modal information of different signals irrespective of its signal to noise ratio. Hence, the proposed SSI based model is tested on simulated signals with known modal parameters at different SNRs and real time signals obtained from PMUs installed on different power systems. The results obtained are compared with that of similar models in the literature.

5.3.1 Synthetic Signals

The simulated signals used for this comparison are given below.

$$\begin{split} Signal\ \ 1 = (2\cos(2\pi * 0.2t + 1.5\pi))\exp(-0.17t) \\ + 2\cos(2\pi * 0.75t + (0.5\pi))\exp(-0.13t) \end{split} \tag{5.21}$$

$$\begin{split} Signal\ \ 2 = 2\cos(2\pi * 0.2t + (1.5\pi))\exp(-0.17t) \\ + 2\cos(2\pi * 0.28t + (0.5\pi))\exp(-0.05t) \\ + (2\cos(2\pi * 0.75t + (4.5\pi))\exp(-0.13t))); \end{split} \tag{5.22}$$

$$\begin{aligned} Signal\ 3 = {} & (2\cos(2\pi * 0.25t + (1.5\pi))\exp(-0.17t)) \\ & + (2\cos(2\pi * 0.33t + (1.5\pi))\exp(-0.12t)) \\ & + (2cos(2\pi * 0.78t + (0.5\pi))\exp(-0.13t)) \\ & + (2cos(2\pi * 0.87t + (0.5\pi))\exp(-0.0702t))); \end{aligned} \tag{5.23}$$

All these signals have a frequency between 0.2 Hz to 0.9 Hz. Signal 1 has a pair of closely spaced modes whereas Signal 2 has two pairs of closely spaced modes. The modal information present in these signals are extracted through the proposed method, Matrix Pencil [93], Eigen Realization Algorithm (ERA) [93], SSI [52], Teager Kaiser [68] and Fourier [60] based methods. As explained in the previous section, the proposed method requires accurate model order estimates for extracting the modal information of the signal precisely. The proposed method uses Exact Model Order algorithm for this purpose. The superiority of this algorithm is proved by comparing it with model order estimation algorithms of ERA and Matrix Pencil based methods in [93] at different SNRs. The results obtained from this comparison is tabulated in Table 5.2.

It is observed from Table 5.2 that accuracy of the modal information extracted through the proposed method, ERA and Matrix Pencil based methods [93] is comparable. However, it is noticed that estimated results in ERA and Matrix Pencil based methods has fictitious modes along with the true modes especially at low SNRs. This occurs due to the poor accuracy of its model order estimation algorithms. These algorithms work based on the ”largest drop method” in which the ratio of singular values of Hankel matrix is compared. However, at low SNRs, there is not much difference between the singular values of the signal and noise subspace. Due to this reason, the largest drop method fails to estimate the accurate model order estimate. If these algorithms are used, separate filtering algorithms will be required for identifying the true modes from the fictitious modes. On the other hand, the eigenvalues of the EMO algorithm is generated from the autocorrelation matrix generated from the signal which is more robust than the similar algorithms in [93]. For instance, the proposed method accurately estimates the model order of the Signal 3 at 15 dB SNR as 4 whereas the model order estimation of the Matrix Pencil and ERA methods are 237 and 292 respectively. Hence, it can be inferred that the EMO algorithm used in the proposed model is better suited for model order estimation than similar algorithms of ERA and Matrix Pencil based methods in [93].

Table 5.2: Comparison of model order and estimated modal parameters of the proposed method with Matrix Pencil [93] and ERA [93] based methods

	SNR = 15 dB			SNR = 20 dB			SNR = 25 dB		
Method	**MO**	**Estimated**		**MO**	**Estimated**		**MO**	**Estimated**	
		Freq (Hz)	**AF**		**Freq (Hz)**	**AF**		**Freq (Hz)**	**AF**
Signal 1									
True value		0.200	0.170		0.200	0.170		0.200	0.170
		0.750	0.130		0.750	0.130		0.750	0.130
Proposed method	2	0.2000	0.1665	2	0.2000	0.1710	2	0.2001	0.1703
		0.7499	0.1292		0.7500	0.1306		0.7500	0.1299
ERA	280	0.2010	0.1719	214	0.2001	0.1694	68	0.2000	0.1692
		0.7498	0.1250		0.7502	0.1296		0.7504	0.1300
	+ 278 modes			+ 212 modes			+ 66 modes		
Matrix Pencil	295	0.2001	0.1695	213	0.2002	0.1708	80	0.2000	0.1701
		0.7501	0.1292		0.7500	0.1306		0.7500	0.1295
	+ 291 modes			+ 209 modes			+ 76 modes		
Signal 3									
True value		0.250	0.170		0.250	0.170		0.250	0.170
		0.330	0.120		0.330	0.120		0.330	0.120
		0.780	0.130		0.780	0.130		0.780	0.130
		0.870	0.070		0.870	0.070		0.870	0.070
Proposed method	4	0.2503	0.1669	4	0.2507	0.1701	4	0.2501	0.1697
		0.3302	0.1189		0.3300	0.1224		0.3300	0.1197
		0.7803	0.1308		0.7802	0.1310		0.7799	0.1294
		0.8700	0.0695		0.8700	0.0706		0.8700	0.0698
ERA	292	0.2504	0.1670	214	0.2498	0.1682	94	0.2497	0.1697
		0.3303	0.1199		0.3299	0.1222		0.3304	0.1216
		0.7799	0.1241		0.7794	0.1302		0.7802	0.1280
		0.8703	0.0702		0.8697	0.0698		0.8699	0.0718
		+ 288 modes			+ 210 modes			+ 90 modes	
Matrix Pencil	237	0.2500	0.1702	109	0.2500	0.1700	8	0.2499	0.1703
		0.3301	0.1187		0.3301	0.1206		0.3300	0.1197
		0.7802	0.1303		0.7800	0.1297		0.7800	0.1300
		0.8699	0.0699		0.8701	0.0707		0.8700	0.0701
		+ 233 modes			+ 105 modes			+ 4 modes	

Table 5.3 compares the frequency and attenuation factor estimates of different synthetic signals obtained through proposed method, Teager Kaiser based method [68], SSI method [52] and Fourier method [60]. The frequency and attenuation factor of a signal is estimated

Table 5.3: Modal parameters of different signals estimated using the proposed method, SSI method [52], Teager Kaiser method [68] and Fourier method [60]

	SNR = 15 dB				**SNR = 20 dB**				**SNR = 25 dB**			
Method	**Estimated**		**Std (%)**		**Estimated**		**Std (%)**		**Estimated**		**Std (%)**	
	Freq (Hz)	**AF**	**Freq (Hz)**	**AF**	**Freq (Hz)**	**AF**	**Freq (Hz)**	**AF**	**Freq (Hz)**	**AF**	**Freq (Hz)**	**AF**
Signal 1												
True	0.200	0.170			0.200	0.170			0.200	0.170		
value	0.750	0.130			0.750	0.130			0.750	0.130		
Proposed	0.2000	0.1665	0.12	1.00	0.2000	0.1710	0.07	0.44	0.2001	0.1703	0.04	0.28
method	0.7499	0.1292	0.08	0.63	0.7500	0.1306	0.05	0.24	0.7500	0.1299	0.02	0.16
SSI	0.1995	0.1681	0.17	0.86	0.2002	0.1700	0.06	0.52	0.2001	0.1697	0.04	0.25
method	0.7499	0.1300	0.07	0.44	0.7501	0.1302	0.04	0.23	0.7500	0.1301	0.02	0.15
Fourier	0.1997	0.1695	0.01	1.53	0.1997	0.1659	0.01	0.87	0.1997	0.1666	0.05	0.53
method	0.7490	0.1220	1.92	1.14	0.7324	0.1270	0.01	0.57	0.7324	0.1265	0.02	0.23
Teager	0.2008	0.1750	0.06	0.49	0.2009	0.1719	0.03	0.27	0.1996	0.1722	0.02	0.14
Kaiser	0.7505	0.1287	0.04	0.28	0.7501	0.1290	0.02	0.18	0.7500	0.1299	0.01	0.12
Signal 2												
True	0.200	0.170			0.200	0.170			0.200	0.170		
Value	0.280	0.050			0.280	0.050			0.280	0.050		
	0.750	0.130			0.750	0.130			0.750	0.130		
Proposed	0.2008	0.1730	0.32	1.85	0.1999	0.1703	0.11	1.04	0.200	0.1700	0.09	0.53
method	0.280	0.0488	0.05	0.4	0.2799	0.0504	0.04	0.25	0.280	0.0501		0.16
	0.750	0.1299	0.09	0.47	0.750	0.1302	0.05	0.37	0.750	0.1295	0.02	0.16
SSI	0.2148	0.1477	3.37	5.76	0.2119	0.1535	2.94	4.51	0.2078	0.1575	2.47	3.70
method	0.2641	0.0779	3.33	5.28	0.2681	0.0671	2.92	4.09	0.2720	0.0624	2.49	3.68
	0.7501	0.1315	0.07	0.39	0.7499	0.1286	0.05	0.29	0.7499	0.1302	0.02	0.15
Fourier	0.26630	0.0524	0.01	0.1	0.2663	0.0525	0.01	0.06	0.2663	0.0524	0.01	0.04
method	0.7590	0.1350	1.37	1.08	0.7640	0.1369	0.75	0.63	0.7656	0.1384	0.01	0.02
Teager	0.1997	0.1854	0.32	1.85	0.2011	0.0.1673	0.11	1.04	0.2013	0.1684	0.09	0.53
Kaiser	0.2801	0.0497	0.04	0.02	0.2799	0.0492	0.06	0.09	0.2800	0.0494	0.07	0.02
method	0.7502	0.1241	1.37	1.08	0.7500	0.1330	0.081	0.05	0.7498	0.1335	0.02	0.09
Signal 3												
True	0.250	0.170			0.250	0.170			0.250	0.170		
value	0.330	0.120			0.330	0.120			0.330	0.120		
	0.780	0.130			0.780	0.130			0.780	0.130		
	0.870	0.070			0.870	0.070			0.870	0.070		
	0.2503	0.1669	0.34	1.27	0.2507	0.1701	0.19	0.80	0.2501	0.1697	0.11	0.47
Proposed	0.3302	0.1189	0.17	1.08	0.3300	0.1224	0.08	0.67	0.3300	0.1197	0.05	0.37
method	0.7803	0.1308	0.13	1.22	0.7802	0.1310	0.10	0.58	0.7799	0.1294	0.05	0.32
	0.8700	0.0695	0.07	0.42	0.8700	0.0706	0.04	0.28	0.8700	0.0698	0.02	0.13
	0.2638	0.1625	3.12	2.47	0.2657	0.1590	3.27	2.14	0.2657	0.1599	3.30	1.94
SSI	0.3151	0.1290	3.15	2.03	0.3136	0.1286	3.37	2.04	0.3138	0.1313	3.29	2.30
method	0.7803	0.1302	0.11	0.87	0.7800	0.1291	0.09	0.40	0.7800	0.1310	0.04	0.28
	0.8700	0.0701	0.04	0.29	0.8700	0.0704	0.03	0.22	0.8702	0.0700	0.01	0.10
	0.2330	0.1640	$< 10^{-7}$	0.0113	0.2330	0.1635	$< 10^{-7}$	0.0043	0.2330	0.1656	$< 10^{-7}$	0.0021
Fourier	0.3329	0.1073	$< 10^{-7}$	0.0038	0.3329	0.1078	$< 10^{-7}$	0.0017	0.3329	0.1075	$< 10^{-7}$	0.0021
method	0.7656	0.0864	$< 10^{-7}$	0.0020	0.7656	0.0872	$< 10^{-7}$	0.0013	0.7656	0.0871	$< 10^{-7}$	0.0021
	0.8655	0.0719	$< 10^{-7}$	0.0012	0.8655	0.0717	$< 10^{-7}$	0.0007	0.8655	0.0717	$< 10^{-7}$	0.0021
	0.2519	0.1599	0.08	0.48	0.2518	0.1601	0.06	0.30	0.2516	0.1597	0.02	0.13
Teager	0.3305	0.1275	0.05	0.35	0.3305	0.1279	0.02	0.2	0.3305	0.1195	0.01	0.13
Kaiser	0.7797	0.1354	0.07	0.32	0.7794	0.1361	0.03	0.19	0.7796	0.1287	0.02	0.19
	0.8698	0.0705	0.03	0.17	0.8694	0.0706	0.02	0.11	0.8700	0.0703	0.01	0.06

by taking the average of the estimated values of 50 independent simulations. Before the estimation process, the length and distance between the windows in the Fourier method are set as 500 and 50 samples, respectively. The value of i and j in the SSI based method is set

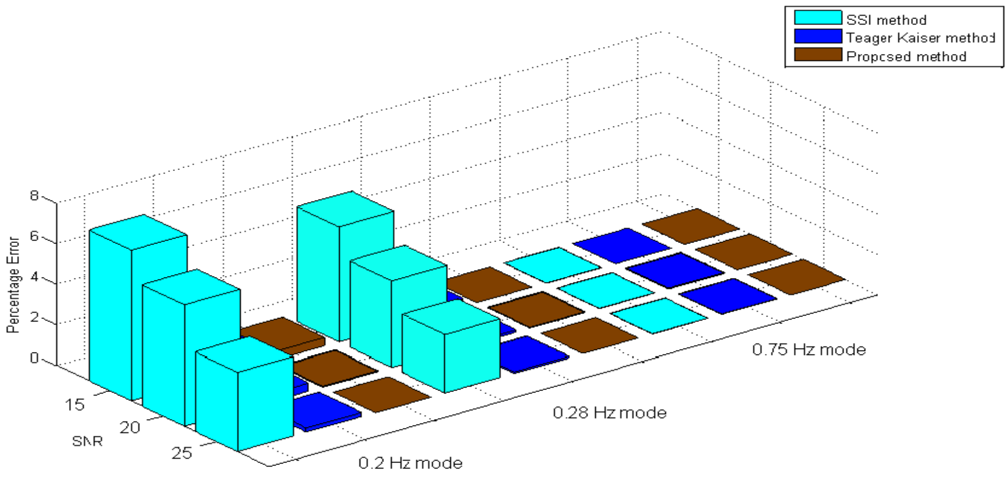

Figure 5.4: Absolute percentage error in frequency estimation of Signal 2 using the proposed method, Teager Kaiser method and SSI method.

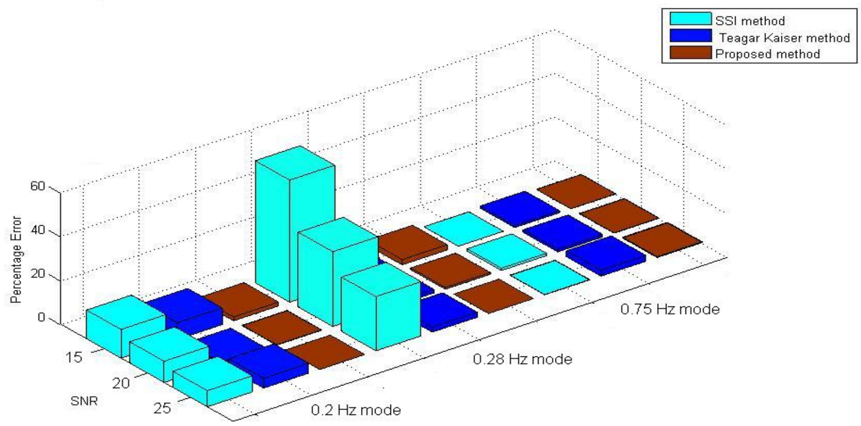

Figure 5.5: Absolute percentage error in attenuation factor estimation of Signal 2 using the proposed method, Teager Kaiser method and SSI method.

as 200 and 1000 respectively. From the tabulated data, it is clear that the Fourier method [60] fails to identify all the modes present in the signal when it has closely spaced modes. This is evident from the estimated values of Signal 2 where the Fourier method estimated the 0.2 Hz and 0.28 Hz modes as one mode. Hence, it can be inferred that this algorithm is not suited for estimating signals with closely spaced modes. The variation of absolute percentage error in the frequency and attenuation factor estimation of Signal 2 at different SNRs obtained using the proposed method, Teager Kaiser method and the SSI based method is plotted in figs. 5.4 and 5.5. It is observed that the frequency estimation error of all the three methods are very small. Hence, it can be concluded that all the methods estimate the frequency of the different modes in the signal accurately. However, it is also observed from fig. 5.5 that the attenuation

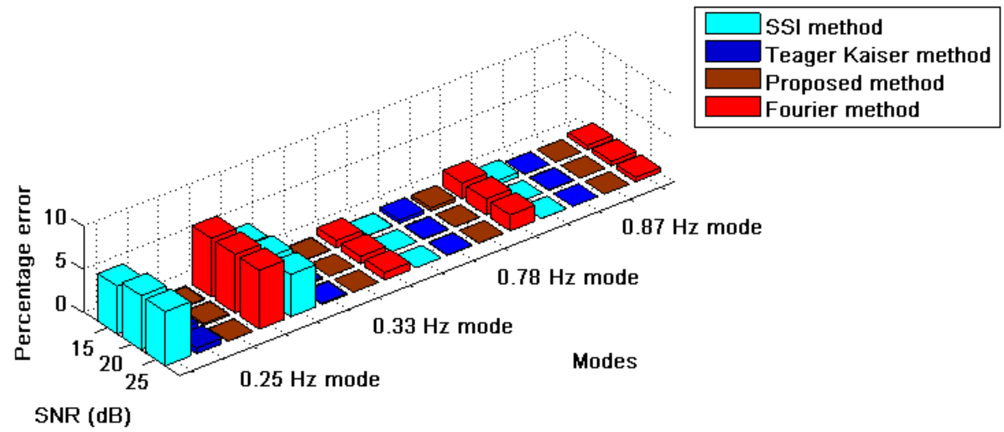

Figure 5.6: Absolute percentage error in attenuation factor estimation of Signal 3 using the proposed method, Teager Kaiser method and SSI method.

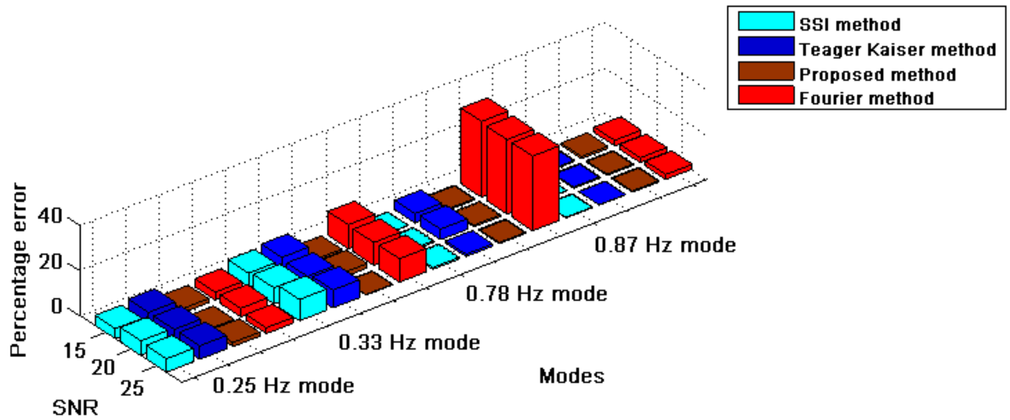

Figure 5.7: Absolute percentage error in attenuation factor estimation of Signal 3 using the proposed method, Teager Kaiser method and SSI method.

factor estimates of the proposed method are more accurate than that of the SSI and Teager Kaiser methods. The maximum attenuation factor estimation error of the SSI based method and Teager Kaiser method are 50% and 7.6% whereas that of the proposed method is less than 2%. Similar observations can be made from figs. 5.6 and 5.7 where variation of absolute percentage error in the frequency and attenuation factor estimation of Signal 3 at different SNRs is plotted. This proves that the proposed method provides more accurate attenuation factor estimates of noise contaminated signals with closely spaced modes as compared to SSI, Teager Kaiser and Fourier methods.

Table 5.4 compares the estimated model order and computation time of different synthetic signals obtained using the proposed method and SSI based method [52] at different SNRs.

Table 5.4: Comparison of model order and computation time for the proposed method with SSI based method

Signal	SNR	SSI Method in [52]		Proposed Method	
		Model order method in [52]	Computation Time (s)	EMO method	Computation Time (s)
Signal 1	15	100	3.29	3	1.96
	20	102	3.32	3	1.96
	25	92	3.09	3	1.80
Signal 2	15	96	3.11	4	1.8
	20	96	3.08	4	1.83
	25	96	3.34	4	1.87

It is noticed that, the model order algorithm in the SSI method overestimates the model order whereas the EMO algorithm estimates the same accurately. For instance, the estimated model order of Signal 1 at 20 dB SNR is obtained as 3 using the proposed method while that of the SSI based method is 102. This overestimation of the model order in the SSI method leads to the presence of fictitious modes in its estimated results. Separate filtering algorithms are used in [52] to identify the true modes of the signal from these fictitious modes. The main disadvantage of this SSI based method is that the computational burden of the whole method increases due to the usage of these filtering algorithms which eventually makes the whole method slow compared to similar algorithms. On the other hand, the proposed method uses EMO algorithm which estimates the model order accurately irrespective of the noise content of the signal. Hence, trivial modes are not present in its estimated results. Therefore, computational time of the proposed method is lesser than the SSI based method in [52]. It is observed that the computational time of the proposed method is less than two seconds for all the signals whereas that of the SSI based method is above three seconds. Thus, it can be concluded that the proposed method is faster than the SSI based method in [52].

5.3.2 Real time PMU data

In this section, real time PMU data corresponding to the probe test data obtained from the WECC system on 14^{th} September 2005 is used for testing the proposed method. The details about the WECC system and the analysis windows used are given in Section 3.3.2. The signal generated from these analysis windows are analyzed using the proposed method, SSI method [52], Teager kaiser [68] method and the Fourier method [60] and the results are tabulated in Table 5.5. Matrix Pencil and ERA methods are not used in this comparison as they have

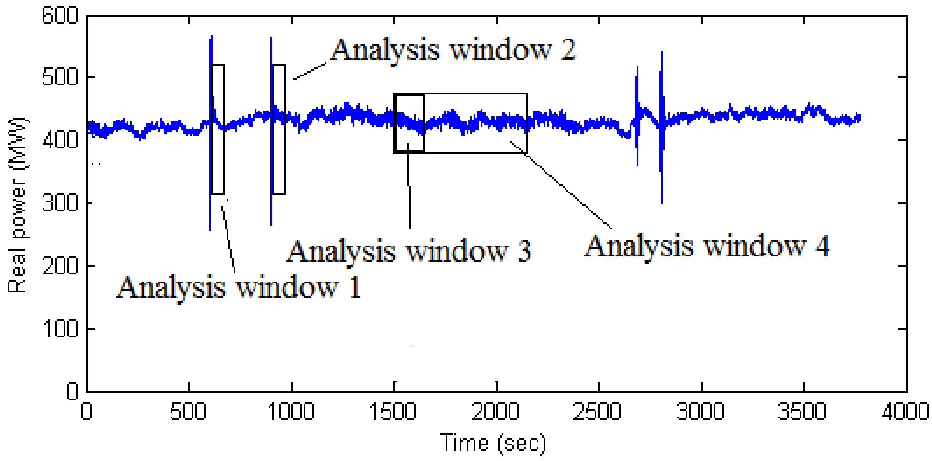

Figure 5.8: Probing data of WECC system [84].

Table 5.5: Estimated modal parameters of WECC system using the proposed method, Teager Kaiser method, SSI method and Fourier method

Window	Estimated value from [84]		Proposed method		SSI method		Fourier method		Teager Kaiser	
	Freq	ζ	Freq	ζ	Freq	ζ	Freq	ζ	Freq	ζ
Window 1	0.318	8.30	0.3208	8.1	0.3266	07.77	0.3497	7.73	0.3201	7.91
			0.6723	12.91	0.6723	012.72	0.6993	3.86	0.5996	21.07
Window 2	-	-	0.3189	8.08	0.3181	7.96	0.3497	8.10	0.3196	8.15
	-	-	0.67693	12.9	0.6993	4.03	0.6702	12.7	0.2121	12.23

Table 5.6: Frequencies and damping ratios of WECC system probe data under different noise levels

Window	SNR=15 dB		SNR=20 dB		SNR=25 dB		SNR=30 dB	
	Frequency (Hz)	ζ	Frequency (Hz)	ζ	Frequency (Hz)	ζ	Frequency (Hz)	ζ
Window 1	0.3192	8.1	0.3184	8.07	0.3185	8.13	0.3188	8.12
	0.6723	12.97	0.6723	12.93	0.6723	12.87	0.6723	12.91
Window 2	0.3204	8.03	0.3211	7.95	0.3196	8.08	0.3189	8.08
	0.67693	12.85	0.67693	12.91	0.67693	12.87	0.67693	12.82

fictitious modes in their estimated results.

It is observed from Table 5.5 that while analyzing the real time signal corresponding to analysis window 1, all the methods under consideration estimated the two modes present in the signal. The dominant mode among them is the 0.318 Hz mode which has a damping factor of 8.3%. It is observed that the proposed method gave near accurate frequency and damping factor estimates of this mode which were closest to the reported values in [84]. The

SSI and Teager Kaiser method provided accurate estimates of the frequency of the signal but damping factor estimates are inaccurate in comparison to the proposed method. The estimated results of the proposed method are almost the same even under highly noisy conditions as evident from Table 5.6. Hence, it can be concluded that the proposed method is best suited for estimation of real time signals as compared to SSI and Fourier methods.

To further prove the superiority of the proposed method over the SSI method in dealing with real time signals of ambient nature, both the methods are compared in terms of computation time. Two analysis windows having lengths of 100 seconds and 600 seconds are used for this purpose. Window 3 is from 1500 seconds to 1600 seconds whereas Window 4 is from 1500 seconds to 2100 seconds. The signals corresponding to these windows are analyzed using the proposed and SSI methods and the results are tabulated in Table 5.7. These simulations was carried out on a computer having Intel Core i5-2400 processor with 4 GB of RAM.

Table 5.7: Simulation time of the proposed method and SSI method

Window	**Length**	**Simulation time (in seconds)**	
		Proposed method	**SSI method**
Window 3	100 seconds	2.8	13.47
Window 4	600 seconds	12.87	59.48

It is observed from Table 5.7 that the computational time of the proposed method is much lesser than that of the SSI method. For instance, the proposed method estimates the modal parameters of the Window 4 in 12.87 seconds while the SSI method takes 59.48 seconds for estimation. The main reason for the increase in the computation time of the SSI method is the overestimation of the model order by its model order algorithm. This results in the presence of fictitious modes in the estimated results, which is removed using a filtering algorithm. This leads to an increase in the computation time of the SSI method. However, the proposed method uses EMO algorithm which estimates the model order accurately. Hence, the filtering algorithm used in the SSI method is not required for the proposed method making it faster than the SSI method.

5.4 Conclusion

An SSI based modal parameter estimation method for identifying the poorly damped modes of low frequency electromechanical oscillations is proposed in this chapter. The proposed method uses an SWT based algorithm for denoising the signal. Further, the model order of the signal, which is a prerequisite for the proper implementation of the SSI method is estimated through EMO algorithm thereby reducing its computational complexity. The ability of the EMO algorithm to estimate the model order accurately is verified by comparing it with the model order algorithms of Matrix Pencil and ERA methods. The robustness of the proposed method is compared with a Fourier based, Teager Kaiser based and another SSI based methods in the literature using synthetic signals and actual PMU data obtained from WECC system. Results confirm that the proposed method estimates all the modes present in the signal with a high degree of accuracy even under high levels of noise.

Chapter 6

An Empirical Wavelet Transform-ESPRIT method for analyzing low frequency oscillations

6.1 Introduction

Accurate knowledge of the low-frequency electromechanical modes in power system gives vital information about the operating characteristics of a power system. The HTLS, ESPRIT and SSI based algorithms proposed in Chapters 3, 4 and 5 help to effectively analyse the poorly damped modes in ringdown and ambient oscillations. However, all these are parametric methods and they require an accurate estimate of the model order for their successful implementation. If the model order is underestimated, one or more modes present in the signal are not identified, whereas overestimation of model order leads to the presence of fictitious modes in the estimated results. However, if the multi-component signal is decomposed into mono-components, then the estimation of model order is not required as the mono components have only one frequency component in them. Thus, the twin issues of estimating the modal parameters of the signal accurately and removal of artificial modes in the estimated results get solved automatically if the signal is decomposed into its mono-components. The decomposition of the signal can be achieved using many techniques like Variational Mode Decomposition (VMD) [94], Empirical Mode Decomposition (EMD) [93] and Wavelet transform. Among these techniques, Wavelet transforms based techniques are one of the easiest and efficient ways for decomposing a multi-component signal into its mono-components by creating a bank of wavelet filters. The Empirical Wavelet Transform (EWT) [95] is a wavelet based method which can efficiently decompose the signal into its mono-components. The main advantage of EWT is that it uses adaptive wavelets i.e. the wavelets used for decomposition are generated based on the information contained in the signal. Due to this property, the EWT can extract different modes of the signal efficiently in comparison to other wavelet based methods, which use a fixed basis for the decomposition process. EWT can decompose stationary as well as non-stationary signals, hence it is one of the perfect choices for analyzing the power system oscillations.

This chapter proposes an Empirical Wavelet Transform-ESPRIT based method for identification of poorly damped modes in power system low frequency oscillations. In this method, EWT is used to decompose the multi-mode signal into its mono-components and the modal parameters of these mono components are calculated using the ESPRIT based technique. The superiority of the proposed method is tested by comparing its performance with that of a VMD-Teager Kaiser based method [94], a Hilbert Huang Transform (HHT) based method [93] and a Continuous Wavelet Transform (CWT) based method [55] in the literature. Test results prove the superiority of the proposed method in identifying the poorly damped low frequency modes present in the power system oscillations.

6.2 Proposed Methodology

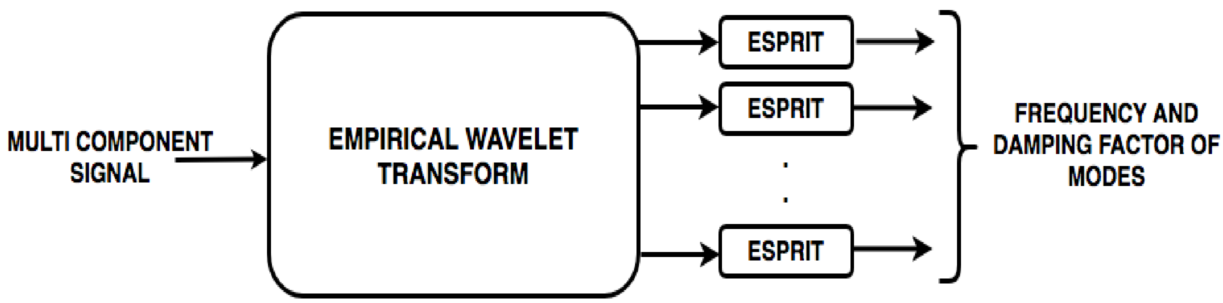

Figure 6.1: Block diagram of the proposed method.

The schematic representation of the proposed method is shown in fig. 6.1. It utilizes a combination of Empirical Wavelet Transform (EWT) and ESPRIT for identifying the poorly damped electromechanical modes present in the power system oscillations. The multi-mode signal under consideration is decomposed using EWT and the modal parameters of these mono components are estimated using ESPRIT. EWT is selected because it uses adaptive wavelets for decomposition process due to which it can efficiently split the multi-mode signal into its mono components whereas ESPRIT method is used because of its capability to provide good accuracy and robustness against noise. A detailed explanation of EWT algorithm is given in the following subsection.

6.2.1 Empirical Wavelet Transform

The Empirical Wavelet Transform (EWT) was proposed by Jerome Gilles in 2013. It can effectively separate the different modes present in the signal using adaptive wavelets. Therefore, this technique is used in the proposed method to separate the multi-component signal into mono-components. A detailed explanation of this method is given in [95, 96]. The main steps of the Empirical wavelet transform are as follows.

Step 1: Obtain the Fast Fourier Transform (FFT) of the signal $x(t)$ under consideration.

Step 2: Plot $X(w)$ and find its highest peak. $X(w)$ is the Fourier transform of $x(t)$.

Step 3: Find out the peaks of $X(w)$ having an amplitude of at least 15% of its highest peak. These peaks represent the dominant modes of the signal. Obtain the frequencies corresponding to these dominant modes.

Step 4: Segment the Fourier spectrum and obtain the boundaries. If $\omega_1, \omega_2, ...\omega_M$ are the peaks of the Fourier spectrum, the corresponding boundaries (σ_i) are obtained using the following equation

$$\sigma_i = \frac{\omega_i + \omega_{i+1}}{2} \qquad i = 1, 2, 3, ...M-1 \tag{6.1}$$

Step 5: Construct filter banks corresponding to these boundaries. The filter bank consists of one low pass filter and M-1 bandpass filters. The filters are developed using the wavelet scaling function (ϕ_1) and the wavelet filter function(ψ_i).

$$\phi_1(\omega) = \left\{ \begin{array}{ll} 1, & if \quad |\omega| \leq (1-\gamma)\sigma_1 \\ \cos(\frac{\pi}{2}\beta(\gamma, \sigma_1)), & if \quad (1-\gamma)\sigma_1 \leq |\omega| \leq (1+\gamma)\sigma_1 \\ 0, & otherwise \end{array} \right\}, \tag{6.2}$$

$$\psi_i(\omega) = \left\{ \begin{array}{ll} 1, & if \quad (1+\gamma)\sigma_i \leq |\omega| \leq (1-\gamma)\sigma_{i+1} \\ \cos(\frac{\pi}{2}\beta(\gamma,\sigma_{i+1})), & if \quad (1-\gamma)\sigma_{i+1} \leq |\omega| \leq (1+\gamma)\sigma_{i+1} \\ \sin(\frac{\pi}{2}\beta(\gamma,\sigma_i)), & if \quad (1-\gamma)\sigma_i \leq |\omega| \leq (1+\gamma)\sigma_i \\ 0, & otherwise \end{array} \right\}, \quad (6.3)$$

Here, γ is a parameter whose value is between 0 and 1. It is used to ensure that two consecutive transition areas are not overlapping. $\beta(\gamma,\sigma_i) = \beta(\frac{1}{2\gamma\sigma_i}(|\omega| - (1-\gamma)\sigma_i)$ is an arbitrary function which exhibits the following properties.

$$\beta(\gamma,\sigma) = \left\{ \begin{array}{ll} 0, & if \quad (\gamma,\sigma) \leq 0 \\ 1, & if \quad (\gamma,\sigma) \geq 0 \\ \beta(\gamma,\sigma) + \beta(1-(\gamma,\sigma)) = 1, & if \quad (\gamma,\sigma)\ \varepsilon\ [0,1] \end{array} \right\}, \quad (6.4)$$

Step 6: Generate the approximation ($W_x(1,t)$) and detail ($W_x(n,t)$) coefficients of the signal under consideration using $\phi_1(\omega)$ and $\psi_i(\omega)$.

$$W_x(1,t) = <x,\phi_1> = IFFT(X(\omega) \times \phi_1(\omega)) \quad (6.5)$$

$$W_x(i,t) = <x,\psi_i> = IFFT(X(\omega) \times \psi_1(\omega)) \quad (6.6)$$

Here, $X(\omega)$ is the FFT of signal x(t). Each row of approximation ($W_x(1,t)$) and detail ($W_x(n,t)$) coefficients represent a separate mode present in the signal $x(t)$.

After the signal is split into its mono components, it is passed to the ESPRIT algorithm for estimating the modal parameters of its mono components. The detailed explanation of the ESPRIT algorithm is given in Section 4.2.2.

6.3 Simulation Results and Discussion

The efficacy of the proposed method in estimating poorly damped modes in power system low frequency oscillations is tested through two case studies. The first case study uses three synthetic signals with known modal parameters whereas the second case study uses real time PMU data from WECC system. The estimated results obtained from these case studies are compared with that of a VMD-Teager Kaiser [94] based method, a Hilbert Huang Transform

(HHT) based method [93] and a Continuous Wavelet Transform (CWT) based method [55] in the literature. The CWT based method uses Morlet wavelet as the mother wavelet for the analysis of real and synthetic signals in these case studies.

6.3.1 Synthetic Signals

Three synthetic signals Signal 1, Signal 2 and Signal 3 are used in this section.

$$\begin{aligned} Signal\ \ 1 = &(2\cos(2\pi * 0.35t + 1.5\pi))\exp(-0.079t) \\ &+ 2\cos(2\pi * 0.87t + (0.5\pi))\exp(-0.039t) \end{aligned} \tag{6.7}$$

$$\begin{aligned} Signal\ \ 2 = &(2\cos(2\pi * 0.71t + 1.5\pi))\exp(-0.04t) \\ &+ 2\cos(2\pi * 1.23t + (0.5\pi))\exp(-0.06t) \\ &+ 2\cos(2\pi * 1.41t + (0.5\pi))\exp(-0.03t) \end{aligned} \tag{6.8}$$

$$\begin{aligned} Signal\ \ 3 = &(2\cos(2\pi * 0.34t)\exp(-0.021t) \\ &+ 2\cos(2\pi * 0.54t)\exp(-0.031t) \\ &+ 2\cos(2\pi * 0.91t)\exp(-0.041t) \\ &+ 2\cos(2\pi * 1.22t)\exp(-0.051t) \end{aligned} \tag{6.9}$$

Signal 1, Signal 2 and Signal 3 has two, three and four modes having frequencies between 0.35 Hz and 1.41 Hz. These signals are corrupted by adding white Gaussian noise and the modal parameters of these corrupted signals are estimated using the proposed method, VMD-Teager Kaiser based method [94], HHT based method [93] and CWT based method [55]. The estimated results are tabulated in Table 6.1.

It is observed from Table 6.1 that, while analysing Signal 1 whose modes are far apart, all the methods identifies both the modes in the signal irrespective of its SNR value. They provided accurate estimates of the frequencies of both the modes present in Signal 1. However,

Table 6.1: Estimated modal parameters of the three signals at different SNRs

Method	SNR = 15 dB Estimated Frequency (Hz)	SNR = 15 dB Estimated Attenuation factor	SNR = 20 dB Estimated Frequency (Hz)	SNR = 20 dB Estimated Attenuation factor	SNR = 25 dB Estimated Frequency (Hz)	SNR = 25 dB Estimated Attenuation factor
			Signal 1			
True value	0.35 0.87	0.078 0.039	0.35 0.87	0.078 0.039	0.35 0.87	0.078 0.039
Proposed method	0.3506 0.8697	0.0724 0.0378	0.3505 0.8699	0.0755 0.0378	0.3505 0.8699	0.0757 0.0382
CWT method	0.3472 0.8792	0.0714 0.0403	0.3472 0.8791	0.0735 0.0399	0.3472 0.8792	0.0736 0.0398
VMD - Teager kaiser method	0.3622 0.8792	0.0839 0.0402	0.3649 0.8791	0.0709 0.0455	0.3682 0.8792	0.0718 0.0413
HHT method	0.3468 0.8041	0.0599 0.0306	0.3494 0.8701	0.0748 0.0359	0.3504 0.8697	0.0753 0.0368
			Signal 2			
True value	0.71 1.230 01.41	0.04 0.06 0.030	0.71 1.230 01.41	0.04 0.06 0.030	0.71 1.230 01.41	0.04 0.06 0.030
Proposed method	0.7101 1.228 1.4103	0.0392 0.0593 0.0276	0.7102 1.2281 1.4104	0.0391 0.0609 0.0283	0.7101 1.2284 1.4104	0.0393 0.0604 0.0287
CWT method	0.7143 1.200 1.4286	0.0371 0.0571 0.0272	0.7143 1.200 1.4286	0.0370 0.0575 0.0276	0.7143 1.200 1.4286	0.0374 0.0578 0.0278
VMD - Teager kaiser method	0.716 1.2173 1.4153	0.0390 0.0674 0.0402	0.7167 1.2176 1.4153	0.0388 0.0690 0.0392	0.7168 1.2176 1.4153	0.0384 0.0681 0.0396
HHT method	0.7772 1.3542	0.0634 0.0144	0.6505 1.3436	0.0624 0.0222	0.71090 1.3510	0.0435 0.0122
			Signal 3			
True method	0.34 0.54 0.91 1.22	0.021 0.031 0.041 0.051	0.34 0.54 0.91 1.22	0.021 0.031 0.041 0.051	0.34 0.54 0.91 1.22	0.021 0.031 0.041 0.051
Proposed method	0.3418 0.5401 0.9103 1.2202	0.0224 0.0325 0.0417 0.0496	0.3408 0.5401 0.9096 1.2201	0.0221 0.0324 0.0419 0.0501	0.3401 0.5401 0.9096 1.2199	0.0218 0.0321 0.0413 0.0501
CWT method	0.3538 0.5682 0.9868 1.3093	0.0179 0.0278 0.0374 0.0497	0.3539 0.5659 0.9868 1.3092	0.0184 0.0279 0.0372 0.0498	0.3539 0.5659 0.9868 1.3093	0.0185 0.0280 0.0374 0.0499
VMD method	0.3336 0.5412 0.9167 1.2167	0.0235 0.0280 0.0407 0.0504	0.3336 0.5412 0.9173 1.2178	0.0251 0.0287 0.0406 0.0506	0.3336 0.5412 0.9165 1.2169	0.0208 0.0300 0.0407 0.0507
HHT method	0.4734 1.0286	0.027 0.0107	0.4432 1.0975	0.0211 0.0103	0.4400 1.0307	0.0347 0.0121

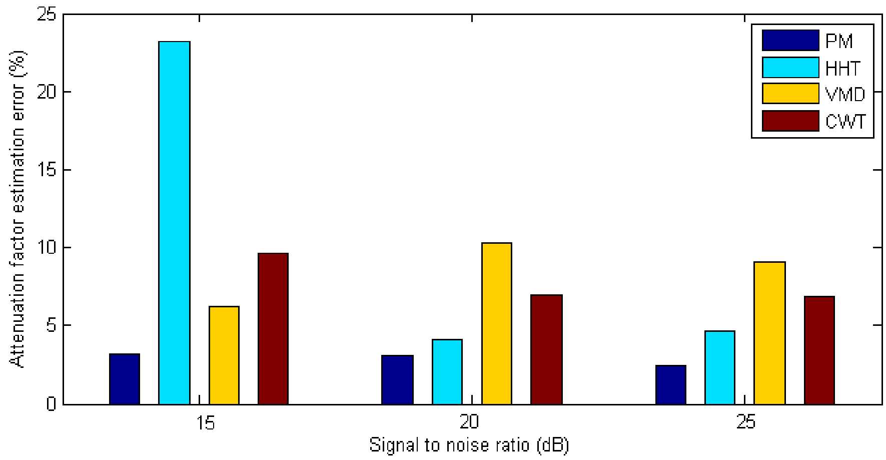

Figure 6.2: Attenuation factor estimation error of 0.34 Hz mode present in Signal 1.

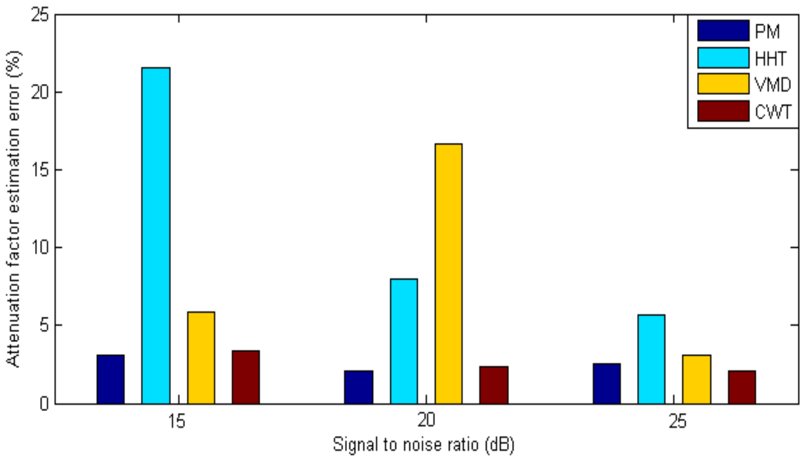

Figure 6.3: Attenuation factor estimation error of 0.85 Hz mode present in Signal 1.

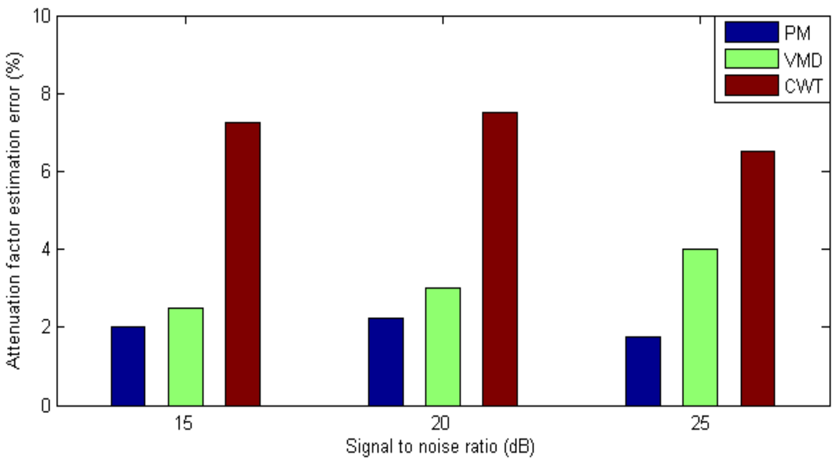

Figure 6.4: Attenuation factor estimation error of 0.71 Hz mode present in Signal 2.

while analysing the attenuation factor estimates of the modes of Signal 1, it is observed that the proposed method gave the most accurate estimates in comparison to that of VMD- Teager

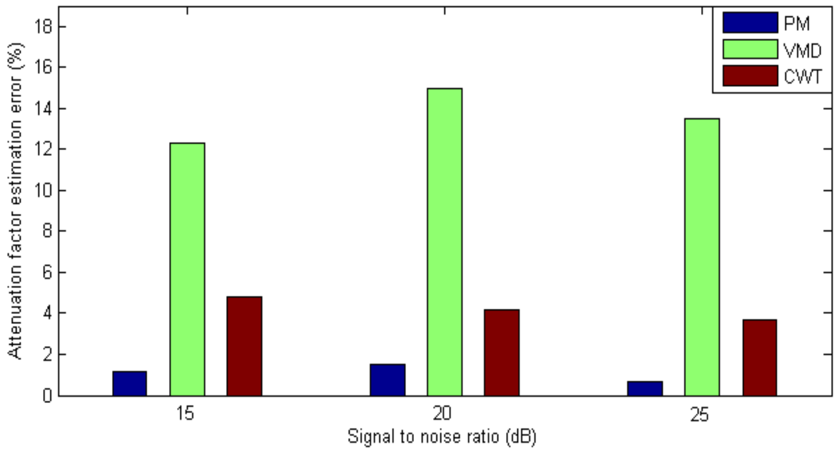

Figure 6.5: Attenuation factor estimation error of 1.23 Hz mode present in Signal 2.

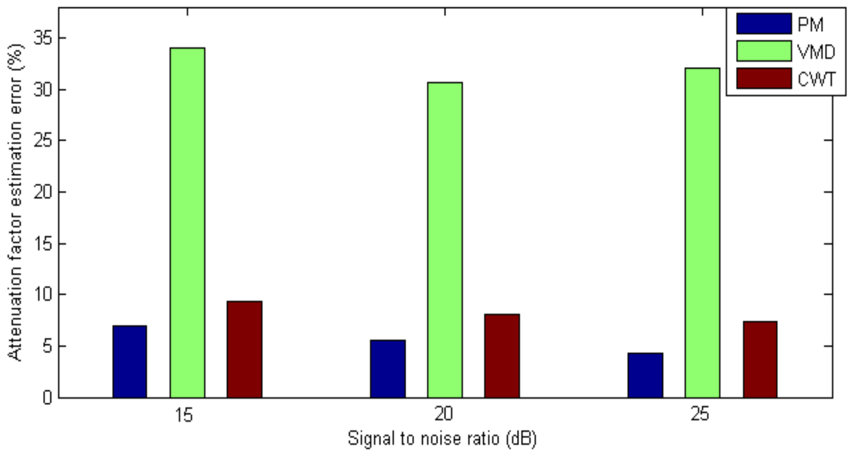

Figure 6.6: Attenuation factor estimation error of 1.41 Hz mode present in Signal 2.

Kaiser method, CWT based method and HHT method. This is clearly evident from figs. 6.2 and 6.3, which show the plot of percentage error in attenuation factor estimation of different methods when the SNR value of the signal is varied from 15 dB to 25 dB. In these figures, PM, HHT, VMD and CWT denote the proposed method, HHT based method, VMD-Teager Kaiser method and CWT based method, respectively. The maximum attenuation factor estimation error of the VMD- Teager Kaiser method, CWT method and the HHT method is found to be 23.2%, 9.6% and 16.66%, respectively, whereas that of the proposed method is only 3.07%. It is observed that while analyzing signals with closely spaced modes, like Signal 2 and Signal 3, the estimates of the HHT method are highly inaccurate. This is due to the usage of Empirical Mode Decomposition (EMD) in HHT method. HHT uses EMD for extracting different modes present in the signal. However, when the signal has closely spaced modes, EMD fails to decompose the signals with closely spaced modes effectively resulting in mode mixing. This phenomenon leads to failure in the identification of one or more modes present in the signal. Hence, it can be inferred that the HHT method is not suitable for estimating signals with closely spaced modes. The other three methods used for modal parameter estimation of Signal 2 and Signal 3 i.e. VMD-Teager Kaiser, CWT and the proposed methods are compared in terms of attenuation factor estimation error. The attenuation factor estimation error of Signal 2 obtained through these three methods are shown in figs. 6.4, 6.5 and 6.6. It is noticed that, among the four methods under consideration, the proposed method has the least attenuation factor estimation error proving that it can accurately estimate the modal parameters of noise contaminated signals with closely spaced modes.

Table 6.2: Modal parameters of Signal 2 estimated at different sampling rates

Sampling(Hz) rate(Hz)	**Frequency (Hz)**	**ATF**	**Estimation error in frequency** (%)	**Estimation error** in **ATF** (%)
	0.7122	0.0404	0.309	1.00
10	1.2223	0.0597	-0.626	-0.50
	1.4106	0.0288	0.042	-4.00
	0.7122	0.0404	0.309	1.00
20	1.2280	0.0609	-0.162	1.50
	1.4106	0.0288	0.042	-4.00
	0.7102	0.0388	0.028	-3.00
30	1.2288	0.0597	-0.097	-0.50
	1.4103	0.0289	0.021	-3.66
	0.7102	0.0391	0.028	-2.25
40	1.2286	0.0596	-0.110	-0.66
	1.4105	0.0290	0.035	-3.33

The data obtained from the PMU will be sampled at frequencies between 10 Hz and 120 Hz [97]. For a parameter estimation algorithm to be implementable, it should estimate the parameters accurately irrespective of the sampling rate of the PMU. The ability of the proposed method to estimate the modal parameters accurately is investigated using Signal 2 at 15 dB SNR and the results obtained are tabulated in Table 6.2. It is seen that irrespective of the sampling rate of the signal, the estimates of the proposed method is much closer to the true modal parameter values. For instance, while estimating the modal parameters of Signal 2 sampled at 10 Hz, the maximum frequency and attenuation factor error of the proposed method is only 0.626% and 4.0%, respectively. It is also observed that the estimation error of both methods decreases with the increase in sampling rate. This proves that the proposed method can accurately estimate the modal parameters of the signal irrespective of its sampling rates.

6.3.2 Real time PMU data

In this section, the proposed method is applied to a real time power system data for the identification of poorly damped modes. The system under consideration is the WECC system. The details about this system is provided in Section 3.3.2. Two signals with the length of 8.6 seconds, as shown in fig. 6.7, generated from this data, is used to compare the proposed method with the VMD-Teager Kaiser based method [94], a HHT based method [93] and CWT based method [55].

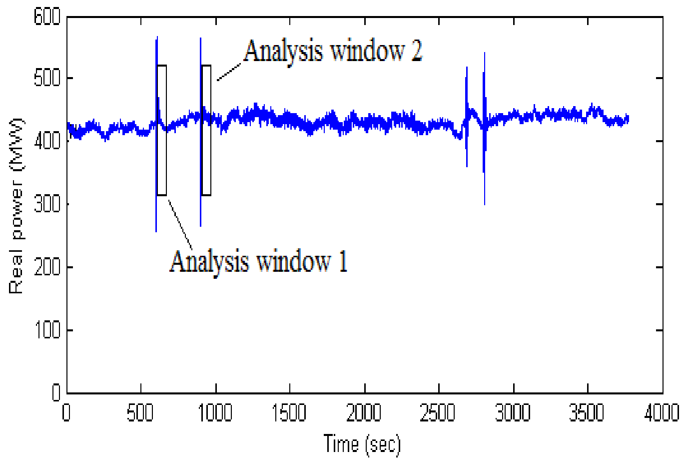

Figure 6.7: Variation of power in Round mountain 1 line of WECC system on 14^{th} September 2005.

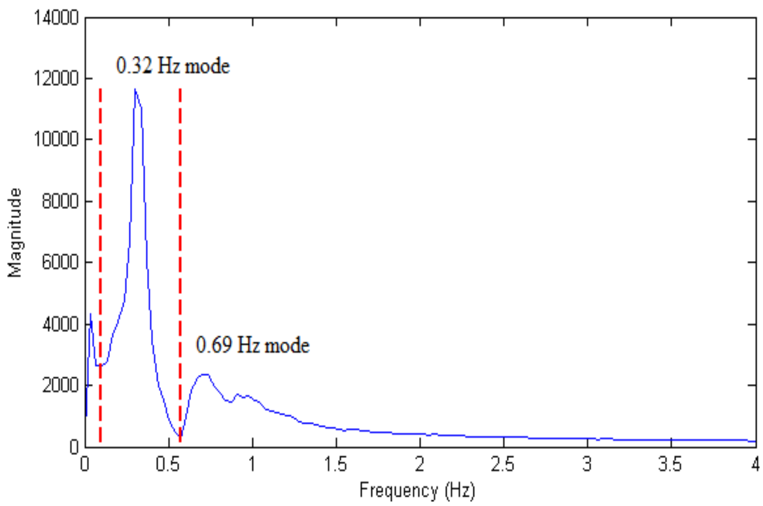

Figure 6.8: FFT plot of signal corresponding to analysis window 1.

Table 6.3 shows the estimated modal parameters of the signals corresponding to analysis windows 1 and 2 obtained through the proposed method, VMD- Teager Kaiser method [94],

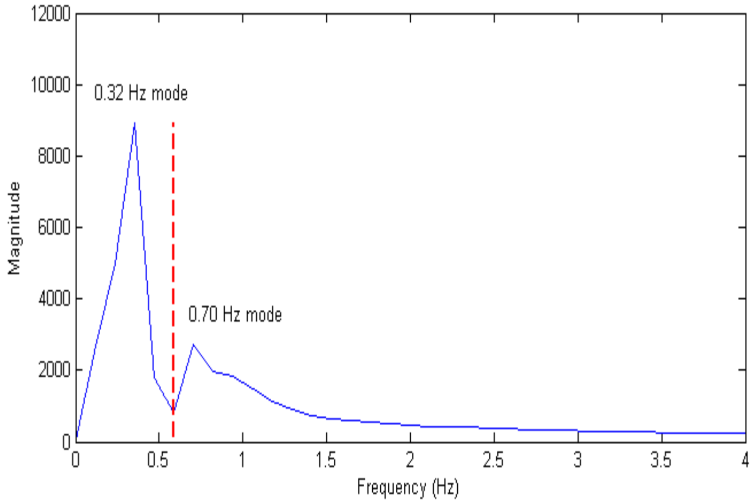

Figure 6.9: FFT plot of signal corresponding to analysis window 2.

Table 6.3: Dominant modes and its parameters of WECC system probe data

Signal	Estimated value from [98]		Proposed method		HHT method		VMD method		CWT method	
	Frequency (Hz)	ς (%)	**Frequency (Hz)**	ς (%)	**Frequency (Hz)**	ς (%)	**Frequency (Hz)**	ς (%)	**Frequency (Hz)**	ς (%)
Analysis window 1	0.32	8.3	0.3201	8.04	0.3543	6.82	0.3029	7.3	0.3205	6.09
			0.6920	12.80	-	-	-	-	0.7891	2.99
Analysis window 2			0.31940	7.73	0.3221	10.86	0.2902	6.99	0.3157	5.36
			0.6892	12.33	-	-	-		0.7576	2.24

Table 6.4: Dominant modes and its parameters of WECC system probe data at different SNRs

Signal	SNR = 15 dB		SNR = 20 dB		SNR = 25 dB		SNR = 30 dB	
	Frequency (Hz)	ς (%)	**Frequency (Hz)**	ς (%)	**Frequency (Hz)**	ς (%)	**Frequency (Hz)**	ς (%)
Analysis window 1	0.3224	7.98	0.3211	8.01	0.3201	8.04	0.3201	8.04
	0.6920	12.81	0.6918	12.82	0.6919	12.80	0.6919	12.80
Analysis window 2	0.3197	7.67	0.3191	7.71	0.3194	7.73	0.3194	7.73
	0.6892	12.33	0.6892	12.33	0.6892	12.33	0.6892	12.33

HHT method [93] and CWT method [55], respectively. The FFT of these signals are plotted in figs. 6.8 and 6.9. It is noticed from these figures that both the signals have two peaks corresponding to two dominant modes present in them. The frequencies of these modes were found to be around 0.32 Hz and 0.70 Hz respectively. It is also noticed that, among the four methods under consideration, only the proposed method and the CWT based method identifies both these modes whereas HHT and VMD- Teager Kaiser based methods identifies only the 0.32 Hz mode. However, the CWT based method estimated the frequency of the 0.70 Hz mode with considerable error. It is also observed that in comparison to the other three methods, the modal parameter estimates of the proposed method for the 0.32 Hz mode are closest to the reported values in [84]. Therefore, it can be inferred that, while analysing real time signals, the proposed method provides more accurate estimates of modal parameters than the VMD- Teager Kaiser [94], HHT [93] and CWT [55] based methods. The estimated results of Table 6.4 indicate that the modal parameter estimates of the proposed method is almost constant even at high levels of noise proving its robustness. Hence, it is proved from Tables 6.3 and 6.4 that in comparison to the other three methods, the proposed method is a better choice for identification of poorly damped modes present in real time signals.

Table 6.5: Dominant modes and its parameters of WECC system probe data obtained through HTLS, EMO ESPRIT, Improved SSI and EWT-ESPRIT methods

Signal	HTLS method		EMO ESPRIT method		Improved SSI method		EWT-ESPRIT method	
	Frequency (Hz)	ς (%)	**Frequency (Hz)**	ς (%)	**Frequency (Hz)**	ς (%)	**Frequency (Hz)**	ς (%)
Analysis window 1	0.3183	8.39	0.3207	8.30	0.3208	8.1	0.3201	8.04
	0.6962	11.83	-	-	0.6723	12.91	0.6920	12.80
Analysis window 2	0.316	8.11	0.3149	7.88	0.3189	8.08	0.3194	7.73
	0.6642	10.51	-	-	0.6769	12.91	0.6892	12.33

To further prove the effectiveness of the proposed EWT-ESPRIT method, it is compared with the HTLS, EMO ESPRIT and SSI based methods proposed in Chapters 3,4 and 5 of this thesis. The real time PMU signals from the WECC system is used for this purpose. It is observed from Table 6.5 that the estimates of the proposed EWT-ESPRIT method are almost similar to the other methods proposed in this thesis. This proves that the proposed EWT-ESPRIT method is accurate like the other methods proposed in this thesis.

6.4 Conclusion

This chapter proposed a EWT-ESPRIT based approach for identifying the poorly damped electromechanical modes in the power system. In this approach, EWT is used to split the signal into monocomponents and the modal parameters of these monocomponents are estimated through ESPRIT algorithm. The performance evaluation of the proposed approach is carried out using synthetic signals with known modal parameters and real-time PMU data from actual power system at different levels of noise. The estimated results of these signals are compared with that of a VMD- Teager based method, a CWT based method and an HHT based method in the literature. Results reveal the superiority of the proposed method over the other three methods. The proposed approach is designed based on the analysis of data received from one PMU in the power system. However, it can be easily extended to analyse data from multiple PMUs with the help of a powerful processor with parallel computing facility at the control centre.

Chapter 7

Conclusions and Future work

This thesis aims to optimally place the PMUs maintaining complete observability of the power system during normal operating conditions and contingencies and develop algorithms for identifying the poorly damped modes in low frequency oscillations utilizing synchrophasor measurements. These low frequency oscillations can be broadly classified into ambient and ringdown type oscillations. The characteristics of the ringdown and ambient oscillations are entirely different. Therefore, separate algorithms are required for the analysis of these oscillations. Hence, four different algorithms using parametric methods are developed for this purpose.

Chapter 1 discusses the basics of Phasor Measurement Units and their applications. A brief explanation of power system stability and small signal stability in particular and the conventional methods for its estimation are also added in this section. It is followed by a detailed literature review on optimal PMU placement and synchronized measurements based estimation of poorly damped modes in power system. The motivation behind selecting this research topic is detailed at the end of this chapter.

In Chapter 2, an optimal placement algorithm using PMUs of varying channel capacity is proposed. The proposed algorithm provides the complete observability of the system under normal operating conditions as well as contingencies like single line outage and PMU outages. Further, it ensures the maximization of measurement redundancy also, which is attainable with the optimal PMU set. In this algorithm, the channel capacity of the PMU placed at a particular bus is determined by the number of interconnections of that bus. Addition of this constraint prevents the placement of a PMU with higher channel capacity at a bus with less number of interconnections. This eventually results in a reduction in the number of PMU channels used for complete observability leading to a reduction in the installation cost. As the observability constraints of this model are non-linear in nature, it is solved using Mixed Integer Quadratic Constrained Programming. The algorithm has been validated on various IEEE test systems and a NRPG -246 bus Indian system. The superiority of using PMUs of varying channel capacity is proved by comparing its performance with that of PMU having fixed channel capacity under normal operating conditions as well as contingencies like single line outage and PMU outages. Similarly, the redundant observability formulation of the proposed model is tested by comparing it with cost minimization model using PMUs with varying channels.

In Chapter 3, a HTLS algorithm for analysing the low frequency modes in ringdown oscillations was proposed. HTLS, being a parametric method, requires an accurate estimate of the model order for its proper implementation. This is obtained based on the number of peaks in the FFT plot of the signal. The fictitious modes, if any, present in the estimated results of the HTLS algorithm are removed by comparing the amplitude of the estimated modes as the amplitude of the true modes are much higher than that of the fictitious modes. The superiority of the proposed method was proven by comparing it with a Fourier based and Prony based models in the literature. Three synthetic signals having known modal parameters and real time signals obtained from PMUs placed in an actual power system is used for this purpose. Results reveal that it performs better than the other two methods irrespective of the reporting rate of the signal and the extent of noise contamination.

An ESPRIT based method for identifying the poorly damped modes in ringdown oscillations occurring in the power system is proposed in Chapter 4. The model order estimates for the ESPRIT method is obtained through EMO algorithm. The effectiveness of the EMO algorithm is tested by comparing it with a similar model order algorithm in the literature. Comparison reveal that the EMO algorithm can effectively estimate the model order of the highly noisy signals also. Further, the effectiveness of the EMO ESPRIT method is verified by comparing it with a ARMA based and Modified Prony based methods in literature. Simulation results show that the proposed method provides an accurate estimate of the modal parameters of the ringdown signals without the presence of fictitious modes irrespective of the noise contamination, presence of close modes in the signal and low PMU reporting rates.

An improved SSI based algorithm for estimating the modal parameters of ambient oscillations occurring in the power system is proposed in Chapter 5. The proposed SSI based method uses a Stationary Wavelet Transform based denoising method for reducing the noise content present in the signal. It also uses EMO algorithm for accurate model order estimation to prevent the occurrence of fictitious modes in the estimated results. The ability of the EMO algorithm to estimate the model order accurately is proved by comparing it with the model order estimation algorithm of a Matrix Pencil and Eigen Realization Algorithm based methods in the literature. Further, the effectiveness of the proposed SSI based method is proved by comparing its performance with a Teager Kaiser based, Fourier based and another SSI based methods in the literature using synthetic and real time signals. The results reveal that the proposed SSI based method estimates all the modes present in ambient type oscillations with a high degree of accuracy even under high noise contamination.

Chapter 6 proposed a method based on a combination of ESPRIT and Empirical Wavelet Transform (EWT) for analysing low frequency oscillations in the power system. In this method, EWT decomposes the signal into its mono-components and ESPRIT algorithm estimates the modal parameters of these mono-components. The EWT can extract different modes of the signal efficiently in comparison to other wavelet methods as it use adaptive wavelets for the decomposition whereas other wavelet methods use fixed basis for the same. Since the signal is decomposed into mono components, model order estimation, which is essential for the modal parameter estimation through ESPRIT technique, is not required. The effectiveness of the proposed method is proven by comparing it with Variational Mode Decomposition (VMD)- Teager Kaiser based method, a CWT based method and an HHT based method in the literature using synthetic and real time signals.

7.1 Major contributions of the thesis

The major contributions of this thesis are summarized as follows:

1. An improved optimal placement algorithm utilizing PMUs of different channel capacity for complete observability along with maximization of measurement redundancy during normal operating condition and contingencies is proposed. Simulation results prove that usage of PMUs with varying channel capacities reduces the total installation cost and improves the utilization of the PMU channels.
2. Two algorithms based on HTLS and ESPRIT were proposed for identifying the poorly damped modes in ringdown oscillations. The model order, which is a prerequisite for these algorithms, is estimated through an FFT based algorithm and EMO algorithm, respectively. Simulation results prove that the proposed methods accurately estimated

the modal parameters of ringdown oscillations irrespective of its noise contamination and PMU reporting rates.

3. A SSI based algorithm for analyzing the modal parameters of ambient oscillations is developed. The noise resistance of the proposed SSI based method is improved with the help of a SWT based denoising algorithm. It also uses EMO algorithm for accurately estimating the model order of the signal so that fictitious modes are not estimated along with the true modes of the signal. Simulation results indicate that the proposed SSI based method effectively identifies the poorly damped modes of ambient oscillation even under high levels of noise and low PMU reporting rates.

4. An EWT- ESPRIT based algorithm for analysing the low frequency oscillations in the power system is proposed. The novelty of this algorithm is that model order estimation which is a prerequisite for the ESPRIT method, is not required for this model. This is due to the usage of EWT, which decomposes the signal into its mono components. Simulation results prove that the proposed EWT ESPRIT method accurately identifies the poorly damped modes in low frequency oscillations irrespective of its noise contamination.

7.2 Future work

As a consequence of the research carried out in this thesis, the following aspects are identified for future research in this area.

1. In Chapters 3-5, different algorithms are proposed for estimating the modal parameters of ambient and ringdown oscillations. In order to identify the type of oscillations so that an appropriate algorithm can be applied, a classifier can be developed to distinguish the signal under consideration as either ringdown or ambient.

2. In Chapter 6, an EWT - ESPRIT method is proposed for analyzing the low frequency oscillations without using model order estimate. The EWT algorithm needs to be fine tuned to accurately estimate the modal parameters of non stationary oscillations occurring in power system.

3. In this thesis, different algorithms are proposed for identifying the poorly damped modes of ambient and ringdown oscillations. However, the possibility of designing a single algorithm, preferably using Wavelet transform based techniques for analyzing the poorly damped modes of both types of oscillations can be investigated.

4. The parametric methods used for the modal parameter estimation in this thesis are computationally intensive due to the usage of Singular Value Decomposition and inverse operations. Hence, further work can be done to reduce the computational complexity of these algorithms.
5. The data used for analysing the low frequency oscillations are obtained from PMUs. However, the measurements obtained from PMUs are prone to different types of errors, which are caused by limited measurement precision, telecommunication equipment, noise, interference from devices, cyber attacks etc. This introduces bad data into the PMU measurements. Hence, an algorithm for detecting the bad data and removing them before passing it to the modal parameter estimation algorithms is essential.

References

[1] S. Zhang, X. Xie, and J. Wu, "WAMS-Based Detection and Early-Warning of Low-Frequency Oscillations in Large-Scale Power Systems," *Electric Power Systems Research*, vol. 78, no. 5, pp. 897–906, 2008.

[2] A. Gomez-Exposito and A. Abur, *Power System State Estimation: Theory and Implementation*. CRC press, 2004.

[3] A. G. Phadke and J. S. Thorp, *Synchronized Phasor Measurements and Their Applications*. Springer, 2008, vol. 1.

[4] A. G. Phadke, "Synchronized Phasor Measurements in Power Systems," *IEEE Computer Applications in Power*, vol. 6, no. 2, pp. 10–15, 1993.

[5] P. Kundur, J. Paserba, V. Ajjarapu, G. Andersson, A. Bose, C. Canizares, N. Hatziargyriou, D. Hill, A. Stankovic, C. Taylor *et al.*, "Definition and Classification of Power System Stability," *IEEE Transactions on Power Systems*, vol. 19, no. 2, pp. 1387–1401, 2004.

[6] P. Kundur, N. J. Balu, and M. G. Lauby, *Power System Stability and Control*. McGraw-hill New York, 1994, vol. 7.

[7] S. A. Hosseini, N. Amjady, and M. H. Velayati, "A Fourier Based Wavelet Approach Using Heisenberg's Uncertainty Principle and Shannon's Entropy Criterion to Monitor Power System Small Signal Oscillations," *IEEE Transactions on Power Systems*, vol. 30, no. 6, pp. 3314–3326, 2015.

[8] T. L. Baldwin, L. Mili, M. B. Boisen, and R. Adapa, "Power System Observability With Minimal Phasor Measurement Placement," *IEEE Transactions on Power systems*, vol. 8, no. 2, pp. 707–715, 1993.

[9] S. Chakrabarti and E. Kyriakides, "Optimal Placement of Phasor Measurement Units for Power System Observability," *IEEE Transactions on Power Systems*, vol. 23, no. 3, pp. 1433–1440, 2008.

[10] M. Hajian, A. M. Ranjbar, T. Amraee, and B. Mozafari, "Optimal Placement of PMUs to Maintain Network Observability Using a Modified BPSO Algorithm," *International Journal of Electrical Power & Energy Systems*, vol. 33, no. 1, pp. 28–34, 2011.

[11] B. Milosevic and M. Begovic, "Nondominated Sorting Genetic Algorithm for Optimal Phasor Measurement Placement," *IEEE Transactions on Power Systems*, vol. 18, no. 1, pp. 69–75, 2003.

[12] H. H. Müller and C. A. Castro, "Genetic Algorithm-Based Phasor Measurement Unit Placement Method Considering Observability and Security Criteria," *IET Generation, Transmission & Distribution*, vol. 10, no. 1, pp. 270–280, 2016.

[13] N. C. Koutsoukis, N. M. Manousakis, P. S. Georgilakis, and G. N. Korres, "Numerical Observability Method for Optimal Phasor Measurement Units Placement Using Recursive Tabu Search Method," *IET Generation, Transmission & Distribution*, vol. 7, no. 4, pp. 347–356, 2013.

[14] J. Peng, Y. Sun, and H. Wang, "Optimal PMU Placement for Full Network Observability Using Tabu Search Algorithm," *International Journal of Electrical Power & Energy Systems*, vol. 28, no. 4, pp. 223–231, 2006.

[15] S. Chakrabarti, G. K. Venayagamoorthy, and E. Kyriakides, "PMU Placement for Power System Observability using Binary Particle Swarm Optimization," in *2008 Australasian Universities Power Engineering Conference*. IEEE, 2008, pp. 1–5.

[16] M. Hajian, A. Ranjbar, T. Amraee, and A. Shirani, "Optimal Placement of Phasor Measurement Units: Particle Swarm Optimization Approach," in *2007 International Conference on Intelligent Systems Applications to Power Systems*. IEEE, 2007, pp. 1–6.

[17] A. Ahmadi, Y. Alinejad-Beromi, and M. Moradi, "Optimal PMU Placement for Power System Observability Using Binary Particle Swarm Optimization and Considering Measurement Redundancy," *Expert Systems with Applications*, vol. 38, no. 6, pp. 7263–7269, 2011.

[18] R. F. Nuqui and A. G. Phadke, "Phasor Measurement Unit Placement Techniques for Complete and Incomplete Observability ," *IEEE Transactions on Power Delivery*, vol. 20, no. 4, pp. 2381–2388, 2005.

[19] F. Aminifar, C. Lucas, A. Khodaei, and M. Fotuhi-Firuzabad, "Optimal Placement of Phasor Measurement Units using Immunity Genetic Algorithm," *IEEE Transactions on Power Delivery*, vol. 24, no. 3, pp. 1014–1020, 2009.

[20] F. Marin, F. Garcia-Lagos, G. Joya, and F. Sandoval, "Genetic Algorithms for Optimal Placement of Phasor Measurement Units in Electrical Networks," *Electronics Letters*, vol. 39, no. 19, pp. 1403–1405, 2003.

[21] C. Peng, H. Sun, and J. Guo, "Multi-Objective Optimal PMU placement Using a Non-Dominated Sorting Differential Evolution Algorithm," *International Journal of Electrical Power & Energy Systems*, vol. 32, no. 8, pp. 886–892, 2010.

[22] R. Sodhi, S. Srivastava, and S. Singh, "Optimal PMU Placement to Ensure System Observability under Contingencies ," in *Power & Energy Society General Meeting, 2009. PES'09. IEEE*. IEEE, 2009, pp. 1–6.

[23] B. Gou, "Generalized Integer Linear Programming Formulation for Optimal PMU Placement," *IEEE Transactions on Power Systems*, vol. 23, no. 3, pp. 1099–1104, 2008.

[24] D. Dua, S. Dambhare, R. K. Gajbhiye, and S. Soman, "Optimal Multistage Scheduling of PMU Placement: An ILP Approach," *IEEE Transactions on Power Delivery*, vol. 23, no. 4, pp. 1812–1820, 2008.

[25] M. Esmaili, K. Gharani, and H. A. Shayanfar, “Redundant Observability PMU Placement in the Presence of Flow Measurements Considering Contingencies,” *IEEE Transactions on Power Systems*, vol. 28, no. 4, pp. 3765–3773, 2013.

[26] S. Chakrabarti, E. Kyriakides, and D. G. Eliades, “Placement of Synchronized Measurements for Power System Observability,” *IEEE Transactions on Power Delivery*, vol. 24, no. 1, pp. 12–19, 2009.

[27] N. P. Theodorakatos, N. M. Manousakis, and G. N. Korres, “A Sequential Quadratic Programming Method for Contingency-Constrained Phasor Measurement Unit Placement,” *International Transactions on Electrical Energy Systems*, vol. 25, no. 12, pp. 3185–3211, 2015.

[28] F. Aminifar, M. Fotuhi-Firuzabad, A. Safdarian, and M. Shahidehpour, “Observability of Hybrid AC/DC Power Systems With Variable-Cost PMUs,” *IEEE Transactions on Power Delivery*, vol. 29, no. 1, pp. 345–352, 2014.

[29] Aminifar, Farrokh and Fotuhi-Firuzabad, Mahmud and Shahidehpour, Mohammad and Khodaei, Amin, “Probabilistic Multistage PMU Placement in Electric Power Systems,” *IEEE Transactions on Power Delivery*, vol. 26, no. 2, pp. 841–849, 2011.

[30] F. Aminifar, M. Fotuhi-Firuzabad, M. Shahidehpour, and A. Khodaei, “Observability Enhancement by Optimal PMU placement Considering Random Power System Outages,” *Energy Systems*, vol. 2, no. 1, pp. 45–65, 2011.

[31] F. Aminifar, M. Fotuhi-Firuzabad, and A. Safdarian, “Optimal PMU Placement Based on Probabilistic Cost/Benefit Analysis,” *IEEE Transactions on Power Systems*, vol. 28, no. 1, pp. 566–567, 2013.

[32] F. Aminifar, M. Fotuhi-Firuzabad, M. Shahidehpour, and A. Safdarian, “Impact of WAMS Malfunction on Power System Reliability Assessment,” *IEEE Transactions on Smart Grid*, vol. 3, no. 3, pp. 1302–1309, 2012.

[33] M. Korkali and A. Abur, “Placement of PMUs with Channel Limits,” in *Power & Energy Society General Meeting, 2009. PES’09. IEEE.* IEEE, 2009, pp. 1–4.

[34] V. Rokkamand and R. Bhimasingu, “A Novel Approach for Optimal PMU Placement Considering Channel Limit,” in *Power System Technology (POWERCON), 2014 International Conference on*. IEEE, 2014, pp. 1164–1171.

[35] M. Korkali and A. Abur, “Impact of Network Sparsity on Strategic Placement of Phasor Measurement Units with Fixed Channel Capacity,” in *Circuits and Systems (ISCAS), Proceedings of 2010 IEEE International Symposium on*. IEEE, 2010, pp. 3445–3448.

[36] O. Gomez, M. Rios, G. Anders *et al.*, “Reliability-Based Phasor Measurement Unit Placement in Power Systems Considering Transmission Line Outages and Channel Limits,” *IET Generation, Transmission & Distribution*, vol. 8, no. 1, pp. 121–130, 2014.

[37] F. Rashidi, E. Abiri, T. Niknam, and M. R. Salehi, “Optimal Placement of PMUs With Limited Number of Channels for Complete Topological Observability of Power Systems Under Various Contingencies,” *International Journal of Electrical Power & Energy Systems*, vol. 67, pp. 125–137, 2015.

[38] Z. Miljanić, I. Djurović, and I. Vujošević, "Optimal Placement of PMUs with Limited Number of Channels," *Electric Power Systems Research*, vol. 90, pp. 93–98, 2012.

[39] Z. Zhao and E. B. Makram, "Optimal PMU Placement Considering Number of Analog Channels," in *North American Power Symposium (NAPS), 2011*. IEEE, 2011, pp. 1–5.

[40] A. M. Najafabadi and A. T. Alouani, *Optimal PMU placement Algorithm with Minimum Measurement Channels*, 2011.

[41] J. Hauer, "Application of Prony Analysis to the Determination of Modal Content and Equivalent Models For Measured Power System Response," *IEEE Transactions on Power Systems*, vol. 6, no. 3, pp. 1062–1068, 1991.

[42] D. Trudnowski, "Order Reduction of Large-Scale Linear Oscillatory System Models," *IEEE Transactions on Power Systems*, vol. 9, no. 1, pp. 451–458, 1994.

[43] D. Trudnowski, J. Johnson, and J. Hauer, "Making Prony Analysis More Accurate using Multiple Signals," *IEEE Transactions on Power Systems*, vol. 14, no. 1, pp. 226–231, 1999.

[44] D. P. Wadduwage, U. D. Annakkage, and K. Narendra, "Identification of Dominant Low-Frequency Modes in Ring-Down Oscillations Using Multiple Prony Models," *IET Generation, Transmission & Distribution*, vol. 9, no. 15, pp. 2206–2214, 2015.

[45] S. Rai, D. Lalani, S. K. Nayak, T. Jacob, and P. Tripathy, "Estimation of Low-Frequency Modes in Power System Using Robust Modified Prony," *IET Generation, Transmission & Distribution*, vol. 10, no. 6, pp. 1401–1409, 2016.

[46] S. Zhao and K. A. Loparo, "Forward and Backward Extended Prony (FBEP) Method for Power System Small-Signal Stability Analysis," *IEEE Transactions on Power Systems*, vol. 32, no. 5, pp. 3618–3626, 2017.

[47] R. Roy and T. Kailath, "ESPRIT-Estimation of Signal Parameters Via Rotational Invariance Techniques," *IEEE Transactions on Acoustics, Speech, and Signal Processing*, vol. 37, no. 7, pp. 984–995, 1989.

[48] P. Tripathy, S. C. Srivastava, and S. N. Singh, "A Modified TLS-ESPRIT-Based Method for Low-Frequency Mode Identification in Power Systems Utilizing Synchrophasor Measurements," *IEEE Transactions on Power Systems*, vol. 26, no. 2, pp. 719–727, 2011.

[49] G. R. Gajjar and S. Soman, "Power System Oscillation Modes Identifications: Guidelines for applying TLS-ESPRIT method," *International Journal of Emerging Electric Power Systems*, vol. 14, no. 1, pp. 57–66, 2013.

[50] S. Rai, P. Tripathy, and S. Nayak, "A Robust TLS-ESPIRIT Method using Covariance Approach for Identification of Low-Frequency Oscillatory Mode in Power Systems," in *Power Systems Conference (NPSC), 2014 Eighteenth National*. IEEE, 2014, pp. 1–6.

[51] X. Wang, F. Tang, X. Wang, and P. Zhang, "Estimation of Electromechanical Modes Under Ambient Condition via Random Decrement Technique and TLS-ESPRIT Algorithm," in *Power System Technology (POWERCON), 2014 International Conference on*. IEEE, 2014, pp. 588–593.

[52] T. Jiang, Y. Mu, H. Jia, N. Lu, H. Yuan, J. Yan, and W. Li, “A Novel Dominant Mode Estimation Method for Analyzing Inter-Area Oscillation in China Southern Power Grid,” *IEEE Transactions on Smart Grid*, vol. 7, no. 5, pp. 2549–2560, 2016.

[53] T. Jiang, H. Jia, J. Zhao, G. Ledwich, D. Wang, J. Zhang, and L. Qiu, “Mode Matching Pursuit for Estimating Dominant Modes in Bulk Power Grid,” *IET Generation, Transmission & Distribution*, vol. 8, no. 10, pp. 1677–1686, 2014.

[54] H. Ghasemi, C. Canizares, and A. Moshref, “Oscillatory Stability Limit Prediction Using Stochastic Subspace Identification,” *IEEE Transactions on Power Systems*, vol. 21, no. 2, pp. 736–745, 2006.

[55] J. L. Rueda, C. A. Juárez, and I. Erlich, “Wavelet-Based Analysis of Power System Low-Frequency Electromechanical Oscillations,” *IEEE Transactions on Power Systems*, vol. 26, no. 3, pp. 1733–1743, 2011.

[56] P. Kang and G. Ledwich, “Estimating Power System Modal Parameters Using Wavelets,” in *Signal Processing and Its Applications, 1999. ISSPA’99. Proceedings of the Fifth International Symposium on*, vol. 2. IEEE, 1999, pp. 563–566.

[57] S. Avdakovic, A. Nuhanovic, M. Kusljugic, and M. Music, “Wavelet Transform Applications in Power System Dynamics,” *Electric Power Systems Research*, vol. 83, no. 1, pp. 237–245, 2012.

[58] D. S. Laila, A. R. Messina, and B. C. Pal, “A Refined Hilbert–Huang Transform With Applications to Interarea Oscillation Monitoring,” *IEEE Transactions on Power Systems*, vol. 24, no. 2, pp. 610–620, 2009.

[59] R. W. Wies, J. W. Pierre, and D. J. Trudnowski, “Use of ARMA Block Processing for Estimating Stationary Low-Frequency Electromechanical Modes of Power Systems,” *IEEE Transactions on Power Systems*, vol. 18, no. 1, pp. 167–173, 2003.

[60] Z. Tashman, H. Khalilinia, and V. Venkatasubramanian, “Multi-Dimensional Fourier Ringdown Analysis for Power Systems Using Synchrophasors,” *IEEE Transactions on Power Systems*, vol. 29, no. 2, pp. 731–741, 2014.

[61] T. Jin, S. Liu, and R. C. Flesch, “Mode Identification of Low-Frequency Oscillations in Power Systems Based on Fourth-Order Mixed Mean Cumulant and Improved TLS-ESPRIT Algorithm,” *IET Generation, Transmission & Distribution*, vol. 11, no. 15, pp. 3739–3748, 2017.

[62] K. Salunkhe, G. Gajjar, A. Kulkarni, and S. Soman, “A Combined Model and Measurement Based Scheme for Assessment of Poorly Damped Power Swings,” in *2016 IEEE Annual India Conference (INDICON)*. IEEE, 2016, pp. 1–6.

[63] M. Scionti and J. Lanslots, “Stabilisation diagrams: Pole identification Using Fuzzy Clustering Techniques,” *Advances in Engineering Software*, vol. 36, no. 11-12, pp. 768–779, 2005.

[64] T. Jin, S. Liu, R. C. Flesch, and W. Su, “A Method for the Identification of Low Frequency Oscillation Modes in Power Systems Subjected to Noise,” *Applied Energy*, vol. 206, pp. 1379–1392, 2017.

[65] J. C.-H. Peng and N.-K. C. Nair, "Enhancing Kalman Filter for tracking Ringdown Electromechanical Oscillations," *IEEE Transactions on Power Systems*, vol. 27, no. 2, pp. 1042–1050, 2011.

[66] M. Yazdanian, A. Mehrizi-Sani, and M. Mojiri, "Estimation of Electromechanical Oscillation Parameters using an Extended Kalman Filter," *IEEE Transactions on Power Systems*, vol. 30, no. 6, pp. 2994–3002, 2015.

[67] M. Yazdanian, A. Mehrizi, and M. Mojiri, "A Novel Approach for Ringdown Detection using Extended Kalman Filter," in *IECON 2013-39th Annual Conference of the IEEE Industrial Electronics Society*. IEEE, 2013, pp. 3270–3274.

[68] I. Kamwa, A. K. Pradhan, and G. Joos, "Robust Detection and Analysis of Power System Oscillations Using the Teager-Kaiser Energy Operator," *IEEE Transactions on Power Systems*, vol. 26, no. 1, pp. 323–333, 2011.

[69] K. Mandadi and B. K. Kumar, "Identification of Inter-Area Oscillations Using Zolotarev Polynomial Based Filter Bank With Eigen Realization Algorithm," *IEEE Transactions on Power Systems*, vol. 31, no. 6, pp. 4650–4659, 2016.

[70] G. R. Gajjar and S. Soman, "Analysis of Sustained Oscillations in Power Systems Observed through Wide Measurements," in *2017 IEEE PES Asia-Pacific Power and Energy Engineering Conference (APPEEC)*. IEEE, 2017, pp. 1–6.

[71] F. Aminifar, A. Khodaei, M. Fotuhi-Firuzabad, and M. Shahidehpour, "Contingency-Constrained PMU Placement in Power Networks," *IEEE Transactions on Power Systems*, vol. 25, no. 1, pp. 516–523, 2010.

[72] J. Philip and T. Jain, "An Improved Redundant Observability Model for Optimal Placement of PMUs with Different Channel Capacities," *WSEAS Transactions on Power Systems*, vol. 13, no. 37, pp. 377–385, 2018.

[73] A. Enshaee, R. A. Hooshmand, and F. H. Fesharaki, "A New Method for Optimal Placement of Phasor Measurement Units to Maintain Full Network Observability Under Various Contingencies," *Electric Power Systems Research*, vol. 89, pp. 1–10, 2012.

[74] NRPG Data, "*Indian Institute of Technology Kanpur* [online]," http://iitk.ac.in/eeold/facilities/Researchlabs/PowerSystem/NRPG-DATA.pdf, accessed: 02 Jan 2016.

[75] R. Kumar and V. S. Rao, "Optimal Placement of PMUs with Limited Number of Channels," in *North American Power Symposium (NAPS), 2011*. IEEE, 2011, pp. 1–7.

[76] Z. Miljanić, I. Djurović, and I. Vujošević, "Multiple Channel PMU placement Considering Communication Constraints," *Energy Systems*, vol. 4, no. 2, pp. 125–135, 2013.

[77] S. Mukhopadhyay, V. K. Agrawal, S. K. Soonee, P. Agarwal, R. Anumasula, and C. Kumar, "Detecting Low Frequency Oscillations Through PMU-Based Measurements for Indian National Grid," in *Power Systems Computation Conference (PSCC), 2016*. IEEE, 2016, pp. 1–7.

[78] M. Glickman, P. O'Shea, and G. Ledwich, "Estimation of Modal Damping in Power Networks," *IEEE Transactions on Power Systems*, vol. 22, no. 3, pp. 1340–1350, 2007.

[79] D. Xu, R. He, and T. Xu, "A New Approach to Power System Electromechanical Oscillation Research," *Power Systems and Communications Infrastructures for the Future*, 2002.

[80] L. L. Grant and M. L. Crow, "Comparison of Matrix Pencil and Prony Methods for Power System Modal Analysis of Noisy Signals," in *North American Power Symposium (NAPS), 2011*. IEEE, 2011, pp. 1–7.

[81] D. P. Wadduwage and U. Annakkage, "Improving Matrix Pencil and Hankel Total Least Squares Algorithms for Identifying Dominant Oscillations in Power Systems," in *2015 IEEE 10th International Conference on Industrial and Information Systems (ICIIS)*. IEEE, 2015, pp. 13–18.

[82] H. Akaike, "A New Look at the Statistical Model Identification," *IEEE Transactions on Automatic Control*, vol. 19, no. 6, pp. 716–723, 1974.

[83] S. Vanhuffel, H. Chen, C. Decanniere, and P. Vanhecke, "Algorithm for Time-Domain NMR Data Fitting Based on Total Least Squares," *Journal of Magnetic Resonance, Series A*, vol. 110, no. 2, pp. 228–237, 1994.

[84] *Report and Data of WECC. [Online]. Available: ftp://ftp.bpa.gov/pub/ WAMS Information/.*

[85] *PDCI Probe Testing Plan, 2005. [Online]. Available: http://www.transmission.bpa.gov/business/operations/SystemNews/.*

[86] S. K. Jain and S. N. Singh, "Exact Model Order ESPRIT Technique for Harmonics and Interharmonics Estimation," *IEEE Transactions on Instrumentation and Measurement*, vol. 61, no. 7, pp. 1915–1923, 2012.

[87] S. K. Jain, P. Jain, and S. N. Singh, "A Fast Harmonic Phasor Measurement Method for Smart Grid Applications," *IEEE Transactions on Smart Grid*, vol. 8, no. 1, pp. 493–502, 2017.

[88] N. Zhou, J. W. Pierre, and J. F. Hauer, "Initial Results in Power System Identification From Injected Probing Signals Using a Subspace Method," *IEEE Transactions on Power Systems*, vol. 21, no. 3, pp. 1296–1302, 2006.

[89] S. N. Sarmadi and V. Venkatasubramanian, "Electromechanical Mode Estimation Using Recursive Adaptive Stochastic Subspace Identification," *IEEE Transactions on Power Systems*, vol. 29, no. 1, pp. 349–358, 2014.

[90] L. Liu and J. Jiang, "Using Stationary Wavelet Transformation for Signal Denoising," in *Fuzzy Systems and Knowledge Discovery (FSKD), 2011 Eighth International Conference on*, vol. 4. IEEE, 2011, pp. 2203–2207.

[91] W. G. Morsi and M. El-Hawary, "A New Perspective for the IEEE Standard 1459-2000 Via Stationary Wavelet Transform in the Presence of Nonstationary Power Quality Disturbance," *IEEE Transactions on Power Delivery*, vol. 23, no. 4, pp. 2356–2365, 2008.

[92] J. G. Philip and T. Jain, "Analysis of Low Frequency Oscillations in Power System Using EMO ESPRIT," *International Journal of Electrical Power & Energy Systems*, vol. 95, pp. 499–506, 2018.

[93] J. Hauer, E. Martinez, A. Messina, and J. Sanchez-Gasca, "Identification of Electromechanical Modes in Power Systems," *Special Publication, TP462, IEEE Power & Energy Society, Tech. Rep.*, 2012.

[94] H. Xiao, J. Wei, H. Liu, Q. Li, Y. Shi, and T. Zhang, "Identification Method for Power System Low-Frequency Oscillations Based on Improved VMD and Teager–Kaiser Energy Operator," *IET Generation, Transmission & Distribution*, vol. 11, no. 16, pp. 4096–4103, 2017.

[95] J. Gilles, "Empirical Wavelet Transform." *IEEE Transactions on Signal Processing*, vol. 61, no. 16, pp. 3999–4010, 2013.

[96] K. Thirumala, A. C. Umarikar, and T. Jain, "Estimation of Single-Phase and Three-Phase Power-Quality Indices Using Empirical Wavelet Transform," *IEEE Transactions on Power Delivery*, vol. 30, no. 1, pp. 445–454, 2015.

[97] K. Martin, G. Benmouyal, M. Adamiak, M. Begovic, R. Burnett, K. Carr, A. Cobb, J. Kusters, S. Horowitz, G. Jensen *et al.*, "IEEE Standard for Synchrophasor Measurements for Power Systems," *IEEE Transactions on Power Delivery*, vol. 13, pp. 73–77, 2011.

[98] *Report on the Grid Disturbance on 30th July [Online]. Available:http://www.cercind.gov.in/2012/orders.*